Time and Energy Optimal Trajectory Generation for Coverage Motion of Industrial Machines

(産業機械の領域被覆動作のための時間／エネルギー最適軌道生成)

July, 2023

Doctor of Philosophy (Engineering)

Mathias Sebastian Halinga

マティアス　セバスチャン　ハリンガ

Toyohashi University of Technology

Declaration of Authorship

I, Mathias Sebastian Halinga, declare that this thesis titled, " Time and Energy Optimal Trajectory Generation for Coverage Motion of Industrial Machines" and the work presented in it are my own. I confirm that:

- This work was done wholly or mainly while in candidature for a research degree at this University.
- Where any part of this thesis has previously been submitted for a degree or any other qualification at this University or any other institution, this has been clearly stated.
- Where I have consulted the published work of others, this is always clearly attributed.
- Where I have quoted from the work of others, the source is always given. With the exception of such quotations, this thesis is entirely my own work.
- I have acknowledged all main sources of help.
- Where the thesis is based on work done by myself jointly with others, I have made clear exactly what was done by others and what I have contributed myself.

Signed: 

Date: July, 2023

Abstract

In the manufacturing industry, industrial machines including Computer Numerical Control (CNC) and industrial robots are widely used because of their accuracy, flexibility, and high production rates to meet the demands for precise products. Coverage motion is one of the dominant motions of industrial machines for manufacturing tasks such as milling, polishing, painting, additive manufacturing, laser cutting, and inspection. To achieve high accuracy, these tasks require precise motion; on the other hand, the tasks are repetitive and are performed for a long time, which leads to high energy consumption. Energy saving is needed given the current worldwide situation of high energy costs, environmental effects, and depletion of energy sources. In addition, shorter operating times are key for industrial machines to meet high production demands and guarantee profits. To attain shorter operation times, machines are typically operated at higher velocities, thus leading to high energy consumption and low precision. Precise motion is vital for machines to manufacture high quality products. Therefore, industrial sector is driven by a high need for machines with accurate motion, shorter operation times, and energy saving.

Coverage motion optimization is one of the methods that play a major role in reducing time and energy consumption while increasing motion accuracy of the machine. It is a feasible and less costly method that does not require replacing existing machine components with new ones or modifying the control law. Motion optimization is categorized into geometric path optimization and trajectory generation while considering objective functions such as smoothness, time, cost, and energy consumption. In the literature, many studies focused on motion optimization and implemented the two processes separately; simultaneous path optimization and trajectory generation are relatively unexplored. By integrating geometric path optimization and trajectory generation, industrial machines can realize high quality products with higher

machine performance and ensure environmental sustainability. Due to the high demand for reducing production costs and environmental sustainability, objective functions of smoothness, time, energy or both time and energy consumption are crucial to be considered for performance enhancement. Moreover, time and energy are two conflicting objectives; the trade-off between time and energy should be determined. This thesis discusses several approaches of industrial machines coverage motion optimization for accuracy and performance enhancement using trajectory (velocity) optimization with simultaneous geometric path optimization. The proposed approaches can be used for machine operations such as milling, laser cutting, inspection, gluing, and polishing that execute point-to-point (PTP) motions.

To enhance machine performance in terms of time and energy consumption while achieving accurate motion in industrial machines, the proposed optimization approaches are described as follows in this thesis: Introductory remarks are presented in chapter 1 followed by a literature review in chapter 2 describing the industrial feed drive systems, related studies in motion optimization, and optimization methods. Chapter 3 presents the method for simultaneous path and trajectory (velocity) optimization used to improve machine efficiency in a coverage motion for industrial machines by ensuring the smoothness and satisfaction of the machine constraints. The multi-objective path and trajectory optimization are proposed to obtain a trade-off between time and energy consumption for coverage motion. The Jerk-limited acceleration profile (JLAP) describes the trajectory where the velocity profiles generated for each linear segment attain desirable velocities. The energy model of an industrial two-axis feed drive system is used to solve the optimization problem. Non-dominated Sorting Genetic Algorithm II (NSGA II) generates a Pareto front for trade-off time and energy consumption solutions. Simulation results of the proposed method are validated through experiments using the industrial two-axis feed drive system. Experimental results show the effectiveness of proposed approach where the best trade-off solution achieves time reduction and energy saving of about 10.05% and 2.10%, respectively. Furthermore, optimized path of proposed method lowers maximum error of about 76.6% compared to the optimized path with constant commanded velocity.

In addition, an energy optimization approach for the coverage motion of industrial machines, which simultaneously integrates trajectory generation and geometric path optimization is presented in chapter 4. The modified S-curve profile describes the trajectory along a linear segment with harmonic motion employed for smooth jerk continuity to enhance the motion accuracy.

Energy consumption model of the industrial feed drive system is used to achieve optimal energy. Genetic Algorithm (GA) is applied for the optimization. Experimental validation of the simulation results is carried out using the industrial two-axis feed drive system. Simulation and experimental results show that the energy saving of the feed drive system is achieved under machine kinematic limits that ensure smooth motion, which is approximately 14.6% energy saving compared to an unoptimized solution. Furthermore, the proposed approach is compared with the optimized path generated using the fourth-order motion profile. The results show that the proposed approach increases motion accuracy with high energy saving compared to the fourth-order motion profile.

Chapter 5 describes an approach that proposes optimal motion planning by simultaneous path and velocity optimization to achieve the trade-off between time and energy consumption. The multi-objective optimization model for minimizing time and energy consumption is solved by the NSGA II. The modified S-curve profile describes the trajectory, which ensures smooth jerk continuity. To validate the effectiveness of the proposed approach, simulation and experiments are carried out using the industrial two-axis feed drive system, and the motion accuracy is compared to that of JLAP. Experimental results reveal that the best trade-off trajectory of the proposed approach achieves respectively 13.9% and 3.5% of time reduction and energy saving. The mean tracking error is reduced by 16.2% and 14.9% for the x and y axes, respectively, compared to the JLAP. Lastly, chapter 6 presents the concluding remarks of this thesis as well as future works.

Acknowledgments

First, I would like to thank God Almighty Father for giving me good health, strength, knowledge, ability, and the opportunity to complete my studies and carry them out satisfactorily.

I would like to express my sincere appreciation to my supervisor, Prof. Naoki Uchiyama, for his great support and guidance throughout my studies. Using his knowledge and expertise improved my career in the field of research, which is beneficial to my career and society in general.

I extend my sincere thanks to the committee members: Prof. Kaiji Sato and Prof. Junji Takahashi for their time, effort, and expertise in reviewing my research. Furthermore, it is my pleasure to extend my gratitude to all members of the System Engineering Laboratory for their support and companionship throughout my studies.

A very special gratitude goes to Toyohashi University of Technology for the assistance. In addition, thanks to Monbukagakusho for providing me a scholarship during my studies.

I would like to express my heartfelt gratitude to my beloved wife Salome for her unconditional love, care, and patient. Thanks also to my children Faith and Adriel for being so patient and kind to me.

Last but not least, I would like to express my sincere gratitude to my parents Sebastian and Ernesi for their unconditional support, patients, and prayers. Furthermore, thanks to my brothers, sisters, and Dr. M. Msukwa for their support and encouragement throughout my study.

Contents

List of Figures

List of Tables

Abbreviations

AC	alternating current
ACO	Ant Colony Optimization
ANN	Artificial Neural Network
CNC	Computer Numerical Control
EMF	electromotive force
GA	Genetic Algorithm
JLAP	Jerk-limited acceleration profile
NSGA II	Non-dominated Sorting Genetic Algorithm II
PSO	Particle Swarm Optimization
PTP	point-to-point
SA	Simulated Annealing
2D	two-dimensional space

Chapter 1

Introduction

1.1 Background

Manufacturing sectors around the world use industrial machines extensively to produce precise products at high production rates. Although, these machines such as CNC (Fig. 1.1) are extensively used in manufacturing industries, numerous studies indicate that their efficiency is about 30% [1, 2]. Their manufacturing activities are associated with high energy consumption and environmental concerns attributed to greenhouse gases [3, 4]. Recently, worldwide energy sources are limited, leading to high energy cost. In addition, precise motion and shorter operation times are highly needed for industrial machines to realize high quality products and production profits. Due to technological advancement, industrial machines are more adaptable and flexible, making easier to improve their performance. By improving machine performances, global challenges can be addressed, such as reducing energy consumption and availability of quality products. Therefore, industrial machines performance can be improved in terms of time, energy saving or both time and energy consumption reduction to ensure high production rates, environmental sustainability, and achieve quality products.

Many researchers have drawn attention to enhance the machine performance through different approaches. Energy saving and time reduction are achieved by modeling and parameters optimization methods as proposed in [5–8]. However, ensuring precise motion requires consideration of trajectory generation, which is not taken into account in these studies. Motion accuracy

(a) CNC milling. http://www.stylecnc.com (b) CNC laser cutter. http://www.stylecnc.com

Fig. 1.1: CNC machines.

and energy saving improvement through controller designs in industrial feed drive systems are proposed in [9, 10]. Nevertheless, their applications are limited to industrial systems where controllers are difficult to access. Using a lightweight design to the components of industrial machine systems reduces moving masses, resulting in energy saving [11, 12]. The lightweight design approach reduces energy consumption and environmental impact, but it requires high production costs to replace existing machine components. Trajectory (velocity) optimization for industrial machines are proposed [13–19] for time-optimal and [20–23] for energy optimal along the predefined paths. However, generation of an optimal geometric path is not taken into account. A geometric path has effect on the machine performance, if it is not properly planned consumes more energy and time [24]. In [24–29], geometric paths optimization are proposed that describes path to be represented by x and y coordinates, but a definition or description of the position, velocity, acceleration, and jerk as a function of time during the machine motion is not given which has effect on performance.

In the context described above, achieving quality products and high production rates while maintaining environmental sustainability remains a challenge. Motion optimization for typical CNC machines under their kinematic limits plays a critical role in coverage motion to increase production efficiency and accuracy. Furthermore, it is necessary to consider energy consumption optimization or both time and energy consumption as multi-objective optimization problems to achieve their trade-off since are conflicting with each other.

1.2 Objectives of this study

The aim of this study is to develop and implement simultaneously trajectory and geometric path optimization approaches for the coverage motion of industrial machines based on given working conditions and constraints. The implementation is to improve machine performance for the coverage motion in terms of energy or both time and energy consumption while achieving precise motion. The procedures are as follows:

- To formulate a single-objective model for achieving energy optimal and a multi-objective model for contradictory objective time and energy consumption of coverage motion in industrial machines.
- To implement optimization of the models through simulation to generate the energy optimal solution for single-objective and Pareto-optimal solutions for the trade-off between time and energy consumption of a given working surface with an obstacle or island.
- To perform experiments using an industrial feed drive system to verify the optimization results.

1.3 Thesis contributions and outline

1.3.1 Contributions

The main contributions of thesis are as follows:

- A method for simultaneous trajectory generation and path optimization for the machine coverage motion for the time and energy optimal is proposed. In most cases, trajectory generation and path optimization are implemented separately. Considering trajectory generation and geometric path simultaneously improves accuracy and performance of the machine. Trajectory generation along the path is described by the JLAP. Time and energy Pareto-optimal solutions are generated using NSGA II to complete coverage motion on a given working surface while satisfying constraints including obstacle avoidance

(island). This is accomplished by formulating a multi-objective model to determine trade-off optimal values. Results show the effectiveness of the proposed method in generating a trade-off optimal paths. Therefore, based on the optimal trade-off between time and energy, planners can choose any solution from the Pareto front based on preference. In addition, in most similar studies that implement trajectory generation, a single objective is considered, and therefore this optimization approach addresses the gap in the literature for determining the best trade-off solution between time and energy consumption.

- The modified S-curve is proposed to describe trajectory along the path by introducing the harmonic functions into the JLAP and achieving smooth jerk continuity. Furthermore, an energy optimization approach is proposed for coverage motion of industrial machines, which simultaneously integrates modified S-curve trajectory generation and geometric path optimization. Energy consumption model is used to achieve energy optimal. Simulation and experimental results show that the energy optimal coverage motion is achieved under machine kinematic limits, ensuring smooth motion. Therefore, using the proposed method has practical advantage to improve the efficiency of existing industrial machine systems when energy optimal coverage motion is needed.

- Using the modified S-curve trajectory for motion description, simultaneous trajectory generation and path optimization is proposed for the trade-off between time and energy consumption. The multi-objective optimization model for minimizing time and energy consumption is solved. Simulation and experimental results show that the method achieves trade-off values time and energy consumption as Pareto-optimal solutions. From Pareto front, planners can choose any solution based on their preferences. Furthermore, compared with JLAP, the modified S-curve describes coverage motion with higher accuracy.

- A few steps of the existing NSGA II are implemented/developed differently to ensure a feasible and optimal path solutions during optimization. These steps include the generation of location points, encoding (path representation), initialization of the population, genetic operators (order crossover and inversion mutation), and assignment of fitness to avoid obstacles (islands) in the optimization procedure. In this case, the order/sequence of points on the path solutions during optimization is monitored, and feasible path solutions are generated. Therefore, the proposed method has practical advantages over the

existing NSGA II by ensuring feasible path solutions. Researchers can apply this approach to optimization problems based on coverage paths, while GA or NSGA II are used as optimization methods.

1.3.2 Outline

The remainder of this thesis is organized as follows: Chapter 2 presents related studies for improving machine performance. It describes dynamics and energy consumption model for the industrial feed drive system. This chapter also describes different motion optimizations with trajectory generation and geometric path. In addition, optimization methods for the coverage motion are illustrated. Chapter 3 describes a method for simultaneous path and trajectory optimization coverage motion for time and energy optimal while achieving accuracy motion. The JLAP is employed to describe the trajectory along a linear segment of the path. Chapter 4 introduces an energy optimization approach for coverage motion of industrial machines, which simultaneously integrates modified S-curve trajectory generation and geometric path optimization. Chapter 5 presents an extension of proposed method in chapter 4 to solve the trade-off between time and energy for industrial machines coverage motion, which mainly aims for achieving time and energy Pareto-optimal solutions while ensuring smooth motion. Chapter 6 presents conclusion and future works.

Assumption of the study

The study is proposed for general application purposes for industrial machines with operations such as laser cutting, milling, inspection, gluing, polishing, and additive manufacturing. In cutting/machining operations, the assumption of study is that the cutting force is negligible, so the machine table system exerts sufficient power/force to perform the operation successfully. In addition, offline coverage motion optimization approaches are proposed that consider using a 2D plane as the working surface for the machine operation.

Chapter 2

Literature Review and Preliminaries

2.1 Introduction

Manufacturing sector plays an important role in advancing society and the economy. This is attributed to the use of industrial machines that are very flexible with high precision, accurate, and speed [30]. Industrial machines such as CNC milling, router, grinder, waterjet, and laser cutting are widely used worldwide. However, these machines are associated with high energy consumption despite their wide use in manufacturing [31]. Most of the energy used in the manufacturing sector for operating machines continuously is generated from fossil fuels which results to the greenhouse gases emission and environmental impact [32, 33]. Energy consumption for the machines is due to the electrical consumption of the components, including the auxiliary units, spindle, and feed drives [34]. Auxiliary units consist of computers, hydraulic systems, and cooling systems that consume energy when the machine is operating. The spindle energy is the energy consumed by spindle drives system including rotary motion for the cutting tool. The feed drives energy consumption is associated with energy supply of linear and rotary motion along the axes (axes motion) and energy of carrying the table used to hold workpieces.

Improving energy performance of the machine is one of the effective measure for energy saving and emission reduction with realization of the sustainable manufacturing [35]. A number of studies are presented to reduce energy consumption of industrial machines. Machine parameters

optimization are proposed in [5, 7, 36–38] and modeling approaches to predict energy consumption [39–41]. These approaches involves studying different machine parameters that contribute to energy consumption; requires experimental measurements, validation, and coming up with energy formulation. The energy models formulated are later used to estimate the machine's energy consumption. To achieve energy saving while observing smooth motion, controller designs are proposed for the feed drives systems [9, 10, 42]. The controller design approaches are used in industrial systems with easier access to the controller since it involves modification of the control system.

Furthermore, motion optimization reduces time and energy consumption [13–29]. It is the approach and practice that is less costly to use existing machines efficiently. This is achieved through effective generation of motion input commands to the machine motion. The generated path motion guides the machine to move from one point to another in the intended direction and speed to complete a working surface. During linear motion interpolation from one point to another, execution time and energy consumption are required to move the machine table and complete the motion along the path. Thus, generation of the motion input commands can be incorporated with machine performance measures such as execution time and energy consumption. These measures are incorporated into the motion generation process through designed models. As a result, the performance of the machine can be improved. Currently, motion optimization has commonly been executed by either trajectory generation or geometric path optimization. Both trajectory generation and geometric path optimization have an impact on machine efficiency [43, 44]. The simultaneous trajectory generation and path optimization have not been compressively investigated in the literature. Therefore, it is essential to explore the significance of simultaneous geometric path optimization and trajectory generation for time and energy optimal while achieving accurate motion.

2.2 Industrial two-axis feed drive systems

Most CNC machines consist of feed drive systems, which are employed to move machine tool components and workpieces towards a desired direction or location through axes [43]. A typical structure of a feed drive system is shown in Fig. 2.1 which is composed of a servomotors, couplings, support bearings, ball-screws, encoders, table, and linear guides supporting the table.

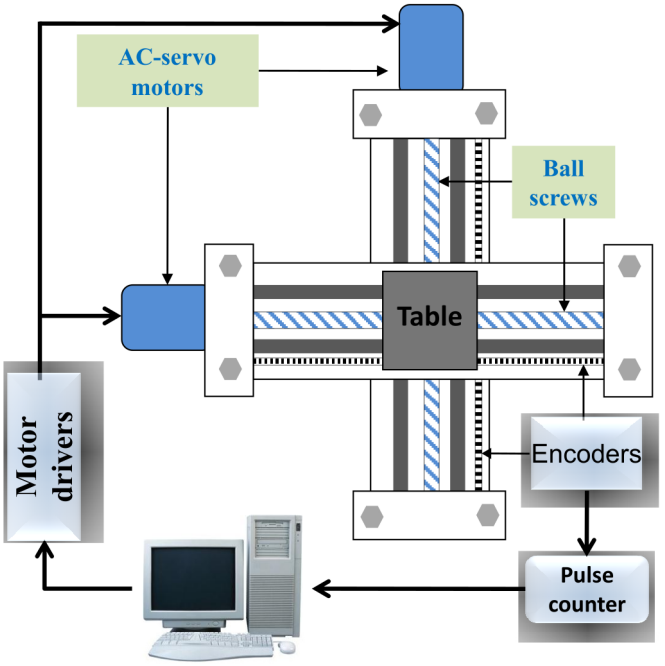

Fig. 2.1: Feed drive system structure.

Feed drive systems are found in industrial machines with applications such as milling, gantry loading, inspection, painting, and laser cutting. These applications are repetitive in nature, leading to high energy consumption. The dynamics including frictions, back electromotive force (EMF) terms, and driven masses of the feed drive systems influence its energy consumption, where the main components affecting energy consumption are motors, bearings, ball-screws, and table [45]. In addition, feed drive systems energy consumption is influenced by the different orientation path motion, movement directions, and working table velocity [46, 47]. Modeling of the energy consumption model of the industrial feed drive system used in this thesis are briefly described as follows.

2.2.1 System dynamics and energy consumption model

Industrial two-axis feed drive system (X-Y table) is commonly utilized in manufacturing industry, where it appears in machineries such as CNC milling, laser cutting, and waterjet. Fig. 2.2 shows the industrial two-axis feed drive system used in this thesis, which consists of a table coupled with ball screws driven by alternating current (AC) servomotors. The dynamics of a

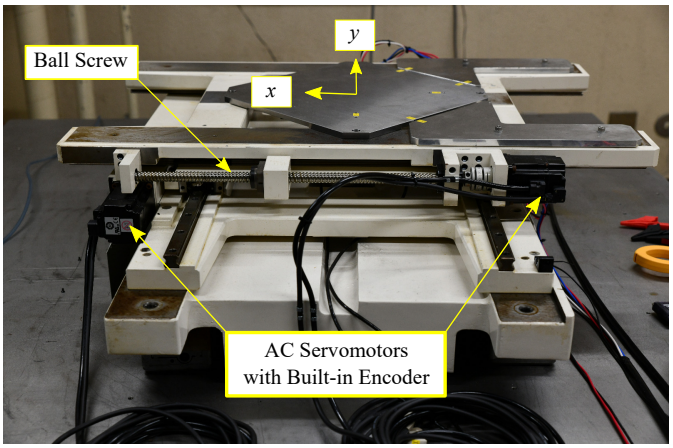

Fig. 2.2: Industrial two-axis feed drive system.

two-axis feed drive system can be generally expressed by decoupled second-order model [42, 48], given as

$$M\ddot{\boldsymbol{x}}(t) + D\dot{\boldsymbol{x}}(t) + F\text{sgn}\left\{\dot{\boldsymbol{x}}(t)\right\} = I_k(t)K_{\text{F}}, \tag{2.1}$$

with

$$M = \text{diag}\left\{m_k\right\}, D = \text{diag}\left\{d_k\right\}, F = \text{diag}\left\{f_k\right\},$$
$$K_{\text{F}} = \text{diag}\left\{k_{\text{F},k}\right\}, k \in \{x, y\},$$

where M, D, F, and K_{F} are matrices of inertia term, viscous friction coefficient, Coulomb friction, and constant force, respectively. $I_k(t)$ and $\boldsymbol{x}(t)$ are the input current vectors and axial positions, respectively. The energy model for the feed drive system is formulated by considering its dynamics as proposed in [49] with three phase AC servomotor used. As the method proposed in [20], the output power P_k is given by

$$P_k(t) = \sqrt{3}\lambda_k V_k(t) I_k(t), \tag{2.2}$$

where $V_k(t)$ and $I_k(t)$ are the instantaneous effective voltage and current of a motor for each axis, respectively. λ_k is the power factor. The effective voltage and current are calculate by

$$V_k(t) = I_k(t)Z + K_{\text{E}}\dot{\boldsymbol{x}}(t), \tag{2.3}$$

with

$$Z = \text{diag}\{z_k\},\ K_\text{E} = \text{diag}\{k_{\text{E},k}\},$$

where z_k and $k_{\text{E},k}$ are the motor impedance and back EMF coefficient of the k^{th} axis, respectively,

$$I_k(t) = \frac{1}{K_\text{F}}[M\ddot{\boldsymbol{x}}(t) + D\dot{\boldsymbol{x}}(t) + F\text{sgn}\,\{\dot{\boldsymbol{x}}(t)\}]. \tag{2.4}$$

The energy consumption model results from the combination of (2.2) - (2.4). The crucial property is that power is a function of velocity and acceleration. As a result, trajectory profiles are used to determine the power. Therefore, the energy consumption model is presented as

$$E = \int_{t_0}^{t_\text{tf}} (|P_x(t)| + |P_y(t)|)dt, \tag{2.5}$$

$$P_k(t) = C_{1,k}\ddot{\boldsymbol{x}}_k^2 + C_{2,k}\dot{\boldsymbol{x}}_k^2 + C_{3,k}\dot{\boldsymbol{x}}_k\text{sgn}\,(\dot{\boldsymbol{x}}_k) + C_{4,k} + C_{5,k}\ddot{\boldsymbol{x}}_k\text{sgn}\,(\dot{x}_k) + C_{6,k}\ddot{\boldsymbol{x}}_k\dot{\boldsymbol{x}}_k,$$
$$\text{for} \quad k = \{x, y\},$$

with

$$\begin{aligned}
C_j &= \text{diag}\{c_{j,k}\},\ j = \{1, 2, ..., 6\},\\
c_{1,k} &= \sqrt{3}\lambda_k m_k^2 \frac{z_k}{k_{\text{F},k}^2},\\
c_{2,k} &= \sqrt{3}\lambda_k d_k \left(\frac{z_k d_k}{k_{\text{F},k}^2} + \frac{k_{\text{E},k}}{k_{\text{F},k}}\right),\\
c_{3,k} &= \sqrt{3}\lambda_k f_k \left(\frac{2z_k d_k}{k_{\text{F},k}^2} + \frac{k_{\text{E},k}}{k_{\text{F},k}}\right),\\
c_{4,k} &= \sqrt{3}\lambda_k f_k^2 \frac{z_k}{k_{\text{F},k}^2},\\
c_{5,k} &= 2\sqrt{3}\lambda_k f_k m_k \frac{z_k}{k_{\text{F},k}^2},\\
c_{6,k} &= \sqrt{3}\lambda_k m_k \left(\frac{2z_k d_k}{k_{\text{F},k}^2} + \frac{k_{\text{E},k}}{k_{\text{F},k}}\right),
\end{aligned} \tag{2.6}$$

Table 2.1: Energy coefficients of each drive axis.

k^{th}axis		$c_{1,k}$[Ws^4/m^2]	$c_{2,k}$[Ws^2/m^2]	$c_{3,k}$[Ws/m]	$c_{4,k}$[W]	$c_{5,k}$[Ws^2/m]	$c_{6,k}$[Ws^3/m^2]
x	$\dot{\boldsymbol{x}} \geq 0$	2.684	546.357	45.135	0.663	2.2667	90.838
	$\dot{\boldsymbol{x}} < 0$	2.684	476.807	-52.3333	0.891	-3.093	90.838
y	$\dot{\boldsymbol{y}} \geq 0$	2.101	534.437	50.851	0.856	2.682	79.682
	$\dot{\boldsymbol{y}} < 0$	2.101	494.006	-48.999	0.795	-2.584	79.682

Table 2.2: Parameters values of each drive axis.

k^{th}axis	m_k[Ns^2/m]	d_k[Ns/m]	f_k[N]	$k_{\text{F},k}$[N/A]
x	86.76	558.62	47.50	235.62
y	99.65	795.5	58.00	331.12

where $c_{j,k}$ is the j^{th} energy coefficient for the k^{th} axis. E is the total energy consumption for the feed drive system from time t_0 to t_{tf}. $P_x(t)$ and $P_y(t)$ are the power at time t for the x and y axes, respectively.

The energy consumption model parameters and coefficients used in this thesis are identified experimentally with industrial two-axis machine (Fig. 2.2) as described in [49]. Machine coefficients and parameters are presented in Tables 2.1 and 2.2, respectively.

2.2.2 Energy measurement method

Energy consumption for the feed drive system are measured using a power meter analyzer (HIOKI13390) connected between a motor driver and a motor, directly measuring its power consumption. The analyzer measures energy using an integration measurement approach, in which the power is integrated every 50 ms of data update. The energy consumption is measured in x and y axes. When the machine moves, the measurement value of energy consumption for the two axes is displayed on the display channel. The total energy of the two axes is recorded, and the sum is the energy consumption of the machine. To avoid inaccuracy in energy measurements, the experiment can be repeated several times for the same motion, and the average energy consumption is calculated.

2.3 Coverage motion optimization

Motion optimization is a way to plan machine motions moving from one point to another that are efficient and feasible. It aims to obtain optimal coverage motion that passes all the required points on the working surface while avoiding obstacles (islands) and with no overlapping of points or path. The objective functions such as energy consumption, production time, production costs, and surface roughness are considered in coverage motion optimization to achieve the optimality for given decision variables and constraints. The optimization can be set as single-objective or multi-objectives for two or more objectives. Offline or online optimizations can be performed, where optimal motions generated are used as input commands to the machine tool. These commands define the operations and movements of the machine table or cutting tool, workpiece, and activities performed. The coverage motion optimization is applied to many machine application, such as milling [24, 25, 50], grinding [51], painting [52], polishing [53], laser cutting [54, 55], and inspection [56]. These industrial motions can be optimized in two ways: geometric path optimization/planning and trajectory generation.

2.3.1 Geometric path optimization

Path optimization refers to the generation of an optimal geometric path, where the sequence of points for machine to move along the path is represented by the x and y coordinates, but the definition of control motion time input from one point to another is not given. During optimization process, optimal geometric path is generated based on selected objectives while taking account of the surface working conditions such as islands/obstacles. To define the given working surface to the optimization process, sequences of points are generated and used as path references. The working surface to be covered is discretized to create sequences of several equidistant grid points (path locations). The discretization method is widely used because it is easier to mark the points on a working surface and incorporated into optimization algorithms.

A number of methods are suggested to optimize geometric paths for industrial machines, including CNC that perform PTP motions. Path optimization method for cavity milling is proposed in [25], aiming to achieve the best trade-off between processing time, cost, and energy. The path for the free-form surface CNC milling is optimized to achieve energy saving and carbon emission

reduction [24]. Path optimization method is proposed in [26] to improve smoothness efficiency in pocket milling using a contour strategy. Geometric path optimization for CNC milling to achieve the shortest path is proposed [27]. A toolpath optimization approach is presented to minimize machining time on several linear segments in the area to be machined [29]. In [55], toolpath optimization for sheet metal laser cutting is proposed to achieve time optimal path. Optimization of the path for drilling holes on flat surfaces is proposed to minimize airtime from one point to another [57]. Toolpath optimization for the energy optimal hole drilling is proposed in [58]. Optimization of polishing coverage path and material removal is proposed to ensure high profile accuracy and surface quality [59]. Laser cutting path optimization is proposed in [60], the trade-off between shortest path distance and time are achieved. Toolpath generation for polishing the surface area of the freeform is proposed in [53]. However, these studies present path optimization methods; trajectory generation, including velocity, acceleration, and jerk, are not considered. As a result, the optimized geometric path motion can generate high operating speeds, excessive accelerations, and vibrations of the machine's mechanical structure, which affect accuracy and performance [61]. To ensure smooth motion for optimized paths, it is necessary to incorporate trajectory generation.

2.3.2 Trajectory generation

Trajectory generation is described as the definition of reference machine motion commands such as position, velocity, acceleration, and jerk as a function of time while moving from one point to another [62]. These are inputs to the feed drives to direct machine motion interpolation while satisfying its kinematic limits. It is essential to observe machine kinematic limits including velocity, acceleration, and jerk to achieve smooth coverage motion. For PTP motion, interpolation of these commands/variables generates a trajectory or motion profiles for each linear segment depending on the direction of the axes. Motion profile or trajectory generation for the linear segments needs to be performed for the machine to follow. During trajectory generation, objective functions such as time and energy can be considered to achieve optimality of the machine motion. Trajectory generation can be performed using functions such as trapezoidal velocity profiles and JLAP. These are simple motion profiles widely used in industrial machines, consist of acceleration, constant velocity, and deceleration times. The trapezoidal velocity profile describes motion along the linear segment consisting of three phases: constant

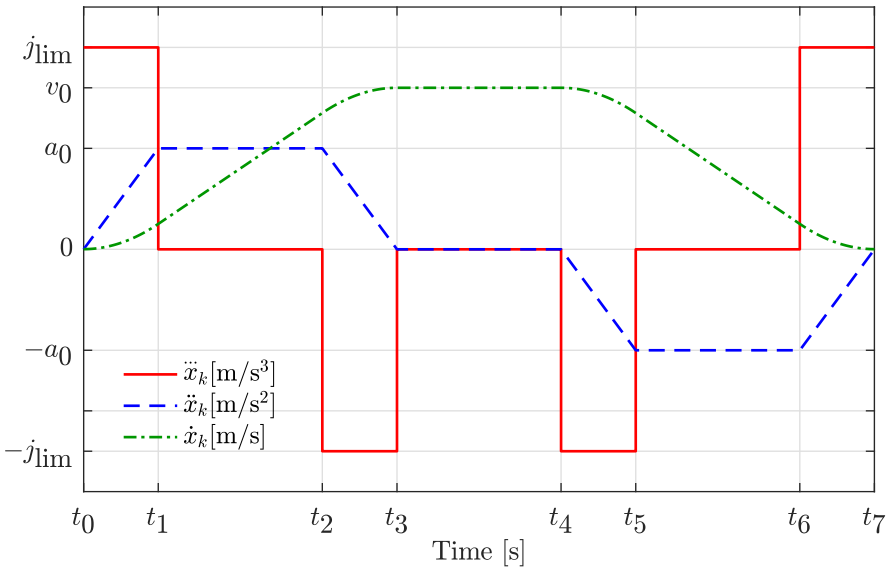

Fig. 2.3: Illustration of a jerk-limited acceleration profile.

acceleration, constant velocity, and constant deceleration with three time motion intervals [63]. In [20, 64], trapezoidal velocity profiles are used to increase motion accuracy and energy saving in industrial machines. The trade-off between time and energy is achieved in [65] while trapezoidal velocity is used to describe the motion along the path. However, trapezoidal profiles are used in these studies, there is a sudden change of acceleration values and the occurrence of infinite jerk values when the profile change from one phase to another, for example from constant acceleration to constant velocity phase. The discontinuous acceleration and infinite jerk occurrence at phase transitions lead to machine excitation and affect machine performance [66]. To overcome this problem, the limitation of jerk to the profile is proposed and used in different studies.

Jerk-limited acceleration profile

The JLAP or S-curve trajectory is the motion profile used to generate smooth trajectories for the linear contours by ensuring the jerk is limited. The trajectory is generated in seven segments of motion time intervals with continuous acceleration profile. The time intervals are used to divide the trajectory of a linear segment in transitions including linear acceleration/deceleration, constant acceleration/deceleration, and constant velocity. Fig 2.3 shows the JLAP trajectory.

The definition of jerk in each time interval is given as

$$\dddot{\boldsymbol{x}}_k(t) = \begin{cases} j_{\mathrm{lim},k}, & t_0 \leq t < t_1, \\ 0, & t_1 \leq t < t_2, \\ -j_{\mathrm{lim},k}, & t_2 \leq t < t_3, \\ 0, & t_3 \leq t < t_4, \\ -j_{\mathrm{lim},k}, & t_4 \leq t < t_5, \\ 0, & t_5 \leq t < t_6, \\ j_{\mathrm{lim},k}, & t_6 \leq t < t_7, \end{cases} \tag{2.7}$$

where $j_{\mathrm{lim},k}$ is the jerk limit for the k^{th} axis. The time interval are calculated from velocity, acceleration, and jerk. The time intervals are defined as

$$\begin{aligned} t_{\mathrm{a},1} &= t_1 - t_0 = t_3 - t_2 = t_5 - t_4 = t_7 - t_6, \\ t_{\mathrm{c},1} &= t_2 - t_1 = t_6 - t_5, \\ T_{\mathrm{c},1} &= t_4 - t_3, \end{aligned} \tag{2.8}$$

where $t_{\mathrm{a},1}$ is the linear acceleration/deceleration period, $t_{\mathrm{c},1}$ is the constant acceleration/deceleration period, and $T_{\mathrm{c},1}$ is the constant velocity period.

The JLAP is optimized to increase the efficiency of the machine while achieving smooth motion using JLAP. In literature, different efficiency measures are considered to improve machine performance. Time-optimal trajectory generation is presented in [16, 67–69] using the S-curve profile for PTP motion. The optimization of the feedrate for the five-axis machine is performed in [15]; the optimal feedrates are obtained from the velocity, acceleration, and jerk limit to ensure machining accuracy while satisfying the kinematic limits of the machine. Motion profiles for the feed drive system along the predefined path are generated using the JLAP for the trade-off between cycle time and motion accuracy [21]. To achieve energy optimal paths of industrial machines while achieving smooth motion, S-curve trajectories are optimized [20, 70]. In addition, JLAP is optimized to achieve the trade-off between time and energy consumption for PTP motion for the feed drive systems [49].

Smooth continuity in velocity and acceleration with jerk limitation during linear interpolations as described using JLAP lessen machine excitation and improve efficiency. However, the jerk limitation is associated with sudden changes in the jerk value at phase transitions that degrade

the accuracy of the machine. For some applications, smooth jerk continuity during interpolation along the path is required to ensure higher accurate motion and energy reduction. This can be achieved by modifying the JLAP and introducing the harmonic motion to the constant jerk phase.

2.3.3 Simultaneous trajectory generation and geometric path optimization

Machine motion optimization for a given working surface as described above can be performed in two ways either geometric path optimization or trajectory generation, where trajectory generation is performed on a predefined geometric path. However, both geometric path and trajectory generation influence machine performance. Hence, it is essential to plan a motion that considers the geometric path and trajectory optimization simultaneously.

For a given working surface, for example 2D geometry (Fig. 2.4) whereby no information on the geometric path is given, the geometric path needs to be determined. In addition, for machine to complete the coverage PTP motion on the working surface from the start to the end of the motion, there are several different feasible geometric paths. Fig. 2.5 (a) shows one of a feasible geometric path on the 2D geometry. Based on the coverage motion objectives such as time and energy consumption, an optimal geometric path must be determined that satisfies the surface working constraints. Furthermore, in linear motion interpolation, variables such as position, velocity, and acceleration should be defined to direct the motion from one location point to another while satisfying machine kinematic limits. Interpolation of these variables generates a trajectory or motion profile for each linear segment depending on the direction of the axes (Fig. 2.5. (b)). Different motion profiles such as trapezoidal and S-curve trajectories can be used to describe the trajectory for PTP linear interpolations. During trajectory generation, objectives such as time and energy can be considered. Therefore, consideration of simultaneous geometric path and trajectory optimization highly improves machine performance while achieving motion accuracy. The optimization parameters are defined based on the geometric path and trajectory generation definition of the working surface.

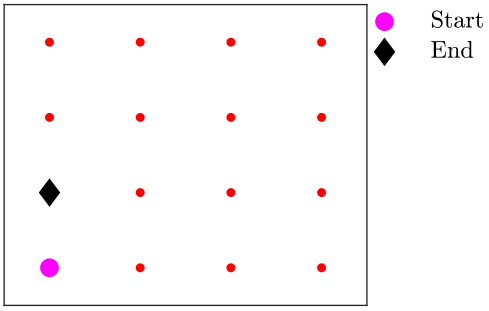

Fig. 2.4: Illustration of a working surface.

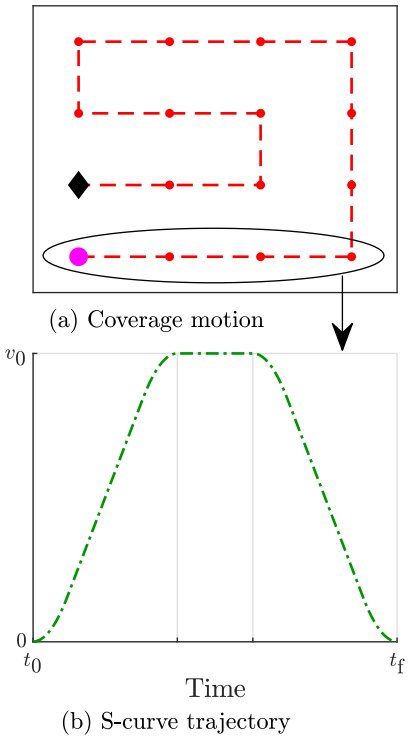

Fig. 2.5: Illustration of a coverage motion.

2.4 Optimization methods

Optimization methods are techniques used to find the best values for a given set of objective functions, optimization parameters, and constraints of the optimization model. There are several methods used for optimization and can be categorized into two groups: deterministic and stochastic. Deterministic methods such as gradient descent and linear programming are used to find optimal solutions to optimization problem by directly applying some steps or exploiting

predefined features of a given problem. On the other hand, stochastic methods including GA and Particle Swarm Optimization (PSO) use randomness search in some constructive way to attain optimal solutions [71].

Recently, in motion optimization, stochastic methods using different algorithms are proven to be effective in finding global optimal solutions to the optimization problems [72]. In [25], GA is used for generating and optimizing toolpaths for cavity milling to find the best trade-off between processing time, cost, and energy. Li *et al.* [24] propose energy optimal toolpath for the free-form surface milling, GA is used as optimization algorithm. PSO and GA are used to find time-optimal path machine motion [29]. GA is used to determine an optimal machining sequence for different areas of a flat workpiece in [28]. For CNC drilling path optimization, Ant Colony Optimization (ACO) algorithm is used to achieve shorter operating time [73]. In [74], ACO is used to find the shortest path for the robotic path planning. Artificial Neural Network (ANN) is used for optimal selection of milling toolpath strategies [75]. Yang *et al.* propose a time-optimal trajectory optimization in industrial machines using PSO [76]. Lu *et al.* [67] propose a time-optimal trajectory generation using the S-curve motion for the machine tool along the predefined path by PSO. For robotic path planning, Xue uses NSGA II for shorter paths, safety, and smoothness [77]. In [78], NSGA II is used to generate Pareto solutions set for time and cost in travel planning. NSGA II is used to solve the multi-objective optimization for energy minimization energy, time, and surface roughness for hole path drilling in CNC machines [58].

These stochastic algorithms can be easily linked to different optimization models and explore a wide range of applications [79]. Based on problem formulation, optimization parameters, and constraints, algorithm is set up to find feasible solutions. Optimized results support decision-making process. The problem considered can be described as single-objective optimization in which the best single solution is determined, or multi-objective optimization that takes into account more than one objective in order to give a set of compromised solutions for the trade-off between them.

2.4.1 Single-objective optimization methods

Problems requiring optimization of only one objective function are termed as single-objective optimization problem. The optimization aims to find best solution for the defined problem such as execution time, energy consumption, shorter path, and surface smoothness. The main goal is to find a solution with the best objective value that outperforms other solutions. Since one best solution is determined, it is easier for the decision maker to only select the obtained best optimized solution. The general mathematical expression of single-objective with assumption of minimization problem is given as

$$\begin{aligned} F(\boldsymbol{u}) &= \min_{\boldsymbol{u}}\{f(\boldsymbol{u})\}, \\ &\text{subject to} : \boldsymbol{u} \in U, \end{aligned} \tag{2.9}$$

where $f(\boldsymbol{u})$ is the objective function to be minimized. $\boldsymbol{u}$ is the optimization parameter vector; $\boldsymbol{u} = [u_1, u_2, ...u_n]$, n is the total number of optimization parameters.

There are several optimization methods for single-objective functions, including numerical, enumerative, and stochastic methods. To achieve a globally optimal solution, stochastic optimization methods are recently been used to determine an optimal solution for single-objective functions, including path optimization [29, 73, 74], trajectory generation [28, 67], and process improvement [80, 81]. Simulated Annealing (SA), GA, ANN, ACO, and tabu search are some of the stochastic optimization methods that solve problems while ensuring global optimal convergence [71]. The selection among these methods depends on the problem that needs to be considered. The use of a GA is shown to suit optimization problems of a combinatorial nature with a high chance of finding global optimal results quickly [82, 83]. Therefore, in the case of a coverage motion optimization problem which is a combinatorial problem in nature, a GA is one of the methods that can be used to determine an optimal solution. Following problem optimization process, a single global optimal solution that outperforms all other solutions is selected as the best solution.

Genetic Algorithm

Genetic Algorithm (GA) is a population-based global search that uses genetic operators to find optimal solutions [82]. It is a randomized search and optimization method based on natural genetics and selection that uses inheritance, variation, and survival struggle mechanisms [84]. With a given single-objective function problem, optimization parameters, and constraints, the algorithm can be executed to find a single-objective optimal solution. The representation of the solution to the GA is achieved by using encoding. Different ways of encoding such as binary, real, and integers (numbering) are commonly used to represent the solution [85]. Binary encoding is the approach whereby the representation of genes uses 0's and 1's, for the real encoding uses continuous numbers for genes representation, and the numbering is used to represent the solution in optimization using positive integers. For the path optimization problems, numbering or integers encoding is used to represent the solutions. An array of integers with no repetition represents a path, which is a solution. A solution in GA is called a chromosome or individual, consisting of discrete units called genes that correspond to each integer in the path representation. Each gene has a particular value or feature for the individual solution. A collection of individuals is called a population. The algorithm finds an optimal global solution as the search evolves iteratively. In Fig. 2.6, the optimization steps of GA is shown, and these steps are briefly described as follows.

Step 1) Population initialization: This is the process to generate non-optimal solutions to be optimized during the optimization process. In coverage motion optimization, population of candidate solutions are generated using numbering encoding that contains several path options. Random initialization is a common method used to maintain the diversity and optimality of the solutions, while other initializations method such as heuristic can be incorporated to increase the convergence of the algorithm [86].

Step 2) Fitness evaluation: During optimization, fitness function is incorporated into the algorithm to determine the value of objective function. Each solution in the population is evaluated using a defined fitness function. A fitness value is the output of a problem-solving algorithm that indicates how good the solution is.

Step 3) Selection: Some solutions in the population are selected as parents to create a new solutions called offspring for the next generation. The selected solutions are entered into the

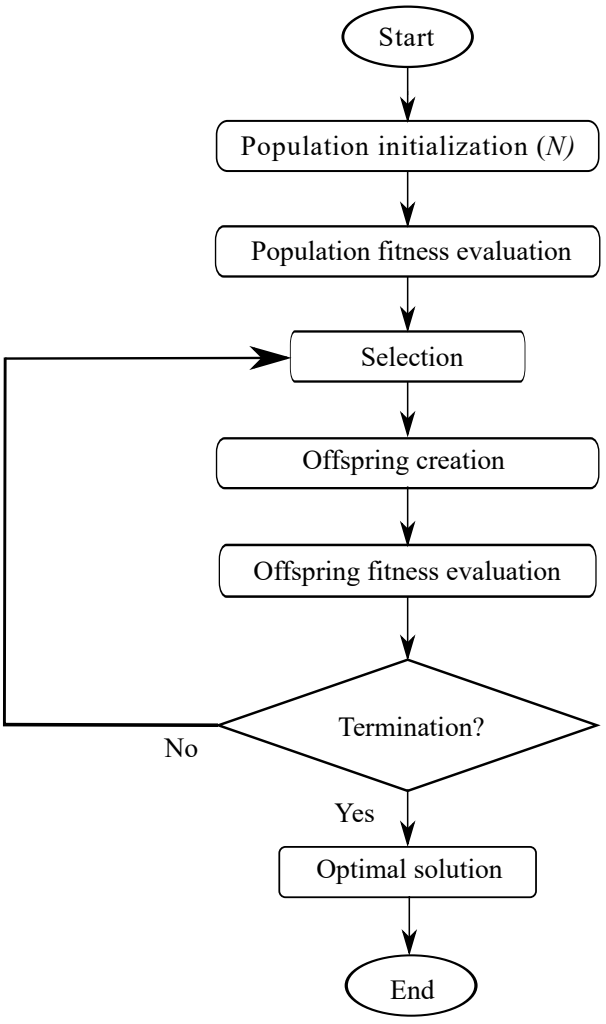

Fig. 2.6: Illustration of a GA flow chart.

mating pool to undergo the recombination process in order to create offspring. Proper selection of parents is essential to maintain good diversity and convergence of the algorithm. One of the selection methods is the roulette wheel selection operator, which provides the chance for each individual solution to get selected and reduces premature convergence of the solution to a local minimum [82]. In addiction, elitism method is incorporated to the algorithm. Elitism means that in an iterative process, few best individuals found so far during each search are kept to the next generation.

Step 4) Offspring creation: The new solutions called offspring are created in mating pool aiming to improve the search toward optimal solution during the iteration process. In the

recombination process, crossover and mutation are used as genetic operators. Crossover is a recombination process that creates offspring from a pair of parents that exchange their genes, creating two offspring [87]. Good genes from parents are expected to appear more frequently in the offspring, eventually leading to convergence and overall good solutions. Therefore, crossover leads to convergence of algorithm by making the individuals in the population alike. Mutation is a slight random change in some genes in the solution. The mutation maintains diversity in the population and assists the algorithm search to escape from converging to the local optima [88]. During optimization process, algorithm is sometimes executed by incorporating some of the modifications to operators to improve the operation to achieve feasible solutions. This can be accomplished using a local search technique in mutation operation. During crossover and mutation operations, each offspring must be created without integers being repeated, ensuring that the path are feasible. After offspring creation, offspring created in the mating pool become a new population.

Step 5) Fitness evaluation of offspring: The created offspring are evaluated using a defined fitness function to determine the optimized value. The fitness values achieved are used in a selection process to determine parents, which are later used in creating offspring for the next generation or the calculated values become the final solutions values of optimization when the algorithm termination condition is met.

Step 6) Termination condition: In order to terminate the optimization of algorithm, termination condition is set. Fitness value evaluation criteria is used to decide on the termination condition. A maximum number of iterations is predefined and selected based on trial runs; the number is selected by which the optimal fitness values do not change. When the terminating condition of the algorithm is met, the new population becomes a final solutions and the solution with best fitness value is selected as the best solution.

2.4.2 Multi-objective optimization methods

Multi-objective optimization involves optimizing a number of objectives either by maximizing or minimizing the values of their respective objective functions. The goal of optimization is to find trade-off between contradictory objectives. A set of trade-off solutions help in the decision-making process by providing a compromise between contradictory objectives, which are used

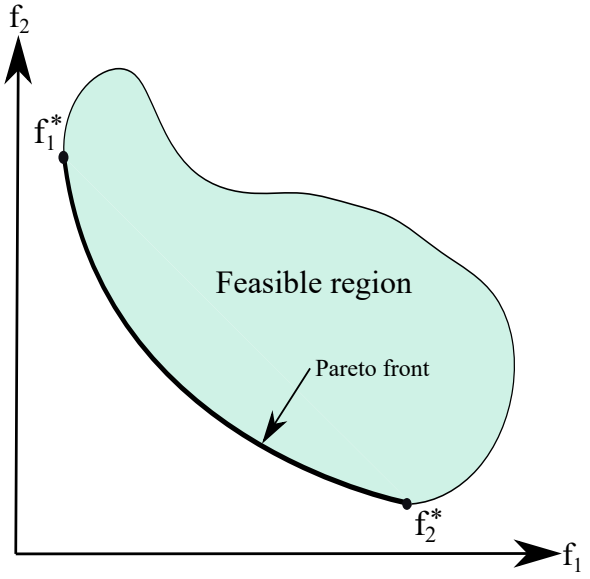

Fig. 2.7: Illustration of a feasible solutions and Pareto front of two-objective functions.

as references to reach a final decision. The multi-objective optimization with assumption of minimization problems is expressed in general mathematical form as

$$F(\boldsymbol{u}) = \min_{\boldsymbol{u}}\{f_1(\boldsymbol{u}), f_2(\boldsymbol{u}), f_3(\boldsymbol{u}), ..., f_n(\boldsymbol{u})\}, \quad (2.10)$$
$$\text{subject to} : \boldsymbol{u} \in U,$$

where $\boldsymbol{u}$ is optimization parameter vector: $\boldsymbol{u} = [u_1, u_2, u_3, ...u_m]$ with m as the number of parameters in feasible solution space U, $f_n(\boldsymbol{u})$ is the n^{th} objective function, and the integer $n \geq 2$ is the number of objectives.

There are two methods that are commonly used in finding feasible solutions for more than one objective function to be optimized simultaneously, namely scalarization and Pareto [89]. Scalarization is a method of finding an optimal solutions by recursively converting multi-objective optimization problems into a set of single-objective subproblems [90]. Some of the scalarization approaches include weighted sum, weighted Chebyshev, and ϵ-constraint. For scalarization optimization, varying parameters such as weight- or ϵ-vectors and optimizing the scalarized function, different Pareto-optimal solutions can be found. However, combining objectives into a single-objective subproblems can lead to the possibility that the search direction is at one

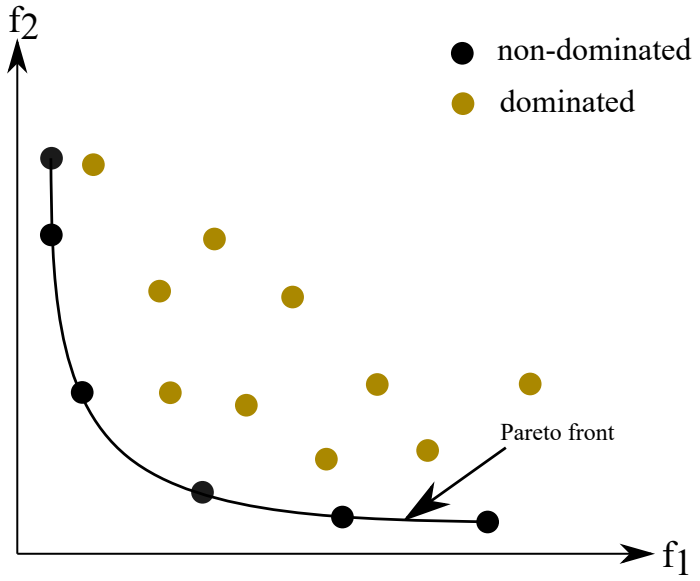

Fig. 2.8: Illustration of a dominance approach during optimization.

point and the diversity of solutions degraded as the results will be a bias in finding a trade-off solutions [91, 92].

Pareto method is a technique for simultaneously direct searching for the optimal solution of each objective function, and a set of the optimal trade-off between the contradictory objectives is represented on the Pareto-optimal front [89]. Fig. 2.7 shows a feasible region where several set of feasible solutions are generated using the Pareto method within the objective function space, and the optimal results are represented on the Pareto front. There are several Pareto approaches such as evolutionary multi-objective optimization (EMO) algorithms and deep learning multi-objective optimization. The evolutionary optimization includes NSGA II, NSGA III, and Strength Pareto Evolutionary Algorithm 2. Multiple trade-off solution results are generated for each simulation run during optimization, and the solutions are distributed on the Pareto front.

The concept of dominance is used to determine the Pareto-optimal solutions, and dominance classifies the solutions generated into dominated and non-dominated. The dominance is executed by help of constraints handling methods and Pareto ranking technique [93, 94]. Fig. 2.8 shows non-dominated and dominated solutions displayed on objective function space. A set of non-dominated solutions is found with wide trade-off among the objectives on the Pareto front.

Pareto optimization method starts with non-optimal random solutions. Several simulation runs are performed to execute an optimization algorithm to generate Pareto solutions. At each iteration, the algorithm searches for global optimal convergence and determines multiple non-dominated trade-off solutions. In addition, as the algorithm runs iteratively, different operators of an algorithm are used to improve the solutions toward optimality. The final optimal values on the Pareto front are achieved when one objective function value cannot be improved without degrading the other objective function value. Therefore, the Pareto-optimal front is a front comprising a collection of optimal non-dominated solutions with full convergence. Pareto-optimal solutions are achieved that provide a set of non-dominated solutions with the exact values of the objective functions; but the best trade-off solution between the objectives is not indicated. Therefore, it is essential to find the best trade-off solution.

To determine the best trade-off solution among Pareto-optimal solutions, one of the methods used is the normalization of objective function optimal values achieved on the Pareto front. Each objective function value is normalized to the entries in the positive unit range [0, 1] without a change in their ordinal positions. The normalization is carried out using the values obtained as follows;

$$\overline{f_{ij}^{*}} = \frac{f_{ij}^{*} - f_{i}^{min}}{f_{i}^{max} - f_{i}^{min}} \quad \text{for} \quad i = 1, ..., n, \quad \text{and} \quad j = \{1, 2, ..., m\}, \tag{2.11}$$

where f_i^{min} and f_i^{max} are the minimum and maximum value of the i^{th} objective functions. f_{ij}^{*} is the j^{th} individual solution of the i^{th} objective function with m number of the solutions. $\overline{f_{ij}^{*}}$ is the normalized value.

Fig. 2.9 shows a representation of two objective functions with normalized solutions features on the Pareto front. After normalization, some of the important solutions points on the Pareto front can be easily indicated. The anchor point is the best point/solution for each objective function from the Pareto front, taking the example for the two objectives as shown in Fig. 2.9, each objective achieves one anchor point; therefore, there are two anchor points. In addition, for the case of minimization problem, the utopia point is obtained by intersecting the minimum value of one objective function with the minimum value of another objective function. When the Pareto front solutions are normalized, the utopia point is the origin point (0,0) as shown in Fig. 2.9. The origin point is used as a reference to find the best trade-off optimal solution

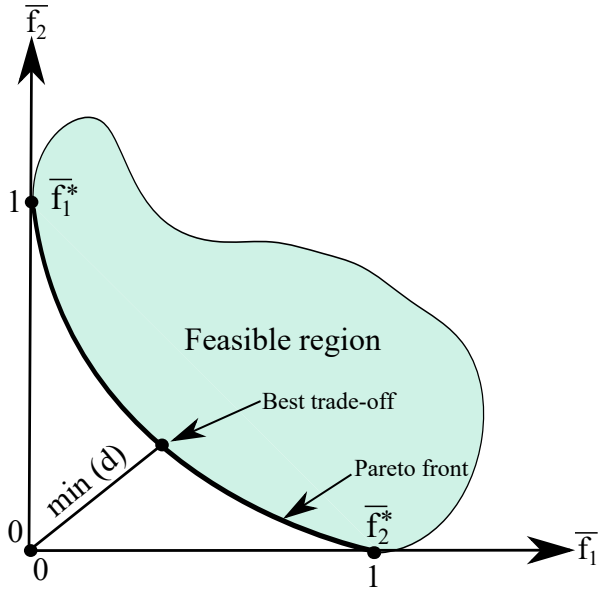

Fig. 2.9: Illustration of a normalization for optimal solutions.

on the Pareto-optimal front. The best trade-off solution is the one with the shortest distance from the origin as shown in Fig. 2.9. NSGA II is one of the Pareto optimization method used for combinatorial optimization problem and its procedures are described as follows.

Non-dominated Sorting Genetic Algorithm II (NSGA II)

This is the optimization method that is population-based algorithm and used to find Pareto-optimal solutions to multi-objective optimization problems [93, 95]. The algorithm generates Pareto-optimal solutions with good convergence and diversity, and iterations are used in the search process. At each run, solutions of each objective are generated and their relationship are determined using the Pareto dominance approach, in addition, population solutions are improved by algorithm operators such as crossover and mutation [93]. The algorithm maintains the diversity and elitism of the solutions using density estimation, crowding distance operator, and genetic operators [95].

To implement an optimization problem in algorithm, first, it starts with defining the problem at hand to suit the algorithm. The optimization problem is defined by three components which are; set of the objective functions, optimization parameter vector, and set of constraints which

determine or ensure feasibility of the solutions. The goal is to find optimal combinations of optimization parameters for the objective functions and obtain the Pareto-optimal solutions while running within given constraints. NSGA II are shown to be an effective evolution algorithm for optimizing several multi-objective problems, including combinatorial problems [77, 96, 97], to generate Pareto-optimal solutions. Therefore, with the aim of simultaneous trajectory generation and path optimization of machine coverage motion, the algorithm can be executed, and Pareto-optimal solutions can be effectively determined.

Path optimization is a combinatorial problem; integers/numbering encoding is used to represent solutions in the algorithm. In addition, since NSGA II adapts some strategies from the GA, optimization steps such as population initialization, fitness evaluation, offspring creation, and termination condition, are executed similarly to those described in the GA in section 2.4.1. Iteratively, the algorithm finds Pareto-optimal solutions that trade-off between the contradictory objectives. The following is a description of the NSGA II operation steps, and Fig. 2.10 shows its flow chart.

Step 1) Population initialization: This is a set of non-optimal solutions of size N that are generated at the start of optimization. Numbering encoding generates a population of candidate solutions that contain several path solutions. These solutions can be generated randomly and incorporated with other initialization methods, such as heuristics, to increase the convergence of the algorithm.

Step 2) Fitness evaluation: In order to determine the value of each objective function, the fitness functions are incorporated into the optimization algorithm. Based on the number of objective functions, more than one fitness function is assigned. Each solution in the population is evaluated using a defined fitness functions. A fitness values are output of a problem-solving algorithm.

Step 3) Non-dominating sorting and selection: The generated population solutions are sorted based on their dominance to generate non-dominated Pareto fronts in the population of size N [93, 95]. For each solution, a comparison is made with every other solution in the population to determine its non-domination. The solutions are identified and classified into different non-dominated ranks. The ranks of non-dominated solutions form multiple Pareto fronts, numbered from first, second, and higher. In addition, the crowded-distance comparison approach is incorporated into the algorithm to maintain a good spread in the obtained solutions. Following

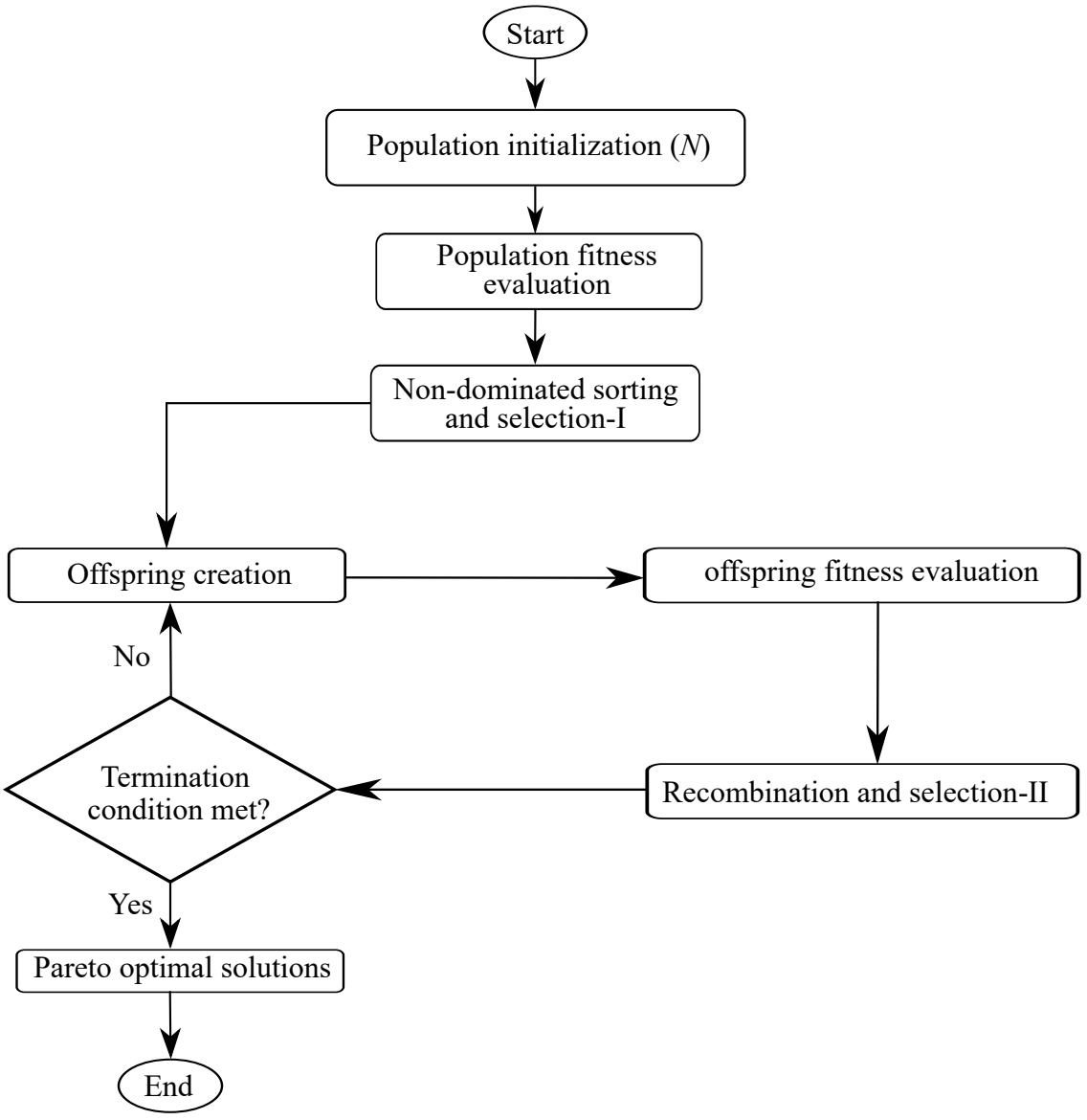

Fig. 2.10: Illustration of a NSGA II optimization process.

the non-dominated process, some solutions are selected from the population to become parents. Parents are selected by the binary tournament based on crowding-distance and assigned Pareto front ranks. The parent population is used to generate offspring by crossover and mutation.

Step 4) Offspring creation: As the iteration process continues, offspring solutions are created in mating pool to improve the search for optimal solutions. Genetic operators of crossover and mutation are used in the mating pool to improve solutions by generating offspring. It is a necessity to ensure the correct sequence of the integers in the created offspring, this is achieved

using the genetic operators that maintain the order of the integers. The crossover process is a recombination process in which two offspring are produced from a pair of parents that exchange their genes, resulting in two offspring. The crossover pushes the algorithm towards convergence by making the solutions look alike. In addition, the mutation is used to introduce slight changes to some of the genes of the solutions to maintain diversity.

Step 5) Recombination and Selection II: The generated offspring population is combined with the parent population to form the population size of $2N$. Recombination of parent and offspring populations ensures elitism [96]. Non-dominating sorting is performed to determine different Pareto fronts classified into ranks. In addition, the crowding-distance approach maintains diversity among non-dominated solutions. Using the binary tournament, crowding-distance approach, and assigned ranks of Pareto fronts, solutions are selected to create a new population of N [93]. The selected solutions are used to create a parent population for the next generation or the final Pareto-optimal solutions when the termination condition is met.

Step 6) Termination condition: A termination condition is set to terminate the optimization of an algorithm after several runs. To select the termination condition, evaluation criteria of fitness values are used. It is selected based on trial runs in which the optimal fitness values do not change, and a maximum number of iterations can be predefined.

Chapter 3

Time and Energy Optimal Trajectory Generation for Coverage Motion using a Jerk-limited Acceleration Profile

This chapter proposes a path and trajectory optimization method for time and energy optimal coverage motion of industrial machines. JLAP is used to describe motion along the path with variable velocities depending on the length of the linear segment with full utilization of the machine performance. An energy model of a feed drive system is used to calculate the energy consumption to move along the path consisting of several linear segments. Multi-objective optimization is implemented to find trade-offs between conflicting objectives of time and energy consumption using NSGA II. The Pareto front is generated to represent the trade-off between time and energy for a geometric path. The best trade-off solution is chosen as the optimal point nearest to the origin of the normalized objective function space. Experimental verification is carried out with a two-axis industrial machine, which demonstrates the effectiveness of the approach. The proposed approach achieves the best trade-off solution with the time reduction and energy-savings of approximately 10.05% and 2.10%, respectively. In addition, a proposed path solution is compared to the case that constant velocity commands are used in path optimization. The maximum error reduction is 76.6% compared to the constantly commanded velocity approach.

In this chapter, simultaneous trajectory generation and path optimization are considered for the machine coverage motion because, in most cases, the two methods are implemented separately: trajectory generation [13–23] and path optimization [24–29]. Consideration of machine kinematic limits and geometric path simultaneously improves the accuracy, performance, and energy consumption of the industrial machine. Moreover, the proposed method has advantages for each linear segment to attain the desired velocity to ensure motion smoothness compared to the widely used approach of constant velocity command in path optimization [24, 25]. Optimization of time and energy to generate the best trade-off solution addresses the gap in the literature for considering both objectives simultaneously. Most similar studies that implement trajectory generation consider a single objective [13–20, 22, 23]. Because time and energy are two conflicting objectives, multi-objective optimization of time and energy is critical.

This chapter is organized as follows: Section 3.1 presents the related works. A description of trajectory representation is described in Section 3.2. Objective functions are given in Section 3.3, followed by the optimization algorithm in Section 3.4. Section 3.5 presents the optimization results. Section 3.6 discusses the experimental process and results, followed by concluding remarks in Section 3.7

3.1 Related works

Industrial machines need efficiency improvements since they are frequently used for a long time with repetitive tasks. Machine efficiency improvement can be achieved through trajectory generation while observing machine kinematic limits. A feedrate optimization approach is proposed by Endo *et al.* for accurate prediction of cycle time for CNC machine path [13]. Feedrate optimization with higher-order constraints is presented using a heuristic trajectory generation algorithm for curved and linear toolpath to attain time-optimality satisfying machine tool drive constraints [14]. Sun *et al.* propose feedrate optimization for the five-axis machine; the optimal feedrates are obtained from the velocity, acceleration, and jerk limit to ensure the required machining accuracy while satisfying the machine kinematic limits [15]. Uchiyama *et al.* propose trajectory generation for a PTP motion for energy reduction and smooth motion generation [20]. In [18], an optimal and improved control motion is proposed, attained through accurate

dynamic modeling and generating the trajectories with continuity. A minimum-time trajectory generation using jerk-limited feedrates of a given PTP motion CNC toolpath is proposed [16]. Cycle time and motion accuracy trajectory generation is proposed for the two-axis feed drive system [21]. In [17], time-optimal trajectory generation is presented with consideration to kinematic and dynamic constraints for robotic manipulator along fully specified paths. Shen *et al.* [19] propose a time-optimal motion for ensuring the continuity of the acceleration trajectory for the robotic system path-constrained. A minimum-energy trajectory generation on robotic systems is proposed for PTP motion using trapezoidal and cycloidal speed profiles [22]. Zhou *et al.* [23] propose minimum-energy trajectory planning for robotic system of sculptured surface machining. These studies show the necessity of trajectory generation/optimization in the coverage motion to improve machine efficiency in energy savings, cycle time, and motion smoothness. Generally, the time and energy consumed by industrial machines are affected not only by trajectory but also by the path. To further reduce time and energy consumption, optimal path selection is crucial [44, 58]. However, in these studies mentioned above, trajectory generation is implemented along the predefined contour paths.

In addition, the geometric path has an impact on machine efficiency; path optimization is another approach used in improving machine efficiency. Zhou *et al.* [25] propose a toolpath optimization method. An improved GA is used to generate and optimize the toolpath for cavity milling with simultaneous optimization of cutting parameters and the toolpath aiming to attain the best trade-off path between processing time, cost, and energy. In [24], a toolpath optimization method for the free-form surface milling is proposed. An image process method on path optimization is proposed in [26] to improve the efficiency in pocket milling using a contour milling strategy. Hatem *et al.* [27] propose an algorithm for geometric path optimization for CNC milling to achieve the shortest path. Path optimization is proposed through a discretization framework [28], GA is used in toolpath optimization to minimize machining time and jerk for the machine efficiency improvement. In [29], toolpath optimization to minimize machining time on several linear segments in the area to be machined is proposed, in which GA and PSO are used for optimization. Edem and Mativenga propose a feed-axes energy model to estimate time and power consumption for the CNC toolpath [98]. The model is used to analyze the impacts of toolpath selection and geometry. However, these studies present path optimization methods; trajectory generation, including velocity, acceleration, and jerk, is not considered. As a result, the optimized geometric path motion can generate high operating speeds, excessive

accelerations, and vibrations of the machine's mechanical structure, which affect accuracy and performance. In addition, the same constant velocity command approach is used in [24, 25] for geometric path optimization. For several linear segments of coverage motion, the commanded constant velocity may not be achieved by shorter segments leading to higher machine excitation. Therefore, it is of great importance to consider trajectory generation in path optimization to improve motion accuracy and efficiency.

3.2 Trajectory representation

3.2.1 Path geometry

The path geometry is a series of location points for the coverage motion. For example in pocket milling, tool motion from one location point to another creates a linear segment. As shown in Fig. 3.1, motion from $\boldsymbol{a}$ to $\boldsymbol{b}$ passes through several location points to create a linear segment with motion distance L. The path consists of several linear segments. Motion $\boldsymbol{a}$ to $\boldsymbol{b}$ is the first segment and $\boldsymbol{b}$ to $\boldsymbol{c}$ is the second segment up to the end of the path. The connection of linear segments defines the generated geometric path.

For a given working surface whereby no information of the geometric path is given, the geometric path needs to be determined. To complete the coverage motion on the working surface from the start to the end of the motion, there are several different feasible paths. It is important to find the optimal geometric path based on objectives set for the coverage motion while satisfying the surface working constraints including obstacle avoidance (island) in this chapter. However, trajectory and machine kinematic limits such as velocity, acceleration, and jerk are not considered during geometric path optimization.

In linear motion interpolation, variables such as position, velocity, and acceleration are commanded to direct the motion from one location point to another while satisfying machine kinematic limits. Interpolation of these variables generates a trajectory or motion profile for each linear segment depending on the direction of axes. Trajectory generation for the linear segments needs to be performed for the machine to follow. The machine kinematic limits velocity, acceleration, and jerk should be observed to achieve the smooth coverage motion. Therefore,

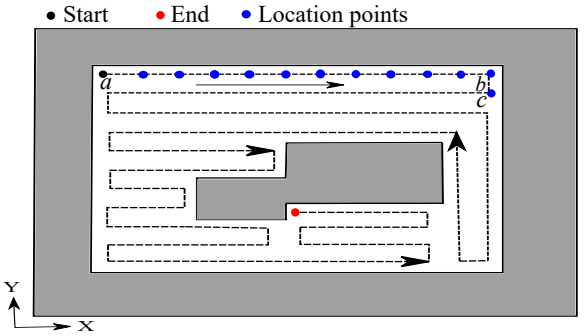

Fig. 3.1: Illustration of a path geometry.

to increase the efficiency of the industrial machine, the objective functions of time and energy consumption for the coverage motion with simultaneous geometric path optimization and trajectory generation are considered.

3.2.2 Trajectory representation of a linear segment

It is crucial to ensure smooth kinematic profiles during trajectory generation to maintain accuracy and avoid exciting the machine [99, 100]. JLAP is used to generate smooth trajectories for accurate linear contours in path optimization. It is the trajectory with continuous acceleration profiles generated from seven segments motion time intervals. The definition of the jerk in each time interval is

$$\dddot{\boldsymbol{x}}_k(t) = \begin{cases} j_{\mathrm{lim},k}, & t_0 \leq t < t_1, \\ 0, & t_1 \leq t < t_2, \\ -j_{\mathrm{lim},k}, & t_2 \leq t < t_3, \\ 0, & t_3 \leq t < t_4, \\ -j_{\mathrm{lim},k}, & t_4 \leq t < t_5, \\ 0, & t_5 \leq t < t_6, \\ j_{\mathrm{lim},k}, & t_6 \leq t < t_7. \end{cases} \tag{3.1}$$

The time intervals are determined by velocity, acceleration, and jerk limit, with the assumption that acceleration and deceleration are the same as the behaviour of industrial machines. The

definition of the time intervals are

$$\begin{aligned} t_{\mathrm{a},1} &= t_1 - t_0 = t_3 - t_2 = t_5 - t_4 = t_7 - t_6, \\ t_{\mathrm{c},1} &= t_2 - t_1 = t_6 - t_5, \\ T_{\mathrm{c},1} &= t_4 - t_3, \end{aligned} \tag{3.2}$$

where j_{lim} is the jerk limit for the k^{th} axis, $t_{\mathrm{a},1}$ is the linear acceleration/deceleration period, $t_{\mathrm{c},1}$ is the constant acceleration/deceleration period, and $T_{\mathrm{c},1}$ is the constant velocity period.

For a linear segment distance L of the geometric path, all machine kinematic limits should be satisfied to determine feasible and optimal coverage motions. The kinematic limits jerk, acceleration, and velocity must be j_{lim}, a_{lim}, $v_{\mathrm{lim}} > 0$, and satisfy the following requirements:

$$\begin{aligned} |\dddot{\boldsymbol{x}}_k(t)| &\leq j_{\mathrm{lim},k}, \\ |\ddot{\boldsymbol{x}}_k(t)| &\leq a_{\mathrm{lim},k}, \\ |\dot{\boldsymbol{x}}_k(t)| &\leq v_{\mathrm{lim},k}, \end{aligned} \tag{3.3}$$

where $\boldsymbol{x}_k(t)$ is the displacement of axis k. $j_{\mathrm{lim},k}$, $a_{\mathrm{lim},k}$, and $v_{\mathrm{lim},k}$ are the jerk, acceleration, and velocity limits, respectively. In this chapter, PTP linear contours are used with zero velocity, acceleration, and jerk at the start and final position of the linear segment.

3.3 Objective functions

3.3.1 Motion time

Motion time is the total time needed in moving the machine table to complete the motion along the path. During motion, the time for each linear segment, as suggested in [20], is calculated using (3.4). The total motion time is a summation of all segment times of the path. The time for each linear segment is calculated as

$$T_i = T_{\mathrm{c},i} + 2t_{\mathrm{c},i} + 4t_{\mathrm{a},i}, \tag{3.4}$$

where T_i is the required time for motion distance of the i^{th} segment, $T_{\text{c},i}$ is the constant velocity period of the i^{th} segment, $t_{\text{c},i}$ is the constant acceleration/deceleration period of the i^{th} segment, and $t_{\text{a},i}$ is the linear acceleration/deceleration period of the i^{th} segment.

3.3.2 Energy consumption

For linear segment trajectory, position, velocity, and acceleration determine the energy consumption for industrial feed drive systems [20]. The important property is that power is a function of velocity and acceleration. Therefore, the power can be estimated from trajectory profiles. The energy consumption model used in this chapter as described in section 2.2 incorporates dynamics of feed drive systems. The representation of power formulation is given as

$$\begin{aligned} P_k = C_{1,k}\ddot{\boldsymbol{x}}_k^2 + C_{2,k}\dot{\boldsymbol{x}}_k^2 + C_{3,k}\dot{\boldsymbol{x}}_k \text{sgn}(\dot{\boldsymbol{x}}_k) + C_{4,k} \\ + C_{5,k}\ddot{\boldsymbol{x}}_k \text{sgn}(\dot{\boldsymbol{x}}_k) + C_{6,k}\ddot{\boldsymbol{x}}_k\dot{\boldsymbol{x}}_k, \quad \text{for} \quad k = \{x, y\}. \end{aligned}$$

Energy consumption is calculated for each linear segment along the path during machine coverage motion. The summation of energy for all segments gives the total energy of the coverage motion. Energy consumption for the linear segment is given by

$$E = \int_{t_0}^{t_{\text{tf}}} (|P_x(t)| + |P_y(t)|)dt, \tag{3.5}$$

where E is the total energy consumption for the feed drive system, t_0 and t_{tf} are the start and end motion time of the segment, respectively. $P_x(t)$ and $P_y(t)$ are the power at time t for the x and y axis, respectively. Different machine coefficients and parameters used in this chapter are presented in Tables 2.1 and 2.2 of section 2.2, respectively.

3.3.3 Multi-objective model

The multi-objective model is used to obtain the trade-off between time and consumed energy in minimizing both objectives. The representation of the model is expressed as

$$F(\boldsymbol{z}) = \min_{\boldsymbol{z}}\{T(\boldsymbol{z}), E(\boldsymbol{z})\}, \tag{3.6}$$

where T and E are the time and energy consumption for the entire coverage motion, respectively, and $\boldsymbol{z}$ is an optimization parameter vector that consists of variables describing the coverage motion. The optimization parameters are the time intervals and distance for the linear segment described as

$$\boldsymbol{z} = [t_{\mathrm{a},1}, t_{\mathrm{c},1}, T_{\mathrm{c},1}, L]. \tag{3.7}$$

3.4 Optimization of the model using NSGA II

NSGA II starts with initial solutions and then gets modified through the iteration process using different operators. Fig. 3.2 shows an optimization flow process. Each operation step is described as follows.

3.4.1 Location points generation

For the machine table to move from one point to another on the working surface, the series connection of the points defines the path. A series of location points is necessary for path generation to achieve the desired geometric path. After specifying the working surface, point locations are generated on it with equal distance from one point to another, which is 7.5 mm in this chapter. Grid points represent location points and are stored using x and y coordinates. Numbering is assigned for each grid location point.

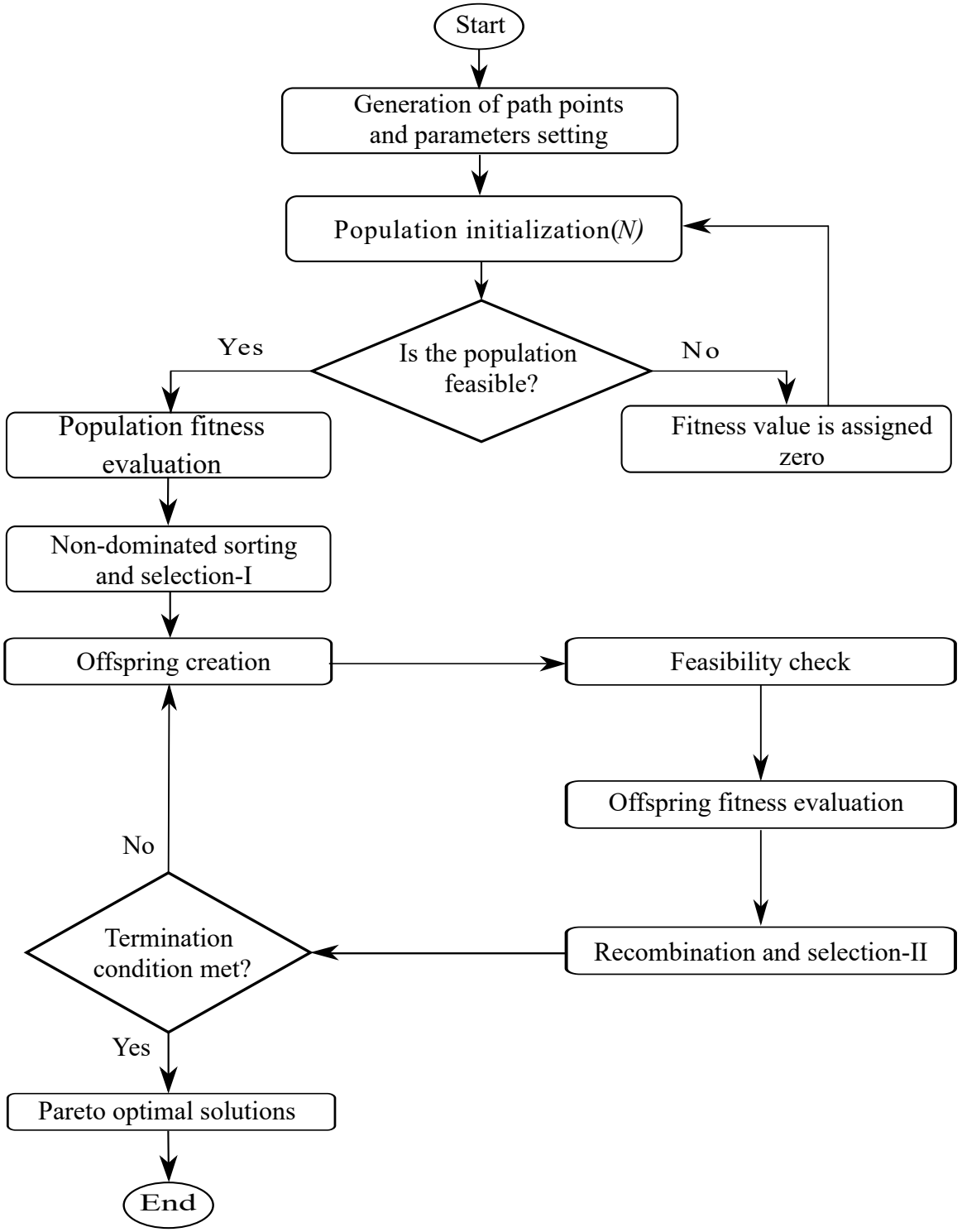

Fig. 3.2: Illustration of a flow chart for NSGA II with feasibility check.

3.4.2 Encoding

Numbers are used to generate different solutions representing different coverage paths. With no repetition, each number/integer represents a location point, in a sequence such as $1 \rightarrow 4 \rightarrow 6 \rightarrow 2 \rightarrow 7 \rightarrow 3 \rightarrow 5$, where the motion starts at 1 followed by 4 up to 5. In NSGA II, each number is a gene with point information; all genes for the path create chromosomes called population. The total number of genes in the path equals the number of series location points representing the geometric path.

3.4.3 Population initialization

The initial population is a set of chromosomes representing different options for the coverage motion. Initialization is a critical step to obtain the best results. If the total population is randomly initialized, an optimal solution is obtained after a long time [86]. Two methods are used for population initialization: random and heuristic. In this chapter, 80% of the population is randomly generated to maintain diversity and optimality in solutions, and the remaining population is heuristically initialized.

3.4.4 Feasibility check

For each generated solution, it is necessary to ensure feasibility that satisfies the constraints of the coverage path. In addition, each integer should be visited only once on its path and the sequence or order of integers should be followed since skipping an integer causes omissions and leads to an infeasible path. The time interval segments should be $0 \leq t_{\mathrm{a}}$, $0 \leq t_{\mathrm{c}}$, and $0 \leq T_{\mathrm{c}}$ and all kinematic limits in (3.3) are satisfied.

3.4.5 Fitness functions

Fitness functions are used to obtain solution values at each algorithm run. The fitness functions are expressed as

$$T = \sum_{i=1}^{n} \left(T_{\mathrm{c},i} + 2t_{\mathrm{c},i} + 4t_{\mathrm{a},i} \right), \tag{3.8}$$

$$E = \int_{t_0}^{t_{\mathrm{tf}}} |P_k(t)| dt, \tag{3.9}$$

where T is the total time, E is the total energy, $T_{\mathrm{c},i}$ is the constant velocity period of the i^{th} segment, $t_{\mathrm{c},i}$ is the constant acceleration/deceleration period of the i^{th} segment, and $t_{\mathrm{a},i}$ is the linear acceleration/deceleration period of the i^{th} segment. $P_k(t)$ is the power at time t for the k^{th} axis, t_0 is the start motion time, and t_{tf} is the end motion time.

3.4.6 Selection

Parents are individuals, as analogous to reproduction, used to create offspring in the recombination process. Individuals in the population of size N are selected to be parents. In this chapter, binary tournament selection is used, as proposed in [93], based on crowding distance comparison.

3.4.7 Crossover operation

The crossover is a recombination process that creates offspring from a pair of parents that exchange their genes, creating two offspring. The crossover probability pc is set to the algorithm as a crossover occurrence in the population. Table 3.1 illustrates the order crossover operation, where a pair of parents is selected, and two random cuts divide parents into three separate groups of genes. For creating the first offspring, the genes between the two cuts in the second parent are copied to fill the position in the offspring while maintaining their position, and

Table 3.1: Crossover process.

Chromosome	Genes
parent (1)	$1 \to 4 \to \underbrace{6 \to 2 \to 7} \to 3 \to 5$
parent (2)	$2 \to 5 \to \underbrace{1 \to 4 \to 7} \to 6 \to 3$
offspring (1)	$6 \to 2 \to \underbrace{1 \to 4 \to 7} \to 3 \to 5$
offspring (2)	$5 \to 1 \to \underbrace{6 \to 2 \to 7} \to 4 \to 3$

Table 3.2: Mutation process.

Chromosome	Genes
parent	$1 \to 4 \to \underbrace{6 \to 2 \to 7 \to 3} \to 5$
offspring	$1 \to 4 \to \overbrace{3 \to 7 \to 2 \to 6} \to 5$

the remaining genes are filled by first parent genes not occupied in the offspring. The second offspring is created copying genes in between the two cuts of the first parent by maintaining their position as in the parent. The remaining part is filled by the genes found in the second parent but not found in the second offspring.

3.4.8 Mutation operation

Mutation operation improves newly formed offspring during the iteration process after the crossover operation by making small changes to the selected genes. In this chapter, inversion mutation is used in combination with a local search to improve the solutions. Table 3.2 shows the mutation process. In inversion mutation, uniformly random two cut points are generated, and the genes between the two cuts are inverted to form new offspring. The local search finds the best new mutated offspring during the inversion process compared to an initial individual; there is no improvement if the initial individual is better than the mutated offspring.

3.4.9 Merging and sorting

After the crossover and mutation process, the newly formed population offspring of size N combine with the initial population parents to form a new population of size $2N$. The formed population is sorted based on their dominance to generate Pareto fronts, starting with the first Pareto front to obtain population size N. The sorted population size N becomes the new population for the subsequent recombination of operation or the final Pareto solutions, as illustrated in Fig. 3.2.

3.4.10 Termination condition

The algorithm runs several iterations to improve solutions, and the maximum number of iterations is predefined. The number is selected based on trial runs by checking if the solutions have no further improvement of the fitness values.

3.4.11 Computation complexity

Computation complexity is the approach that aims to classify and compare the algorithm performance when executing computational problems by evaluating the amount of resources such as time and memory required to run it [101]. Computational complexity depends on the size of the inputs of the computational problems. The notation symbols are used as a language to express the complexity of an algorithm. In running the optimization problem by NSGA II, the resource space complexity is described as $O({n_p}^2)$, where n_p is the population size [102]. Computation time is given by $O(n_{it} n_o {n_p}^2)$, where n_{it}, n_o, and n_p are number of iterations, objectives, and population size, respectively [101, 102]. Thus, the optimization problem in this chapter has a space and time complexity of $O({n_p}^2)$ and $O(n_{it} n_o {n_p}^2)$, respectively.

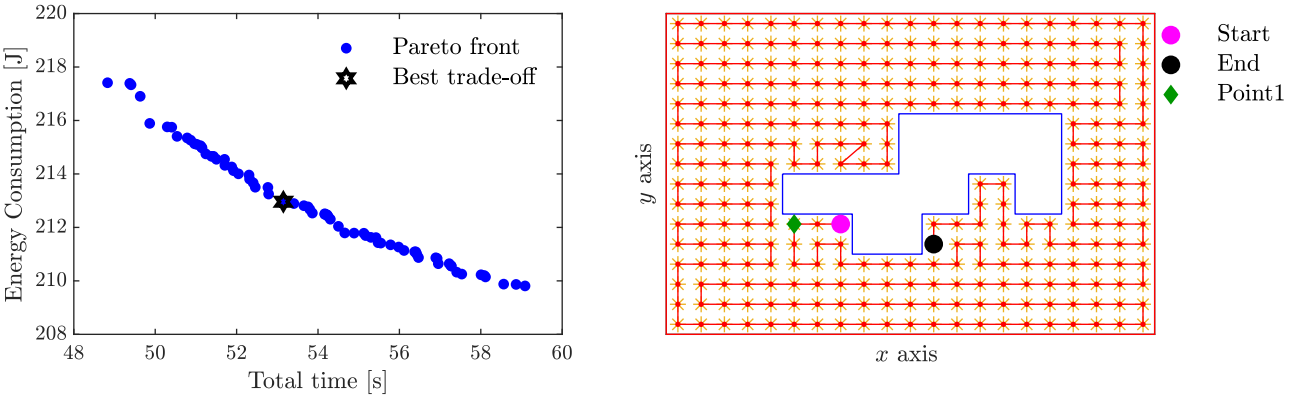

(a) Pareto front

(b) Best trade-off path

Fig. 3.3: Pareto front representing the optimization results and the geometric path at the best trade-off.

3.5 Case study

3.5.1 Optimization condition

The 2D pocket geometry part in Fig. 3.3 (b) is used for path optimization. The working surface dimensions are 158.5 mm x 120 mm with a polygon as the island is used. The axial velocity, acceleration, and jerk machine limits are 0.08 m/s, 1 m/s^2, and 20 m/s^3, respectively. The optimization problems of (3.8) and (3.9) are used as fitness functions in NSGA II to determine optimal motion time and energy consumption along the geometric paths. NSGA II parameters are crossover probability $pc = 0.8$, mutation probability $pm = 0.2$, population size is 200, and maximum iterations number is 100. The parameters are selected based on trial runs of different parameters set of pc, pm, population size, and a maximum number of iterations by checking if the solutions have no further improvement of the fitness values. The optimization is performed in MATLAB® 2021a environment on a laptop computer core i7-1165G7, 2.80 GHz CPU, 16GB RAM, and Windows 10 operating system to generate optimized solutions.

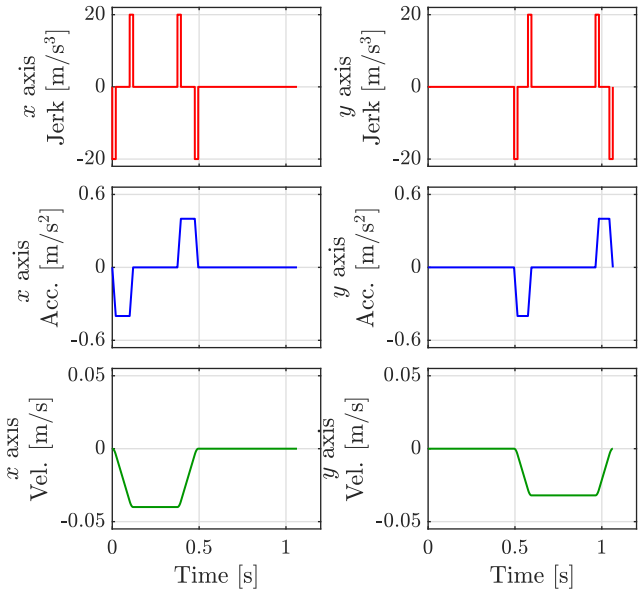

Fig. 3.4: The best trade-off path's generated jerk, acceleration, and velocity for a linear segments in x and y axes.

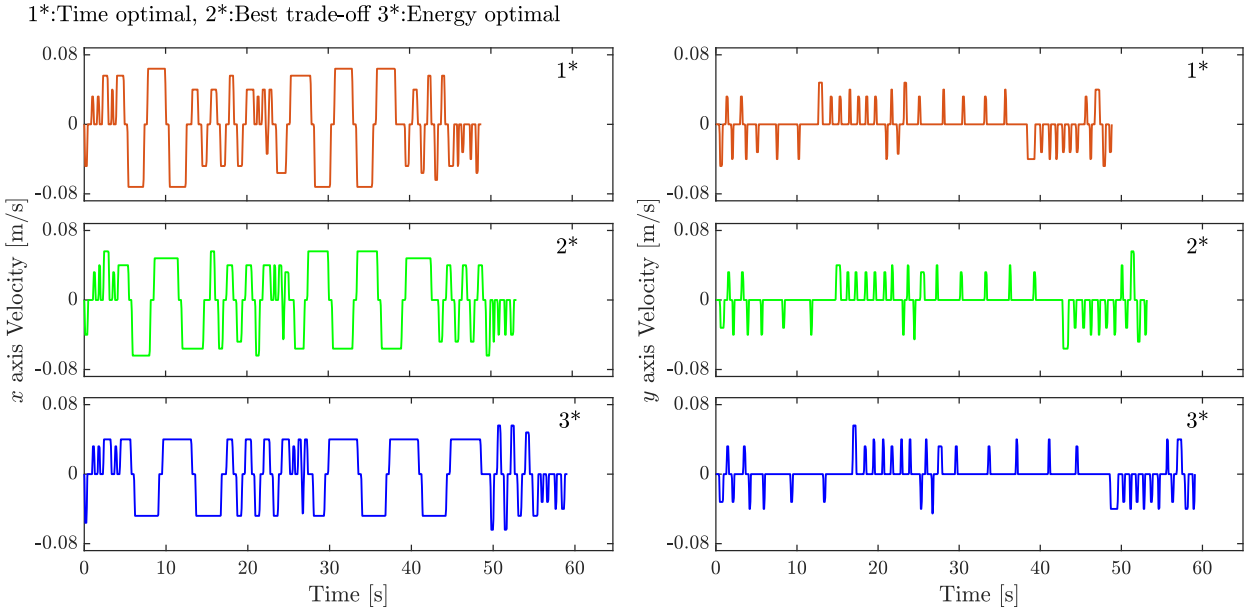

Fig. 3.5: Generated velocity profiles for the time, best trade-off, and energy optimality paths in x and y axes.

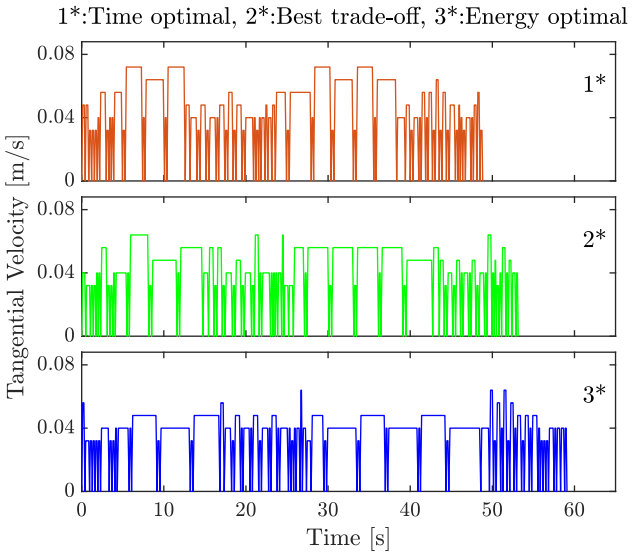

Fig. 3.6: Generated tangential velocities for the time, best trade-off, and energy optimality paths.

3.5.2 Optimization results

The Pareto front is generated after running the algorithm for 100 iterations. Fig. 3.3 (a) shows the Pareto front for the trade-off between total time and energy consumption, and Fig. 3.3 (b) shows the best trade-off geometric path. At the best trade-off point in Fig. 3.3 (a), the energy consumed is 212.96 J and the total time path motion is 53.15 s. At the energy-optimal point, the path motion energy consumption is 209.81 J and the total time is 59.09 s. The energy consumed is 3.15 J, less than the best trade-off path energy consumption. At the time-optimal point, the energy consumption is 217.52 J, which is 4.56 J higher than the best trade-off point, and the total time is 48.83 s. Hence, the best trade-off solution provides time reduction and energy-saving of 10.05% and 2.10%, respectively, compared to the time and energy-optimal solutions. As shown in Fig. 3.3, the Pareto optimal results indicate that the proposed approach is effective in finding the trade-off between two objectives. The computation time for generating the Pareto optimal results (Fig. 3.3) is 754.98 s.

Path motion profiles for jerk, acceleration, and velocity in optimal case of the best trade-off are presented in Fig. 3.4 for the x and y axes, a linear segment motion as shown in Fig. 3.3 (b) from ***Start*** to ***Point1*** is used to generate the motion profiles. Velocity profiles for the time, best trade-off, and energy optimal solutions for both axes are shown in Fig. 3.5. The kinematic

limits of all path motions are obeyed. Further, the proposed approach generates the path motion profiles with variable velocities for each linear segment. Tangential velocity is presented in Fig. 3.6. Trajectories are generated for each linear segment consisting of acceleration, constant velocity, and deceleration periods, which is a profile used in industrial machines to generate a smooth motion [20]. Furthermore, the optimized geometric path has longer segments that minimize the tool's frequent lifting and reduce air time; this contributes to significant time reduction and energy saving.

3.5.3 Motion optimization of the other two working surfaces

Similar optimization procedures presented in section 3.4 are used to generate simultaneous path and trajectory optimal results on two other working surfaces. The working surface of 2D pocket geometry with two islands inside Fig. 3.7 (b) is optimized, the size of the working surface is 110 mm x 140 mm with point locations of equal distances of 10 mm from one point to another. After optimization is run to the maximum number of iterations (100), the trade-off solutions between time and energy consumption are determined. Fig. 3.7 (a) shows the Pareto front for the trade-off solutions between time and energy consumption, and Fig. 3.7 (b) presents the geometric path for the best trade-off solution. The best trade-off solution achieves a time of 26.34 s and energy of 133.29 J, where the energy consumption is 3.24 J less than the overall time-optimal result, and it is 2.98 s faster than the overall energy-optimal solution. Therefore, the best trade-off solution achieves time and energy saving potential of about 10.21% and 2.37%, respectively, compared to the overall extrema among the three optimal cases.

In addition, optimization of the working surface with an island Fig. 3.8 (b) is considered. The size of working surface area is 100 mm x 100 mm, the point locations are generated with equal distance of 10 mm from one point to another. The Pareto front optimal solutions for the trade-off time and energy consumption are generated and shown in Fig. 3.8 (a), with the best trade-off solution achieving time and energy values of 18.29 s and 73.62 J, respectively. The time-optimal path total time is 16.42 s and the energy consumption is 75.62 J, and for the energy-optimal path motion, the total time is 20.57 s with the energy consumption of 72.31 J. Using three optimal cases from simulation, the best trade-off solution achieves time reduction and energy saving of 11.08% and 2.66%, respectively. Fig. 3.8 (b) shows the best trade-off geometric solution.

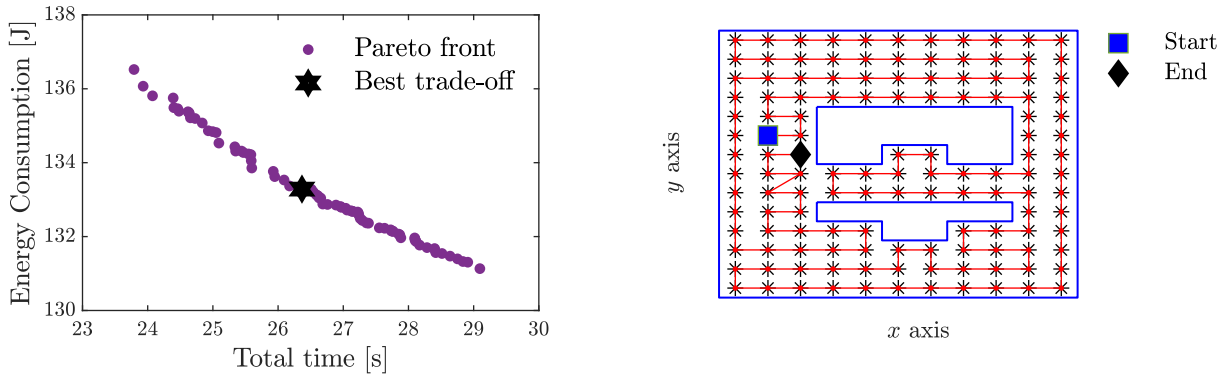

(a) Pareto front

(b) Best trade-off path

Fig. 3.7: Pareto optimal solutions and the geometric path at the best trade-off for working surface two.

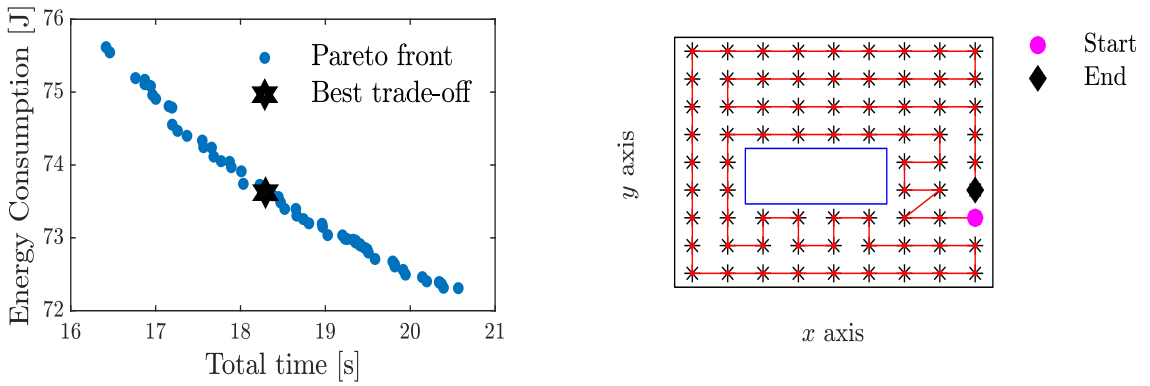

(a) Pareto front

(b) Best trade-off path

Fig. 3.8: Pareto optimal solutions and the geometric path at the best trade-off for working surface three.

3.6 Experiment

3.6.1 Experimental procedure

An industrial two-axis machine, as shown in Fig. 3.9, is used in the experimental verification of the proposed approach. The machine table has two AC servomotors with two ball screw drive systems connected to each axis. The rotary encoders of 76.29 nm resolution are used to measure the axial position of each axis of the table. A sampling time of 0.2 ms is used.

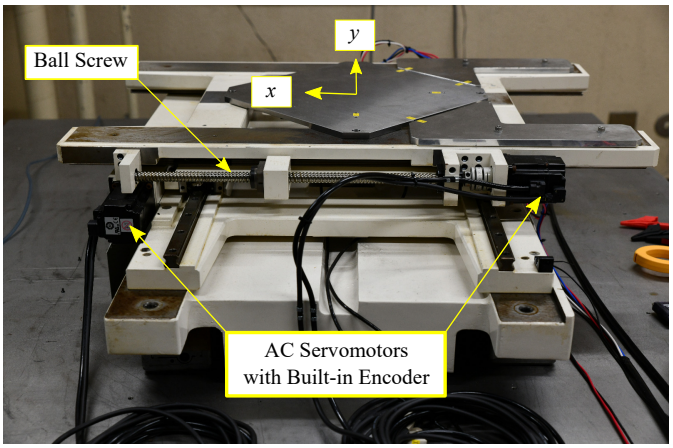

Fig. 3.9: Industrial two-axis feed drive system.

Table 3.3: Selected optimized paths on Pareto front.

No.	Total time [s]	Energy consumption [J]
1	48.83	217.52
2	51.24	214.75
3	53.15	212.96
4	55.30	211.63
5	59.09	209.81

The experiment is conducted on optimized paths from Pareto optimal solutions to verify the simulation results. Five points are selected on the Pareto front for experimental verification: best trade-off, energy-optimal, time-optimal solutions, and two other solutions, as shown in Table 3.3. Reference trajectories of the paths are prepared to move the machine, and the experiment of each path is repeated five times to ensure the repeatability of the results. The electrical power consumption for each axis is recorded by a power analyzer (HIOKI3390). The power analyzer is installed between a motor driver and a motor, directly measuring its power consumption. The analyzer measures energy using an integration measurement approach, in which the power is integrated every 50 ms of data update. When the reference trajectory path moves the machine, the measurement value of energy consumption for the two axes is displayed on the display channel. The total energy of the two axes is recorded. The experiment is repeated five times for each trajectory path, and the average energy consumption is calculated.

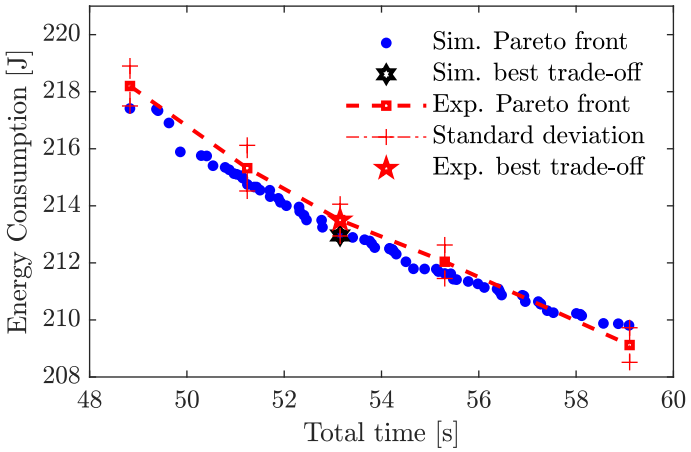

Fig. 3.10: Experimental and simulation results on energy consumption.

3.6.2 Experimental results

Fig. 3.10 presents simulation and experimental average energy consumption for five different paths results selected from the Pareto front. The experimental results obtained are similar to the simulation results. Experimental x and y axes velocity profiles for the time, best trade-off, and energy optimal cases are presented in Fig. 3.11. All the kinematic limits are obeyed and are similar to the velocity profiles for the simulation results (see Fig. 3.5).

The rotary encoder measures the tracking performance for the path motions. Fig. 3.12 shows the x and y axes mean absolute tracking error for the three paths: time, best trade-off, and energy optimal. The tracking error at the time-optimal path is higher in x axis when compared with other paths due to higher velocities attained by different linear segments in the path as shown in Fig. 3.11. The tracking error in y axes is similar in all of the paths since all short segments attain almost the same velocity.

Furthermore, the same constant velocity approach [25] is used for path and trajectory optimization to command all linear segments to achieve the commanded velocity. The selected velocity is 0.04 m/s. The generated path is compared with the optimized best trade-off path of the proposed approach. Fig. 3.13 shows the experimental velocity profiles for the best trade-off and constantly commanded velocity path for the x and y axes. The best trade-off path shows that each segment attains different desirable velocities. For the constantly commanded velocity

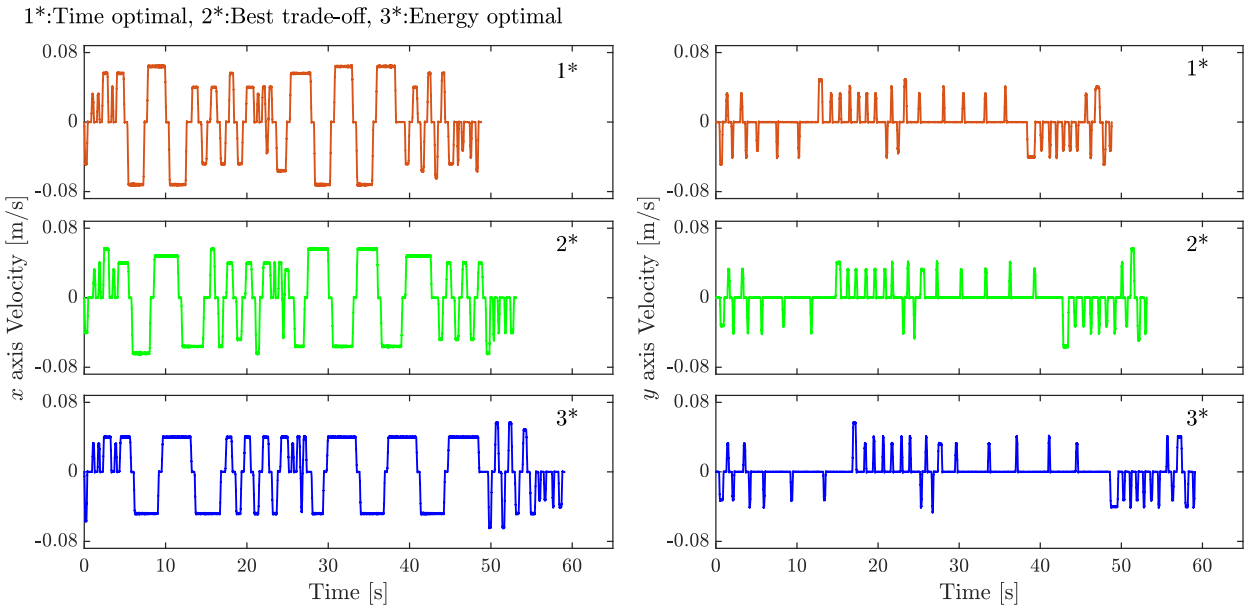

Fig. 3.11: Experimental velocity profiles for the time, best trade-off, and energy optimality paths in x and y axes.

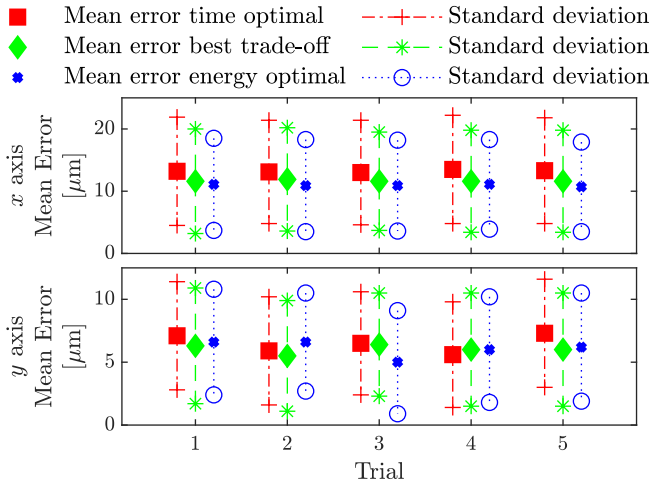

Fig. 3.12: Mean absolute tracking error for the time, best trade-off, and energy optimality paths in x and y axes.

approach, each linear segment tries to attain the desired constant velocity. However, short segments fail to attain it, leading to higher machine excitation and higher maximum errors than the proposed approach. Fig. 3.14 shows the mean absolute tracking error for the best trade-off

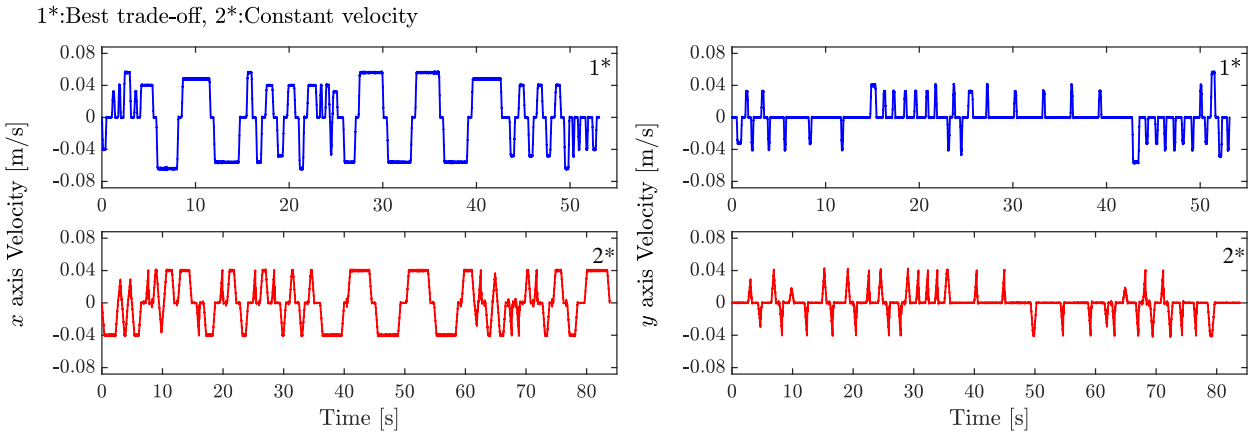

Fig. 3.13: Experimental velocity profiles for the best trade-off and constantly commanded velocity paths in x and y axes.

and constantly commanded velocity approach. There is a slightly higher mean absolute tracking error for the best trade-off path in x axis compared to the constantly commanded velocity path because there are linear segments with higher assigned velocities, which is easier to be tracked by the controller. In the y axis, the constantly commanded velocity path has a higher mean absolute tracking error because almost all the segments have higher velocities compared to the best trade-off path.

Fig. 3.15 shows the maximum error for the two paths. Constantly commanded velocity path has a higher maximum error in both axes. The constant velocity cannot be attained for shorter linear segments, causing higher machine excitation. The best trade-off path has an approximately 76.6% reduced maximum error because all linear segments attain desirable velocities. The above results show that path optimization with variable velocities generates smoother motion profiles than the constantly commanded velocity approach. In addition, the energy consumption for the constant velocity path is 221.47 J, which is 3.8% higher than the best trade-off path.

3.6.3 Discussion

The chapter aims to solve the multi-objective problem of simultaneous path optimization and trajectory generation to minimize time and energy consumption for the coverage motion. As shown in Fig. 3.10, similar Pareto fronts are obtained in both simulation and experimental

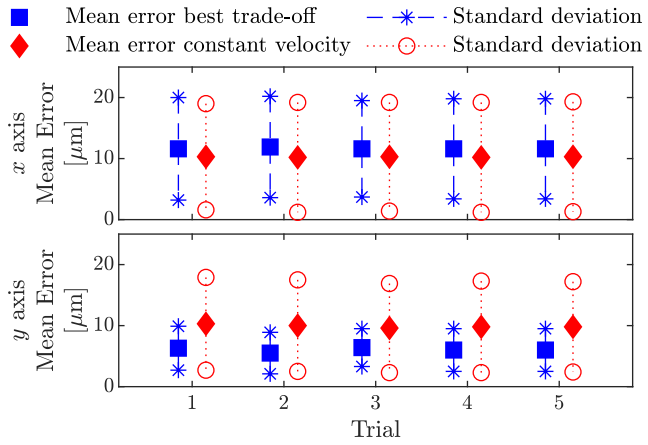

Fig. 3.14: Mean absolute tracking error for the best trade-off and constantly commanded velocity paths in x and y axes.

Fig. 3.15: Maximum error for the best trade-off and constantly commanded velocity paths in x and y axes.

results. The optimal solution for the best trade-off between time and energy consumption is determined. The findings demonstrate that the proposed method can be used to provide a trade-off between time and energy consumption for the coverage motion (see Figs. 3.3 and 3.10). Hence, during process planning, the planner can choose any solution from the Pareto front, depending on the preferences between the two objectives.

Figs. 3.3(b) and 3.5 show simulation results of the generated geometric path and the motion profiles, respectively. From the simulation results, reference trajectories of the paths are prepared to move the machine table. The experimental motion profiles are recorded and plotted; the motion profiles are similar to simulated ones (see Figs. 3.5 and 3.11). From these

results, can be concluded that the proposed method achieve simultaneous path optimization and trajectory generation while obeying kinematic constraints. Unlike the path optimization in [24–29], which mainly generates an optimal geometric path without taking into account kinematic constraints, the proposed method generates the optimal path while considering trajectory generation, including velocity, acceleration and jerk.

The proposed approach is compared with the same constant velocity approach used in path optimization [25]. The selected approach is widely used in practice for geometric path coverage motion optimization. To show the same performance, the mean absolute tracking and maximum error values are shown in Figs. 3.14 and 3.15. The proposed method shows a significant contribution in reducing the maximum error by 76.6%. As a result, it is reasonable to conclude that the proposed method can be used to improve motion performance.

In this chapter, the energy model of an industrial two-axis feed drive system (3.5) is used. Two-axis industrial machine feed drive systems are commonly utilized in the manufacturing industry, where they are found in types of machinery such as CNC milling, laser, and waterjet cutting machines. Therefore, the trajectory generation performance evaluation is performed on an industrial two-axis feed drive system. Since the trajectory evaluation is done on a typical feed drive system, the proposed method can also be applied to machining operations by simply incorporating a cutting force model. In addition, the proposed approach can be appropriate in pocket milling with islands since several linear segments have different lengths.

3.7 Conclusion

This chapter proposes simultaneous path and trajectory optimization to minimize the time and energy consumption of the 2D coverage motion. An energy consumption model for a two-axis industrial machine is used in the optimization. Simulation results are verified using a two-axis industrial machine, which shows the effectiveness of the proposed approach. The best trade-off solution achieves a time reduction and energy savings of 10.05% and 2.10%, respectively. In addition, the proposed method improves the path's accuracy by reducing tracking errors. Results show that an optimized path motion with variable velocities at each linear segment

lowers the maximum error by approximately 76.6% compared to the optimized path using the constant commanded velocity approach.

Chapter 4

The Effectiveness of the Modified S-curve Trajectory for Energy Saving in Coverage Motion

This chapter proposes a coverage motion optimization approach that simultaneously integrates trajectory generation and geometric path optimization for energy saving of industrial machines. PTP coverage motion is generated by linear interpolation of each segment described by the modified S-curve velocity profile. Smooth and accurate transitions between the phase changes in the profile are attained with smooth continuity of machine kinematic limits jerk, acceleration, and velocity, which are crucial to realize accurate motion. GA is used to generate an optimal coverage motion using the convergence approach whereby the converged solution is selected as the final solution achieving minimum energy consumption. The simulation study and experimental validation are provided to illustrate the effectiveness of the proposed technique. In addition, the proposed approach is compared with the optimized path generated using the fourth-order motion profile in terms of energy saving and motion performance. The comparison results show that the proposed approach increases motion accuracy by reducing the absolute mean and maximum tracking error. The proposed approach reduces absolute mean error by about 25.43% and 22.76% for the x and y axes, respectively, and reduces the maximum tracking error by 8.92% for the x axis and 4.14% for the y axis.

This chapter is organized as follows: Section 4.1 describes the related works. In section 4.2, the trajectory generation is presented followed by section 4.3, which presents the two-axis feed drive energy model. Section 4.4 is the description of the optimization approach through simulation to achieve energy saving in coverage motion. Experimental analyses are presented in section 4.5 followed by the discussion in section 4.6. Finally, section 4.7 presents the concluding remarks.

4.1 Related works

Energy saving and motion performance improvement in industrial machines' operation is crucial to enhance productivity and lessen global issues such as energy shortages and environmental concerns [103]. Several approaches are proposed for energy saving of industrial machines. Energy saving and motion accuracy improvement through controller designs in feed drive system are proposed [9, 10]. However, their applications cannot be applied to industrial systems with an inaccessible controllers. Moreover, to improve machine motion performance and energy saving, a number of motion planning optimizations are proposed. Trapezoidal velocity profiles are used to increase motion accuracy and energy saving as proposed in [63, 64]. Trapezoidal velocity profiles are linked to machine excitation caused by abrupt changes in acceleration and infinite jerk values at the phase transitions [104, 105]. To avoid machine excitation, methods such as notch filters and input shaping are used [106]. However, the path geometry may be altered using filters and elongates the cycle times [61, 107]. In addition, to eliminate the occurrence of infinite jerk values in the trapezoidal motion profile, the JLAP is optimized to achieve energy optimal coverage motion. Energy saving trajectory generation for PTP motion of industrial machines is proposed by Uchiyama *et al.* [20], S-curve profile is used to describe the motion. JLAP is used to achieve optimal time and energy in feed drive system for PTP motion [49]. Although the JLAP improves the motion by eliminating the occurrence of infinite jerk values, smooth jerk continuity is crucial to further improve machines' performance by smoothly interpolating at the phase transitions [108, 109]. Hence, it is essential to plan motion with smooth jerk continuity while satisfying the machine kinematic limits.

In addition to the velocity profile significance, geometric path optimization improves the machine performance. There are several studies on geometric path optimization for PTP coverage

motion [58, 110]. In these studies, trajectory (velocity) generation is not considered. In implementing a geometric path optimization, smooth trajectory generation should be considered simultaneously for the coverage motion.

4.2 Trajectory representation

4.2.1 Jerk-limited acceleration profile

The JLAP or S-curve trajectory (Fig. 4.1) is widely used in current industries. It is a trajectory with the confined jerk that provides accurate motion, maintains smooth kinematic profiles during trajectory generation, and reduces machine excitation [13, 99]. The JLAP is a widely used approach to generate smooth trajectories for accurate linear contours and eliminate the occurrences of an infinite jerk values. The trajectory consists of continuous acceleration profiles with linear and constant acceleration/deceleration forming seven motion time intervals, as shown in Fig. 4.1. The definition of the jerk for each segment is given as

$$\dddot{\boldsymbol{x}}_k(t) = \begin{cases} j_{\mathrm{lim},k}, & t_0 \le t < t_1, \\ 0, & t_1 \le t < t_2, \\ -j_{\mathrm{lim},k}, & t_2 \le t < t_3, \\ 0, & t_3 \le t < t_4, \\ -j_{\mathrm{lim},k}, & t_4 \le t < t_5, \\ 0, & t_5 \le t < t_6, \\ j_{\mathrm{lim},k}, & t_6 \le t < t_7, \end{cases} \tag{4.1}$$

where $j_{\mathrm{lim},k}$ is the jerk limit for the k^{th} axis. On the assumption that acceleration and deceleration have the same motion time interval as the typical settings of industrial machines, the time intervals are defined as

$$\begin{aligned} t_{\mathrm{a},1} &= t_1 - t_0 = t_3 - t_2 = t_5 - t_4 = t_7 - t_6, \\ t_{\mathrm{c},1} &= t_2 - t_1 = t_6 - t_5, \\ T_{\mathrm{c},1} &= t_4 - t_3, \end{aligned} \tag{4.2}$$

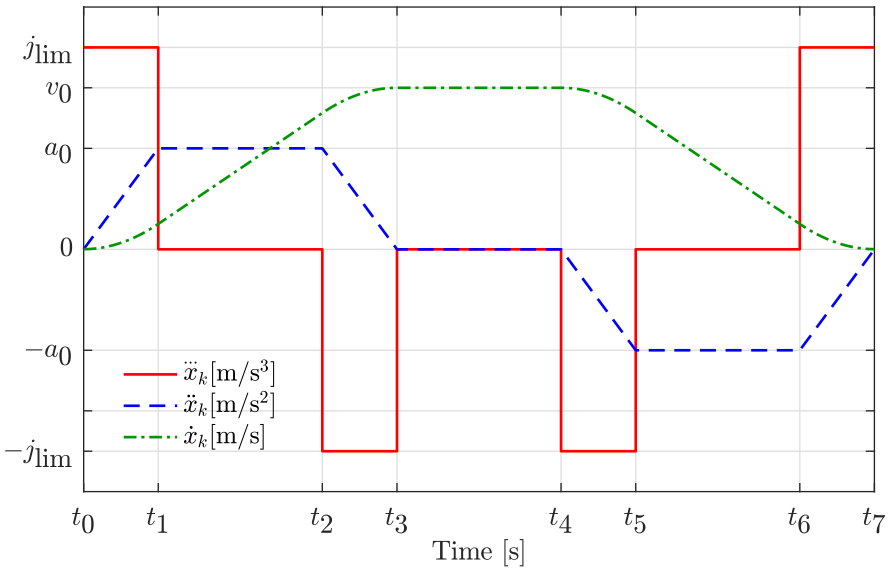

Fig. 4.1: Illustration of a jerk-limited acceleration profile.

where $t_{\mathrm{a},1}$ is the linear acceleration/deceleration period, $t_{\mathrm{c},1}$ is the constant acceleration/deceleration period, and $T_{\mathrm{c},1}$ is the constant velocity period. The time intervals are calculated by velocity, acceleration, and jerk as

$$\begin{aligned} t_{\mathrm{a},1} &= \frac{a_0}{j}, \\ t_{\mathrm{c},1} &= \frac{v_0}{a_0} - t_{\mathrm{a},1}, \\ T_{\mathrm{c},1} &= \frac{(L-S)}{v_0}, \end{aligned} \tag{4.3}$$

where a_0, v_0, j, L, and S are the constant acceleration, velocity, jerk, total motion distance, and total displacement for the acceleration and deceleration, respectively.

The total motion time is therefore summation of all time intervals along the linear segment given as

$$T_1 = T_{\mathrm{c},1} + 2t_{\mathrm{c},1} + 4t_{\mathrm{a},1}. \tag{4.4}$$

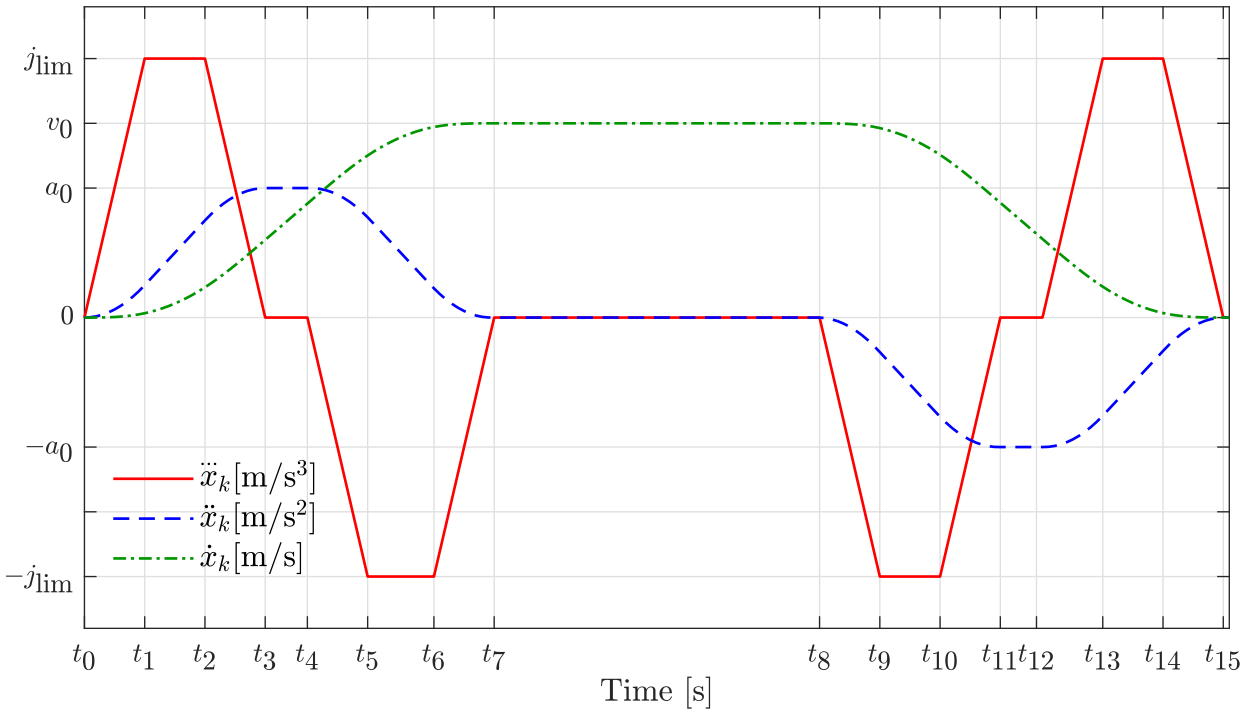

Fig. 4.2: Illustration of a fourth-order motion profile.

4.2.2 Fourth-order motion profile

Fourth-order motion profile is a trajectory profile that imposes a smooth velocity transition between points composed with the trapezoidal jerk profile for the given predefined limits of velocity, acceleration, and jerk [111–114]. The profile is generated based on the fourth-order polynomial S-curve motion profiles that ensures smooth and continuity of the velocity, acceleration, and jerk as function of time. Fig. 4.2 shows the fourth-order motion profile for the jerk, acceleration, and velocity consisting of an acceleration phase from t_0 to t_7, a constant velocity phase from t_7 to t_8, and a deceleration phase from t_8 to t_{15} with the assumption that it is symmetrical trajectory with equal acceleration and deceleration times. The jerk profile consists of linear jerk, constant jerk, and zeros for some of time intervals forming fifteen time periods.

The trajectory of jerk profile is given as

$$\dddot{\boldsymbol{x}}_k(t) = \begin{cases} j_{\text{lim},k}\frac{t}{T_l}, & t_0 \le t < t_1, \quad t_{12} \le t < t_{13}, \\ j_{\text{lim},k}, & t_1 \le t < t_2, \quad t_{13} \le t < t_{14}, \\ j_{\text{lim},k} - j_{\text{lim},k}\frac{t}{T_l}, & t_2 \le t < t_3, \quad t_{14} \le t < t_{15}, \\ 0, & t_3 \le t < t_4, \quad t_7 \le t < t_8, \\ & t_{11} \le t < t_{12}, \\ -j_{\text{lim},k}\frac{t}{T_l}, & t_4 \le t < t_5, \quad t_8 \le t < t_9, \\ -j_{\text{lim},k}, & t_5 \le t < t_6, \quad t_9 \le t < t_{10}, \\ -j_{\text{lim},k} + j_{\text{lim},k}\frac{t}{T_l}, & t_6 \le t < t_7, \quad t_{10} \le t < t_{11}, \end{cases} \tag{4.5}$$

where T_l is the linear jerk period and $j_{\text{lim},k}$ is the jerk limit for the k^{th} axis. Integrating (4.5), acceleration, velocity, and position are determined. The time intervals are determined such that the trajectory satisfies kinematic limits of jerk, acceleration, and velocity defined as follows;

$$\begin{aligned} &T_{l,1} = t_1 - t_0 = t_3 - t_2 = t_5 - t_4 = t_7 - t_6, \\ &T_{l,1} = t_9 - t_8 = t_{11} - t_{10} = t_{13} - t_{12} = t_{15} - t_{14}, \\ &t_{\text{cj},1} = t_2 - t_1 = t_6 - t_5 = t_{10} - t_9 = t_{14} - t_{13}, \\ &t_{\text{ca},1} = t_4 - t_3 = t_{12} - t_{11}, \\ &T_{\text{v},1} = t_8 - t_7, \end{aligned} \tag{4.6}$$

where $T_{l,1}$, $t_{\text{cj},1}$, $t_{\text{ca},1}$, and $T_{\text{v},1}$ are the linear jerk period, constant jerk period, constant acceleration/deceleration period, and constant velocity period, respectively. The total motion time of a linear segment is expressed as the sum of all intervals of time along the segment defined as

$$T_1 = T_{\text{v},1} + 2t_{\text{ca},1} + 4t_{\text{cj},1} + 8T_{l,1}. \tag{4.7}$$

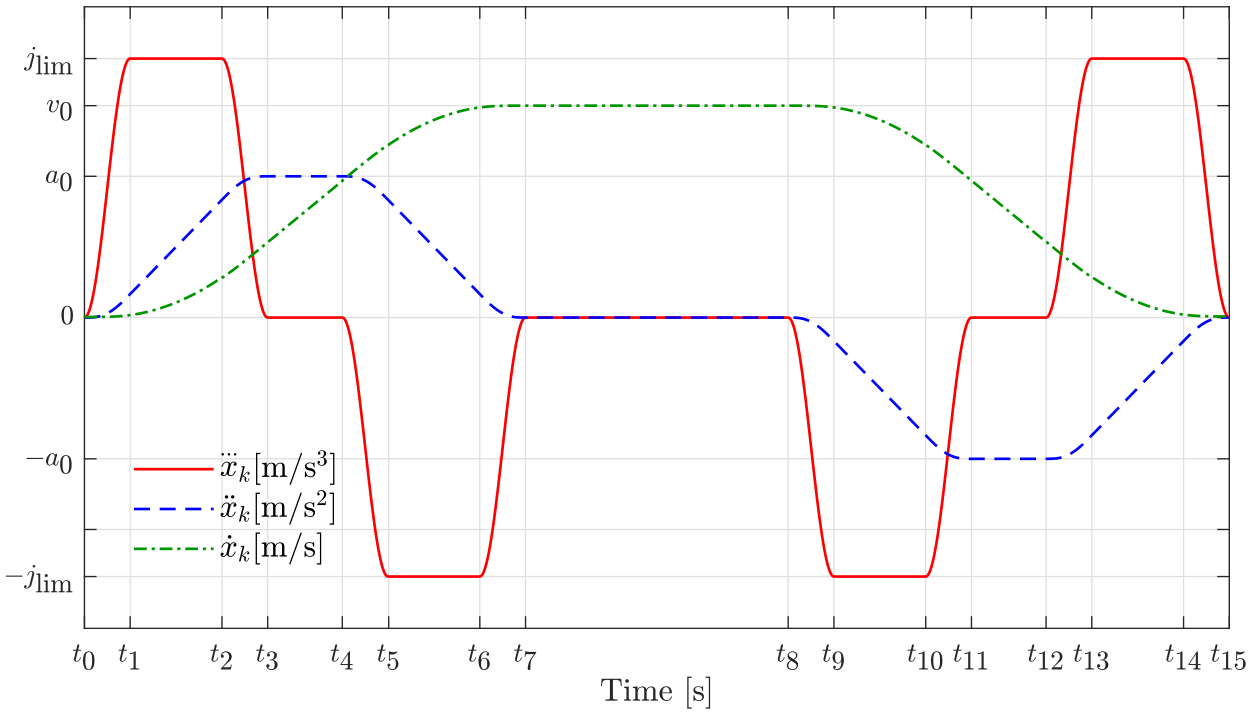

Fig. 4.3: Illustration of a modified S-curve trajectory.

4.2.3 Proposed motion profile

In some applications, smooth jerk continuity is crucial to increase the smoothness of the motion [109, 115]. To further achieve the smooth jerk continuity profile, harmonic functions are incorporated into constant jerk phases of the JLAP (Fig. 4.1) which is called the modified S-curve trajectory. Using the constant jerk phase, the scale parameter β is applied to obtain harmonic motion time segments. As a result, modification of the jerk profile leads to motion phases consisting of fifteen segments. Fig. 4.3 depicts the motion profile for the jerk, acceleration, and

velocity. The jerk trajectory profile for each segment is expressed as

$$\dddot{\boldsymbol{x}}_k(t) = \begin{cases} \frac{j_{\lim,k}}{2}A, & t_0 \le t < t_1, \quad t_{12} \le t < t_{13}, \\ j_{\lim,k}, & t_1 \le t < t_2, \quad t_{13} \le t < t_{14}, \\ \frac{j_{\lim,k}}{2}B, & t_2 \le t < t_3, \quad t_{14} \le t < t_{15}, \\ 0, & t_3 \le t < t_4, \quad t_7 \le t < t_8, \\ & t_{11} \le t < t_{12}, \\ \frac{-j_{\lim,k}}{2}A, & t_4 \le t < t_5, \quad t_8 \le t < t_9, \\ -j_{\lim,k}, & t_5 \le t < t_6, \quad t_9 \le t < t_{10}, \\ \frac{-j_{\lim,k}}{2}B, & t_6 \le t < t_7, \quad t_{10} \le t < t_{11}, \end{cases} \tag{4.8}$$

with

$$A = \left\{1 - \cos(\frac{\pi t}{t_h})\right\} \text{ and } B = \left\{1 + \cos(\frac{\pi t}{t_h})\right\}.$$

By integrating (4.8) while taking into consideration its initial conditions, the acceleration, velocity, and position are determined. Under the assumption that acceleration and deceleration have the same motion time interval, the time intervals are defined as follows:

$$\begin{aligned} &t_{\mathrm{j},1} = t_3 - t_0 = t_7 - t_4 = t_{11} - t_8 = t_{15} - t_{12}, \\ &t_{\mathrm{ca},1} = t_4 - t_3 = t_{12} - t_{11}, \\ &T_{\mathrm{v},1} = t_8 - t_7. \end{aligned} \tag{4.9}$$

The time intervals are calculated as

$$t_{\mathrm{j},1} = \frac{a_0}{j(1-\beta))}, \text{ with } 0 \le \beta \le 0.5, \tag{4.10}$$

$$t_{\mathrm{h},1} = \beta t_{\mathrm{j},1}, \tag{4.11}$$

$$t_{\mathrm{cj},1} = t_{\mathrm{j},1} - 2t_{\mathrm{h},1}, \tag{4.12}$$

$$t_{\mathrm{ca},1} = \frac{v_0}{a_0} - t_{\mathrm{j},1}, \tag{4.13}$$

$$T_{\mathrm{v},1} = \frac{(L-S)}{v_0}, \tag{4.14}$$

where $t_{\mathrm{j},1}$, $t_{\mathrm{ca},1}$, and $T_{\mathrm{v},1}$ are the jerk period, constant acceleration/deceleration period, and constant velocity period, respectively. $t_{\mathrm{h},1}$ and $t_{\mathrm{cj},1}$ are the harmonic jerk period and constant jerk period, respectively. β is the parameter for the jerk fraction period.

Summation of all time intervals along a linear segment gives the total segment motion time defined as

$$T_1 = T_{\mathrm{v},1} + 2t_{\mathrm{ca},1} + 4t_{\mathrm{cj},1} + 8t_{\mathrm{h},1}. \tag{4.15}$$

Motion distance L includes displacements during constant velocity, acceleration, and deceleration. The total acceleration and deceleration displacements are defined as follows:

$$\begin{aligned} S_{\mathrm{acc}} &= \sum_{r=1}^{7} \big(S_r\big), \\ S_{\mathrm{dec}} &= \sum_{r=9}^{15} \big(S_r\big), \\ S &= S_{\mathrm{acc}} + S_{\mathrm{dec}}, \end{aligned} \tag{4.16}$$

where S_{r} represents the displacement of r^{th} segment phase motion time interval.

Parameter β adjusts jerk continuity and the generation of a fifteen-segment velocity profile. From (4.10), for $\beta = 0$, the time is described as follows:

$$t_{\mathrm{j},1} = \frac{a_0}{j},$$

with

$$t_{\mathrm{h},1} = 0, \text{ and } t_{\mathrm{cj},1} = t_{\mathrm{j},1}.$$

The trajectory jerk profile consists of only seven-time intervals with constant jerk phases, as shown in Fig. 4.1. For $\beta = 0.5$, the resulting jerk motion time is given as

$$t_{\mathrm{j},1} = \frac{a_0}{0.5j},$$

with

$$t_{\mathrm{h},1} = 0.5t_{\mathrm{j},1}, \text{ and } t_{\mathrm{cj},1} = 0,$$

the constant jerk phases of JLAP are replaced by harmonic jerk phase motion only.

To achieve feasible trajectory generation, all kinematic limits of the machine should be satisfied. The jerk, acceleration, and velocity limits must satisfy the following limits

$$\begin{aligned} |\dddot{\boldsymbol{x}}_k(t)| &\leq j_{\mathrm{lim},k}, \\ |\ddot{\boldsymbol{x}}_k(t)| &\leq a_{\mathrm{lim},k}, \\ |\dot{\boldsymbol{x}}_k(t)| &\leq v_{\mathrm{lim},k}, \end{aligned} \tag{4.17}$$

where $\boldsymbol{x}_k(t)$ is the displacement of the k^{th} axis for the linear segment motion of distance L. The segment initial and final positions have zero jerk, acceleration, and velocity. j_{lim}, a_{lim}, $v_{\mathrm{lim}}(> 0)$, are their maximum values.

4.3 Energy model of industrial two-axis feed drive system

For industrial feed drive systems, position, velocity, and acceleration can be optimized to reduce energy consumption [20]. Hence, it is essential to incorporate these factors in determining energy consumption in path optimization. The energy consumption model used in this chapter as described in section 2.2 incorporates the dynamics of the feed drive system with the property that power is a function of velocity and acceleration. Energy is calculated for each linear segment. The summation of energy for all segments of the coverage motion results to the total energy consumption. Energy consumption for the linear segment is calculated as

$$E = \int_{t_0}^{t_{\mathrm{tf}}} (|P_x(t)| + |P_y(t)|)dt, \tag{4.18}$$

$$P_k(t) = C_{1,k}\ddot{\boldsymbol{x}}_k^2 + C_{2,k}\dot{\boldsymbol{x}}_k^2 + C_{3,k}\dot{\boldsymbol{x}}_k \text{sgn}\,(\dot{\boldsymbol{x}}_k) + C_{4,k}$$
$$+C_{5,k}\ddot{\boldsymbol{x}}_k \text{sgn}\,(\dot{\boldsymbol{x}}_k) + C_{6,k}\ddot{\boldsymbol{x}}_k\dot{\boldsymbol{x}}_k, \quad \text{for} \quad k = \{x, y\},$$

where E is the total energy consumption for the feed drive system from time t_0 to t_{tf}. $P_x(t)$ and $P_y(t)$ are the power at time t for the x and y axes, respectively. Coefficients of the energy model and machine parameters are presented in Tables 2.1 and 2.2 of section 2.2, respectively.

4.4 Optimization of coverage motion using Genetic Algorithm

4.4.1 Motion optimization

Genetic Algorithm (GA) is a population-based global search method with significant convergence using genetic operators to find an optimal solution [116]. This chapter aims to find optimal energy coverage motion consisting of trajectory and path generation. For the working surface such as the square in Fig. 4.5, there are several feasible solutions for the machine to complete the coverage motion, among which optimal one is required in terms of energy optimality. Machine motion is PTP that consists of several linear segments connected by points forming a path. For optimization, the working surface to be covered is discretized into several equidistant grid points (path locations). An optimal ordering of grid points is a representation of the solution; if all points are visited once, a complete path is generated. To provide displacement information along the linear segment, grid points are stored using the x and y coordinates. For a linear displacement from one point to another, the trajectory, with velocity, acceleration, and jerk, is generated. Based on the above preparations, GA finds optimal trajectories and path based on the feasible connection between the linear segments. For a gene representation in the algorithm execution, each grid point is assigned an integer and permutation encoding is applied to create chromosomes. The problem considered is combinatorial optimization in nature, so the MATLAB® GA toolbox cannot be suitable to find feasible optimal solution. Therefore, in this chapter, different GA iteration steps as shown in Fig. 4.4 are prepared using MATLAB®, and the description of each operation step is presented as follows.

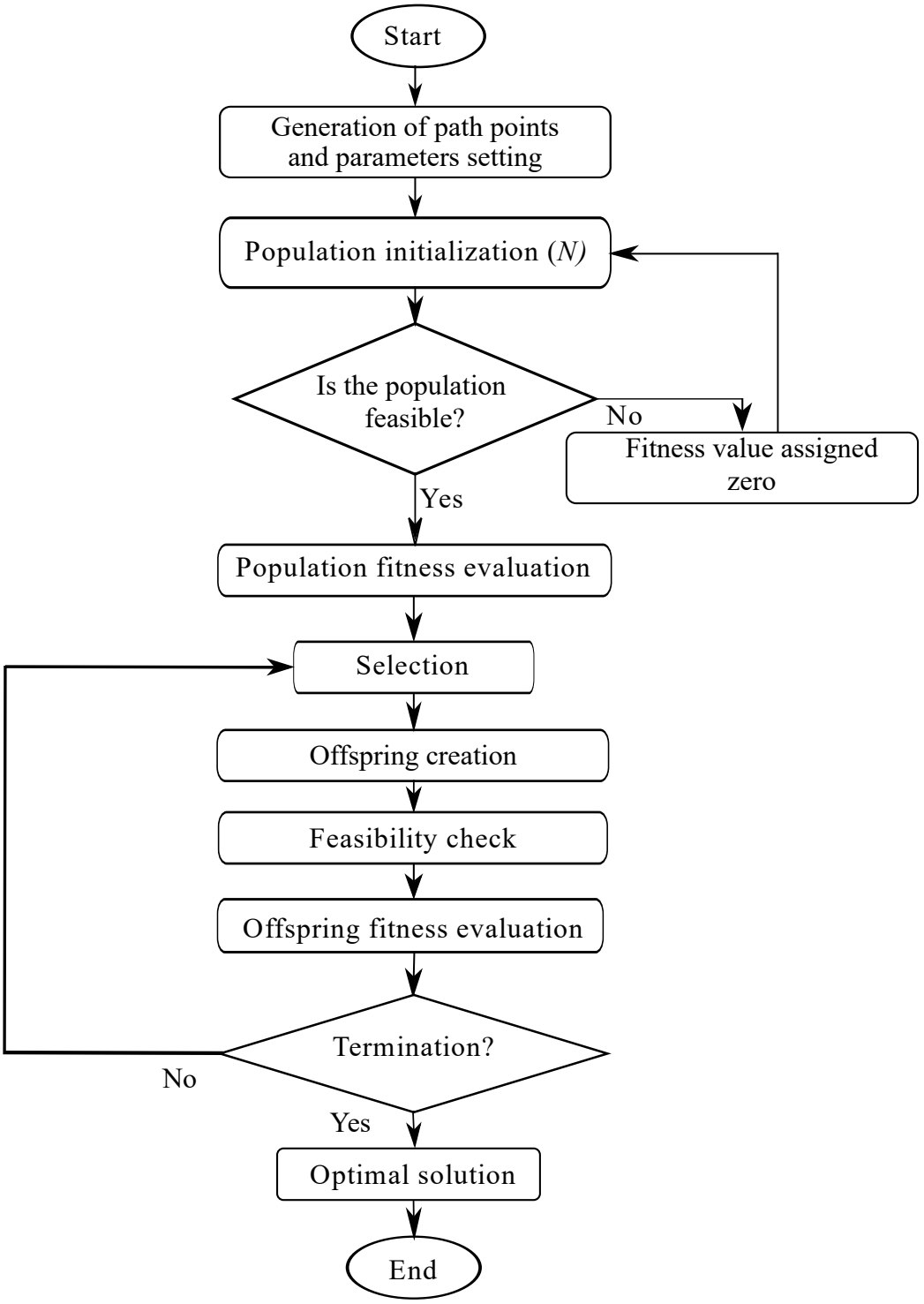

Fig. 4.4: Illustration of the optimization process using GA with feasibility check.

4.4.1.1 Population initialization

Two initialization technique are used: a random initialization and the nearest neighbor. The nearest neighbor method is used to initialize 20% of the population to improve the search process such as diversity.

4.4.1.2 Fitness evaluation and feasibility check

Each coverage motion generated in population is evaluated by using (4.18). To ensure that all the paths in the population are feasible, the time interval segments are $0 \leq t_{\mathrm{h}}$, $0 \leq t_{\mathrm{cj}}$, $0 \leq t_{\mathrm{ca}}$, and $0 \leq T_{\mathrm{v}}$, all kinematic limits in (4.17) are satisfied, and $0 \leq \beta \leq 0.5$.

4.4.1.3 Selection

The selection method is applied to select individuals to be parents for creating new offspring. In addition, solutions are selected for the next generation. Roulette wheel method in combination with elitism is used to ensure parents/solutions with best fitness values are selected.

4.4.1.4 Offspring creation

New population solutions are created using genetic operators. In this chapter, the order crossover and inversion mutation are used in creating offspring from parents. During the crossover and mutation operations, each offspring is created without the integer (path points) being repeated. The crossover operation enriches the population with better individuals, while mutation increases diversity and preventing the solution to be trapped to the local optimum.

4.4.1.5 Replacement and new generation

The genetic algorithm selects a number of individuals to be new generation using roulette wheel and elitism. When the algorithm reaches the termination condition, the new population becomes the final solution.

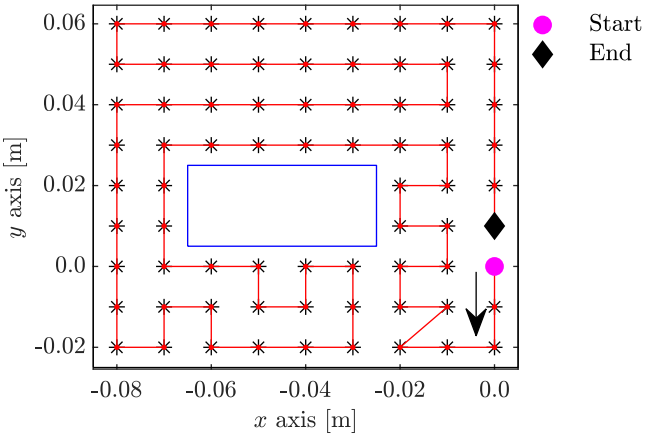

Fig. 4.5: Working surface area.

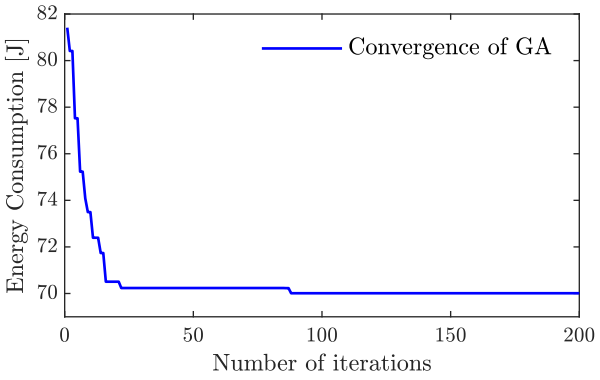

Fig. 4.6: Convergence of optimal solution using modified S-curve.

4.4.1.6 Termination condition

The algorithm runs several iterations to improve the solutions, and the maximum number of iterations is predefined. In this chapter, the maximum number of iterations selected is 200.

Optimization results

To validate the effectiveness of the proposed method, the 2D geometry in Fig. 4.5 is used for trajectory generation and path optimization. The working surface area is 90 mm x 90 mm in size with an island inside size of 40 mm x 20 mm. In this chapter, point locations are generated on the working surface with a 10 mm distance between neighboring points. The

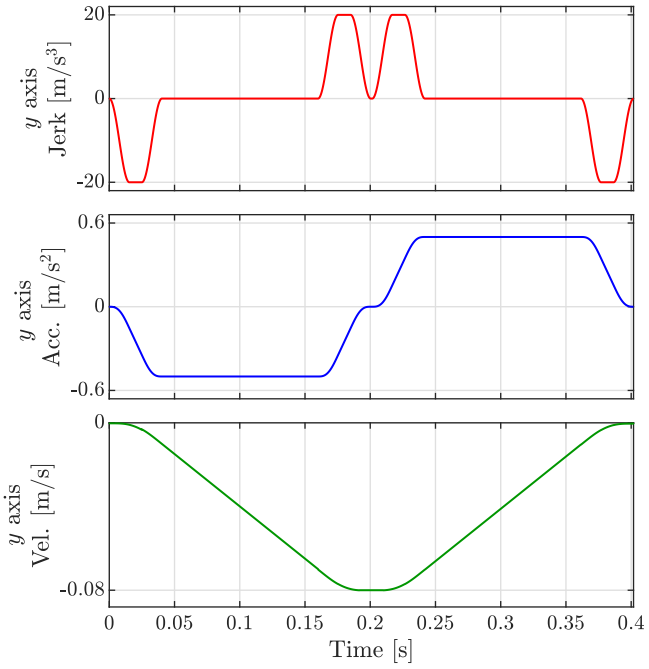

Fig. 4.7: Generated motion profiles for the jerk, acceleration, and velocity.

machine kinematic limits velocity, acceleration, and jerk used are 0.08 m/s, 1 m/s^2, and 20 m/s^3, respectively. The optimization is implemented by MATLAB® 2021a environment on a computer with Windows 10 operating system, core i7-1165G7 processor running at 2.80 GHz, and 16 GB of RAM.

The optimization parameters in GA are set as follows: population size is 100, the maximum number of iterations is 200, crossover probability is 0.8, and mutation probability is set to 0.2. The proposed approach employs GA for the trajectory generation and optimization of the path simultaneously. The final solution is achieved when the optimization algorithm reaches the predefined (200) iterations. Fig. 4.6 shows the convergence of solutions, in which the optimal result is obtained at the iteration number of 83 with the minimum energy value of 70.01 J, equivalent to 14.6% energy saving compared to unoptimized solutions. The proposed approach demonstrates the effectiveness with its convergence. As shown in Fig. 4.5, the feasible optimal coverage motion is attained with the motion from the start to the end point. Fig. 4.7 shows the generated jerk, acceleration, and velocity of the linear segment for the motion from (0,0) to (0,-0.02) m in Fig. 4.5. From the results shown in Figs. 4.5, 4.6, and 4.7, simultaneous trajectory generation and path optimization are achieved with satisfied kinematic limits.

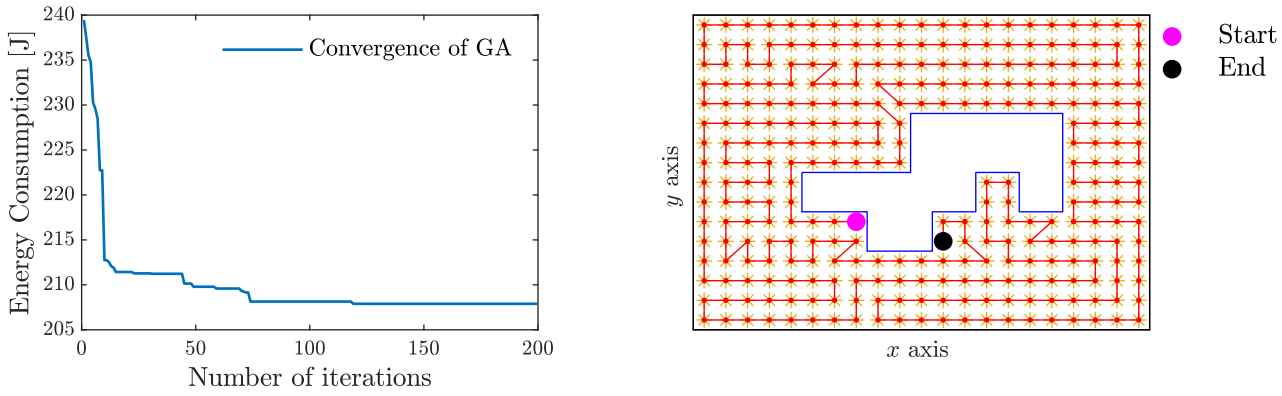

(a) Convergence of optimal solution

(b) Optimal geometric path

Fig. 4.8: Optimal solutions for a working surface two.

4.4.2 Motion optimization of the other two working surfaces

Two other cases or working surfaces are considered for simultaneous trajectory and path optimization using similar strategies presented in section 4.4.1 and GA steps in Fig 4.4 with the maximum number of iterations of 200. The first case is the 2D pocket geometry Fig. 4.8(b) working surface area sized 158.5 mm x 120 mm with an island inside. The path points are generated on it with equal distance between the points, which is 7.5 mm in this case. After optimization is run to the maximum number of iterations (200), an optimal energy coverage solution is determined. Fig. 4.8(a) shows the convergent plot for the GA optimization and Fig. 4.8(b) presents the optimal geometric path generated. The energy optimal value is 207.89 J, with an energy saving of approximately 13.2% compared to an unoptimized solution during the start of optimization.

Furthermore, the working surface Fig. 4.9(b) is optimized, the size of the working surface area is 110 mm x 140 mm with two islands inside and path points are generated with an equal distance of 10 mm from one point to another. An optimal solution for the energy coverage motion optimization problem is determined after running an optimization to the maximum number of iterations defined. Fig. 4.9(a) shows the convergence plot of the algorithm during optimization with the energy optimal achieved of 125.76 J. Energy saving is about 12.14% compared to an unoptimized solution at the start of optimization. Fig. 4.9(b) presents the optimal geometric path solution for machine motion from start to end point.

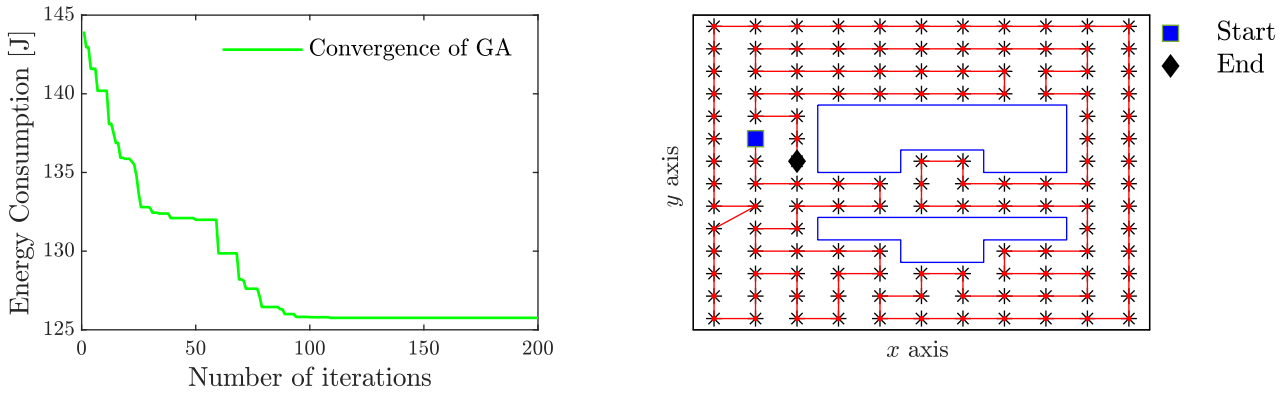

(a) Convergence of optimal solution

(b) Optimal geometric path

Fig. 4.9: Optimal solutions for a working surface three.

4.4.3 Comparative study with the fourth-order motion profile

The proposed approach is compared with the fourth-order motion profile method (Fig. 4.2). The profile is generated based on approach proposed in [111–114]. The motion trajectory is similar to the proposed approach (modified S-curve) that ensures a continuous jerk profile without any sudden change of jerk values that consists of a linear jerk, constant jerk, and zero for some of the time intervals. Furthermore, the trajectory profile ensures that the machines operate to their maximum values of jerk and acceleration with full utilization of the machine capacity, thus increasing the efficiency of the machine [69, 109]. The trajectory obeys machine kinematic limits for velocity, acceleration, and jerk while ensuring its continuity. During the optimization process, similar optimization strategies presented in section 4.4.1 are used. The same case study or working surface Fig. 4.5 is used with the fixed start and end point of motion. The algorithm steps in Fig. 4.4 are used except for the feasibility check. To ensure that all the paths solution are feasible, the time intervals for the fourth-order motion profile are $0 \leq T_l$, $0 \leq t_{\mathrm{cj}}$, $0 \leq t_{\mathrm{ca}}$, and $0 \leq T_{\mathrm{v}}$, all kinematic limits in (4.17) are satisfied while each coverage path in a population is evaluated similarly using the fitness function (4.18).

Optimization results

Running the GA algorithm to the maximum number of iterations (200), the optimal path and trajectory are simultaneously obtained. The convergence plot for the algorithm is as shown

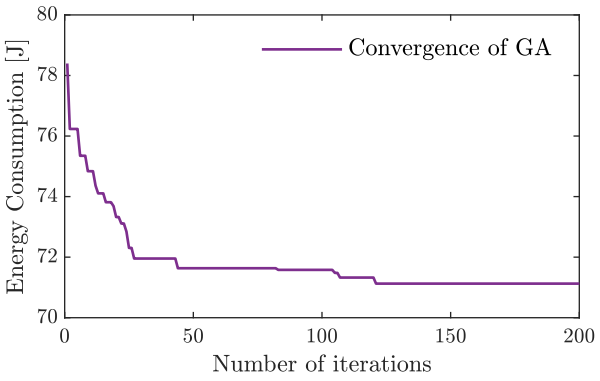

Fig. 4.10: Convergence of optimal solution using fourth-order motion profile.

in Fig. 4.10 with converged optimal solution of 71.13 J achieved at the iteration number 121. In comparison to an unoptimized solution, the energy saving is about 9.27%. Generating the trajectory for a linear segment from (0,0) to (0,-0.02) m in Fig. 4.5 of optimized solution using fourth-order motion profile, the jerk, acceleration, and velocity are shown in Fig. 4.11. All the machine kinematic limits are obeyed and the jerk motion profile with trapezoidal shape is achieved. From these simulation results, comparing the fourth-order motion profile to the modified S-curve, the modified S-curve provides an energy saving of approximately 1.12 J, which is about 1.57%.

4.5 Experiment

4.5.1 Experimental setup

Experiments are carried out on a typical X-Y table system as shown in Fig. 4.12. The table consists of two AC servomotors, which generates linear motion by ball-screws. The position of the table is measured by rotary encoders 76.29 nm resolution with 0.2 ms sampling time. The reference trajectory motions for the modified S-curve and fourth-order motion profile of the optimized path in Fig. 4.5 are prepared and used for experimental verification. The electrical power analyzer (HIOKI3390) installed between a motor and a motor drive is used to measure electrical power consumption. The PD controller is used as the control law to track the reference

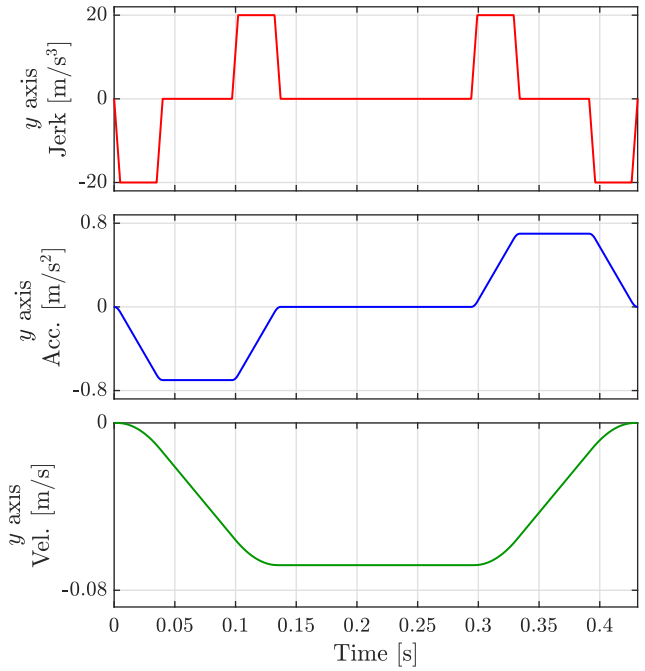

Fig. 4.11: Generated motion profiles for the jerk, acceleration, and velocity by fourth-order trajectory generation.

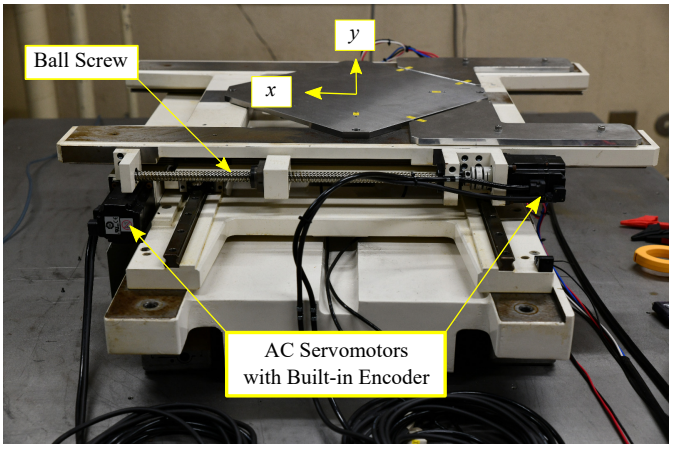

Fig. 4.12: Industrial two-axis feed drive system.

trajectory with proportional and derivative gains of 13000 s^{-2} and 200 s^{-1}, respectively, for each drive axis.

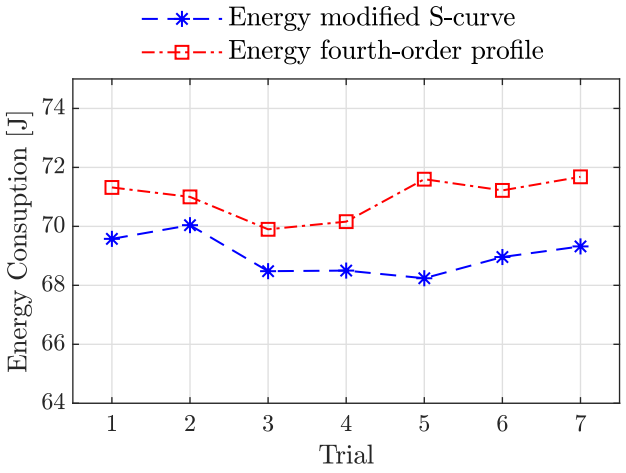

Fig. 4.13: Seven-times experimental trial results of energy consumption with optimized trajectory for the modified S-curve and fourth-order motion profile.

4.5.2 Experimental results

Fig. 4.13 shows the experimental average energy consumption for the optimal coverage motions of two different motion profiles; modified S-curve and fourth-order motion profile. Experiments are carried out seven times for each motion profile, which reveal similar energy consumption results with that of simulation. The average energy consumption for the modified S-curve is about 69.05 J for all experiments and for the fourth-order motion profile is about 70.58 J. These values are almost similar to optimal values obtained by simulation shown in Fig. 4.6 and Fig. 4.10 for the modified S-curve and fourth-order motion profile, respectively. From these experimental energy results, the modified S-curves achieves about 2.17 % energy saving when compared to the fourth-order motion profile.

In addition, Figs. 4.14 and Fig. 4.15 show simulation and experimental velocity profiles for a linear segment in Fig. 4.5 ((0,0)→(0,-0.02) m) of modified S-curve and fourth-order motion profile, respectively. Similar velocity profiles are obtained in experiments and simulation (Figs. 4.7 and 4.11). The motion profiles for the two different trajectories satisfy the machine velocity limits. Furthermore, a rotary encoder is used to measure the tracking performance for the path motions during the experiments. Fig. 4.16 shows mean tracking error results for the proposed approach and fourth-order motion profile in x and y drive axes. The average mean tracking error for the proposed approach are 11.32 μm and 6.21 μm for the x and y axes, respectively. Using the fourth-order motion profile, the average mean tracking error are 15.18 μm and 8.04

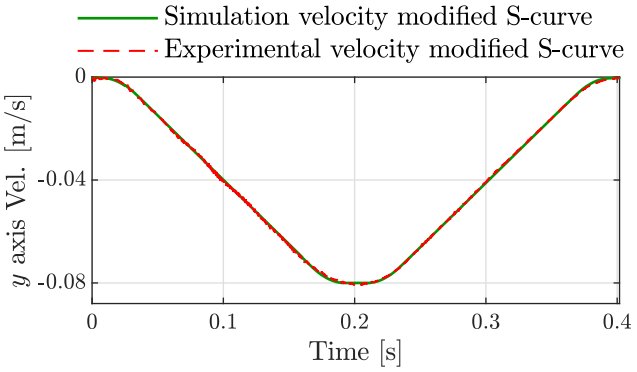

Fig. 4.14: Simulation and experimental modified S-curve velocity profile for a linear segment.

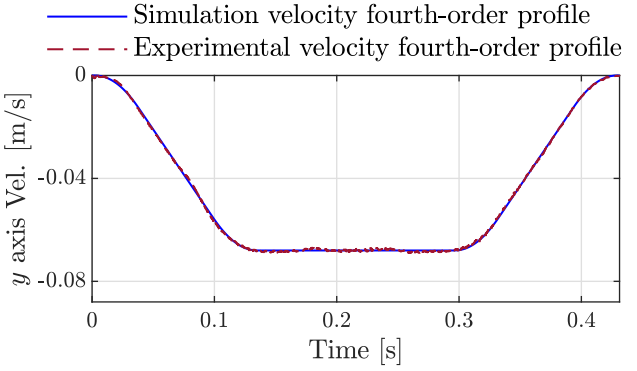

Fig. 4.15: Simulation and experimental fourth-order velocity profile for a linear segment.

μm for the x and y axes, respectively. The proposed approach improves the accuracy by about 25.43% and 22.76% for the x and y axes, respectively, compared to the fourth-order motion profile.

Fig. 4.17 presents the maximum error for the coverage motions. Maximum tracking error for the fourth-order motion profile are 48.51 μm and 30.14 μm in x and y drive axes, respectively, as an average of all trials. The fourth-order motion profile has a higher maximum error in both axis for all trials. The average maximum error for the proposed method is 44.18 μm for the x axis and 28.89 μm for the y axis. The proposed approach improves the motion accuracy for about 8.92% and 4.14% for the x and y axes, respectively.

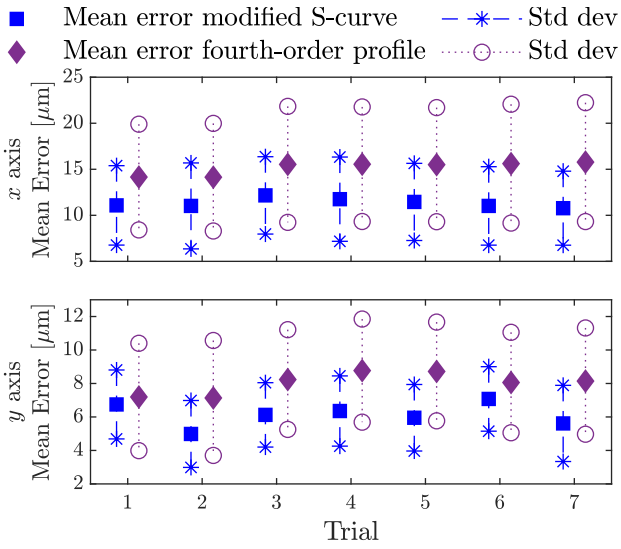

Fig. 4.16: Experimental results of absolute mean tracking error.

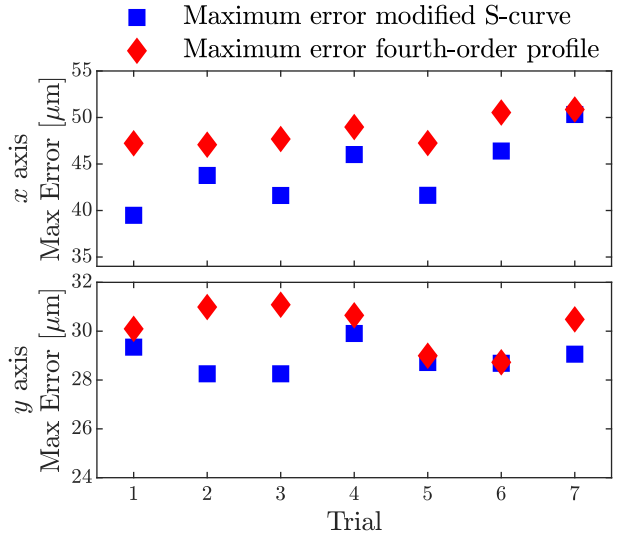

Fig. 4.17: Experimental results of maximum tracking error.

4.6 Discussion

The study in this chapter aims to solve single-objective problem of simultaneous path optimization and trajectory generation for energy saving in coverage motion. Figs. 4.5, 4.8(b), and 4.9(b) show the optimal geometric paths for the three different working surfaces with their

convergence plots during optimization Figs. 4.6, 4.8(a), and 4.9(a), respectively. The generated motion profiles jerk, acceleration, and velocity for the proposed approach is shown in Fig. 4.7. These findings demonstrate that the proposed approach can be used for energy saving in coverage motion. Using the simulation results of the working surface Fig. 4.5, reference trajectories of the coverage path are prepared to move the machine. The experimental motion profile is recorded and plotted as shown in Fig. 4.14; using the linear segment motion profiles from (0,0) to (0,-0.02) m in Fig. 4.5. The experimental motion profile is similar to simulated (Fig. 4.7). The experimental energy consumption is about 69.05 J, also similar to simulation result. From these results, can be concluded that the proposed approach can achieve energy saving in coverage motion with simultaneous path optimization and trajectory generation while obeying the machine kinematic limits.

From the experimental comparison results Figs. 4.13, 4.16, and 4.17 for the energy consumption and motion performance, it shows that the proposed approach outperforms the fourth-order motion profile by achieving lower energy consumption and increase the motion accuracy. Scale parameter β and harmonic motion introduced to the proposed approach contribute to better performance by ensuring smooth jerk continuity and determining energy saving in coverage motion. Hence, the proposed approach can be used for industrial coverage motion planning for energy saving while providing high accuracy motion.

4.7 Conclusion

An energy coverage motion optimization approach for simultaneous trajectory generation and path optimization is proposed. Energy saving in coverage motion is attained, for which modified S-curve is used to describe the motion along the linear segments. The optimized energy result from simulation is almost similar to the experimental result. Its performance is experimentally validated using a typical industrial X-Y table system, which can be applied to many industrial machines for manufacturing tasks such as pocket milling, inspection, polishing, gluing, and laser cutting. In addition, the proposed motion optimization approach increases motion accuracy when compared to the fourth-order motion profile.

Chapter 5

Generation of Time and Energy Optimal Coverage Motion using a Modified S-curve Trajectory

In this chapter an optimal time and energy trajectory generation method with simultaneous path optimization using the modified S-curve is proposed. The modified S-curve generates smooth motion while ensuring continuity of machine kinematic limits jerk, acceleration, and velocity. Using the modified S-curve to describe coverage motion, multi-objective optimization is considered for time and energy consumption, which are two conflicting objectives. NSGA II is used to generate a set of Pareto-optimal solutions using the Pareto dominance approach, which represents the contradictory nature of both objectives. Simulation and experimental results demonstrate the effectiveness of proposed approach using an industrial two-axis feed drive system to achieve the trade-off between time and energy consumption. The best trade-off optimal path is compared to the optimized path generated using the JLAP approach. The comparison shows that the modified S-curve increases the motion accuracy by reducing mean tracking error. Results reveal that the proposed approach can reduce absolute mean tracking error by about 16.2% and 14.9% for the x and y axes, respectively.

This chapter is organized as follows: Section 5.1 presents the related works followed by a description of motion planning described in Section 5.2. An energy consumption model is presented in

Section 5.3, followed by the optimization algorithm in Section 5.4. Section 5.5 presents the simulation, while Section 5.6 describes the experimental results, followed by discussion in Section 5.7. Finally, Section 5.8 presents the concluding remarks.

5.1 Related works

Given the current worldwide situation of an increase in energy costs and environmental problems, energy saving and shorter production time are essential to improve machine performance [16, 103, 117]. Trajectory optimization is one of the approaches widely used to improve the performance of industrial machines while achieving motion accuracy. In [63, 64], trapezoidal velocity profiles are used to achieve optimal energy consumption in a PTP machine motion. Bi-objective optimization between time and energy is proposed in [65], and a trapezoidal velocity profile is used to achieve the trade-off. In these studies [63–65], the motion profiles ensure the continuity of the velocity with limited acceleration. However, trapezoidal velocity profiles in which the machine is accelerated/decelerated at a constant acceleration/deceleration value consist of sudden changes in acceleration and infinite jerk values at the phase transition. As a result, the generated reference trajectories may lead to machine excitation and affect the machine performance [66]. For a smooth change in velocity and acceleration during linear interpolation and to lessen machine excitation, jerk-limited trajectory generation is used. Lu *et al.* [67] propose a time-optimal trajectory generation using the S-curve motion for the machine tool along the predefined path. In [68], an asymmetrical S-curve velocity profile is proposed to achieve the shortest motion time, and the jerk ratio is introduced to limit the jerk value along the path motion. A minimum-time trajectory generation is proposed in [16] via jerk-limited feedrates for the predefined PTP path motion. Furthermore, the JLAP is used to achieve optimal energy or time and energy trajectory generation during machine motion. Nshama *et al.* [49] propose a time and energy consumption optimization method for the two-axis feed drive system, in which the confined jerk profile is used to describe the motion along the path. Energy minimization strategies are proposed in [20, 70], and the acceleration motion times of the S-curve are optimized to reduce energy consumption for PTP motion. The studies [16, 20, 49, 67, 68, 70] present trajectory generation methods to improve machine efficiency, and the jerk limitation

used is associated with sudden value changes at phase transitions. Nevertheless, smooth jerk continuity along the path should be considered to ensure accurate motion and energy reduction.

To further improve the motion, the fourth-order polynomial S-curve function is proposed to ensure a smooth transition of the jerk. In [118], a time-optimal trajectory optimization is presented via the fourth-order S-shaped curve for the coverage motion to attain high machine performance. Fan *et al.* [119] propose the method to increase the machining quality using the fourth-order S-curve trajectory generation along the predefined path. In these studies [118, 119], the rate change of the jerk with respect to time is introduced for jerk continuity, but energy consumption is not taken into account. Furthermore, several S-shaped profiles are proposed to enhance the machine motion accuracy and performance. Lee *et al.* propose a time-optimal trajectory algorithm to achieve the smooth jerk profile using an asymmetric sinusoidal waveform motion, and the method improves the smoothness of the PTP motion compared to the symmetric jerk-limited acceleration profile [120]. Trigonometric functions are proposed to attain a smooth transition of the jerk in [113, 121, 122], the constant jerk phase for the S-curve trajectory along the linear interpolation motion are replaced by trigonometric jerk profile. However, in such a motion, machine cannot operate to their maximum jerk or acceleration values and hence the motion efficiency is limited [69, 109, 122]. For the machines to operate to their maximum values of jerk and acceleration, several approaches are proposed. Wu *et al.* [109] propose a time-optimal PTP motion for a pick and place robot system via an asymmetrical jerk profile to achieve minimum-time and ensure jerk continuity. In [69], a time-optimal trajectory is proposed for the industrial machine, and the piecewise sigmoid function is used to ensure that the machines operate to their maximum values of jerk and acceleration. Using an optimized sinusoidal jerk model, Fang *et al.* propose a time-optimal path that considers both the machine kinematic limits and jerk continuity [105]. However, energy consumption optimization is not taken into account in [69, 105, 109, 113, 120–122], despite the fact that improving profit margins through energy saving and lowering emissions are two important goals in the manufacturing industry.

On the other hand, optimizing geometric paths for the machine coverage motion increases the production efficiency [16, 58]. Several studies have proposed geometric path optimization methods to improve motion performance [24–26, 29]. In these studies, the velocity, acceleration, and jerk machine kinematic limits are not taken into account. As a result, optimized geometric path motion can lead to high operating speeds, excessive accelerations, and vibrations

in mechanical structural parts that affect the machine accuracy and performance. Therefore, trajectory generation with smooth jerk, acceleration, and velocity should be considered during path optimization to further ensure motion accuracy and performance.

5.2 Motion path planning

5.2.1 Modified S-curve trajectory

The modified S-curve trajectory, which is a profile that imposes a smooth jerk transitions consisting of acceleration, constant velocity, and deceleration phases to increase tracking performance, is considered to describe motion along a linear segment for PTP motion. The profile is generated by introducing harmonic motion to the constant jerk phases of the JLAP to ensure smooth jerk continuity and increase motion smoothness. For each jerk constant phase of the JLAP, the phase is divided into three sub-phases consisting of two harmonic motions and the constant jerk value phase, leading to fifteen segments of motion time intervals along the linear segment. The time intervals are calculated as

$$t_{\mathrm{j},1} = \frac{a_0}{j(1-\beta))}, \text{ with } 0 \leq \beta \leq 0.5, \tag{5.1}$$

$$t_{\mathrm{h},1} = \beta t_{\mathrm{j},1}, \tag{5.2}$$

$$t_{\mathrm{cj},1} = t_{\mathrm{j},1} - 2t_{\mathrm{h},1}, \tag{5.3}$$

$$t_{\mathrm{ca},1} = \frac{v_0}{a_0} - t_{\mathrm{j},1}, \tag{5.4}$$

$$T_{\mathrm{v},1} = \frac{(L-S)}{v_0}, \tag{5.5}$$

where a_0, v_0, j are the acceleration, velocity, and jerk, respectively. $t_{\mathrm{j},1}$, $t_{\mathrm{ca},1}$, and $T_{\mathrm{v},1}$ are the jerk period, constant acceleration/deceleration period, and constant velocity period, respectively. $t_{\mathrm{h},1}$ and $t_{\mathrm{cj},1}$ are the harmonic jerk period and constant jerk period, respectively. β is the parameter for the jerk fraction period. L and S are the total distance of a linear segment and the total acceleration and deceleration coverage distance, respectively. The jerk profile equation

is described as

$$\dddot{\boldsymbol{x}}_k(t) = \begin{cases} \frac{j_{\lim,k}}{2}A, & t_0 \le t < t_1, \quad t_{12} \le t < t_{13}, \\ j_{\lim,k}, & t_1 \le t < t_2, \quad t_{13} \le t < t_{14}, \\ \frac{j_{\lim,k}}{2}B, & t_2 \le t < t_3, \quad t_{14} \le t < t_{15}, \\ 0, & t_3 \le t < t_4, \quad t_7 \le t < t_8, \\ & t_{11} \le t < t_{12}, \\ \frac{-j_{\lim,k}}{2}A, & t_4 \le t < t_5, \quad t_8 \le t < t_9, \\ -j_{\lim,k}, & t_5 \le t < t_6, \quad t_9 \le t < t_{10}, \\ \frac{-j_{\lim,k}}{2}B, & t_6 \le t < t_7, \quad t_{10} \le t < t_{11}, \end{cases} \tag{5.6}$$

with

$$A = \left\{1 - \cos(\frac{\pi t}{t_h})\right\} \text{ and } B = \left\{1 + \cos(\frac{\pi t}{t_h})\right\},$$

where $j_{\lim}$ is the maximum jerk of the k^{th} axis. By integrating (5.6), the acceleration, velocity, and displacement profiles are obtained, with time intervals described as

$$\begin{aligned} &t_{\text{h},1} = t_1 - t_0 = t_3 - t_2 = t_5 - t_4 = t_7 - t_6, \\ &t_{\text{h},1} = t_9 - t_8 = t_{11} - t_{10} = t_{13} - t_{12} = t_{15} - t_{14}, \\ &t_{\text{j},1} = t_3 - t_0 = t_7 - t_4 = t_{11} - t_8 = t_{15} - t_{12}, \\ &t_{\text{ca},1} = t_4 - t_3 = t_{12} - t_{11}, \\ &T_{\text{v},1} = t_8 - t_7. \end{aligned} \tag{5.7}$$

The total motion time of the linear segment is the summation of all time intervals given as

$$T_1 = T_{\text{v},1} + 2t_{\text{ca},1} + 4t_{\text{cj},1} + 8t_{\text{h},1}. \tag{5.8}$$

In order to ensure that the machine operates with maximum velocity, acceleration, and jerk values with simultaneously enhancing motion accuracy while achieving optimal time and energy consumption, the selection of optimal parameter β is of importance. Therefore, to achieve optimal time and energy coverage motion during optimization, the parameter selection process is included in the optimization process.

5.2.2 Kinematic limits

For smooth motion along the linear segment, all the machine kinematic limits should be satisfied such that optimal coverage motion values are determined. All three limits of velocity, acceleration, and jerk must be positive, and must satisfy the following requirements:

$$\begin{aligned} |\dddot{\boldsymbol{x}}_k(t)| &\leq j_{\text{lim},k}, \\ |\ddot{\boldsymbol{x}}_k(t)| &\leq a_{\text{lim},k}, \\ |\dot{\boldsymbol{x}}_k(t)| &\leq v_{\text{lim},k}, \end{aligned} \tag{5.9}$$

where $\boldsymbol{x}_k(t)$ is the displacement of the k^{th} axis for the linear segment motion of distance L. In this chapter, PTP linear contours are considered, the jerk, acceleration, and velocity at the initial and final positions of the segment being zero.

5.3 Energy consumption model

This chapter also considers coverage motion of an X-Y table (two-axis feed drive system), which is widely used in industry. The feed drive dynamics are included in the energy consumption model used as described in section 2.2. The energy model is formulated using a two-axis industrial feed drive system with AC 3ϕ servomotors. The crucial property is that power is a function of velocity and acceleration. As a result, trajectory profiles are used to determine the power. The energy consumption model is presented as

$$\begin{aligned} P_k(t) = C_{1,k}\ddot{\boldsymbol{x}}_k^2 + C_{2,k}\dot{\boldsymbol{x}}_k^2 + C_{3,k}\dot{\boldsymbol{x}}_k \text{sgn}\,(\dot{\boldsymbol{x}}_k) + C_{4,k} \\ + C_{5,k}\ddot{\boldsymbol{x}}_k \text{sgn}\,(\dot{\boldsymbol{x}}_k) + C_{6,k}\ddot{\boldsymbol{x}}_k\dot{\boldsymbol{x}}_k, \quad \text{for} \quad k = \{x, y\}, \end{aligned}$$

$$E = \int_{t_0}^{t_{\text{tf}}} (|P_x(t)| + |P_y(t)|)dt, \tag{5.10}$$

where E is the total energy consumption for the feed drive system from time t_0 to t_{tf}. $P_x(t)$ and $P_y(t)$ are the power at time t for the x and y axes, respectively. Machine coefficients and parameters used in this chapter are presented in Tables 2.1 and 2.2 as described in section 2.2, respectively.

5.4 Optimization of coverage motion

5.4.1 Problem formulation

During linear motion interpolation, execution time and energy consumption are required to move the machine table and complete the motion along the path. The dynamics of the machine, velocity, acceleration, and jerk limits during trajectory generation determine the motion time and energy required to complete a linear segment. However, time and energy consumption are two conflicting objectives; determining optimal trajectories that trade-off between time and energy consumption for the optimal path is crucial. This chapter considers simultaneous path and trajectory optimization to achieve optimal time and energy for coverage motion. Therefore, the multi-objective model formulated to obtain the trade-off is described as

$$F(\mathbf{u}) = \min_{\mathbf{u}}\{T(\mathbf{u}), E(\mathbf{u})\}, \tag{5.11}$$

where T and E are the total time and energy consumption for the entire coverage motion, respectively, and $\boldsymbol{u}$ is an optimization parameter vector that consists of variables describing the coverage motion for each segment.

5.4.2 Motion optimization

The motion is optimized to generate the optimal path and trajectories by using NSGA II [93]. The algorithm is a population-based global search that starts with an initial solution and then gets modified through an iteration process to generate the Pareto front solutions. Without combining objectives into a single objective function, NSGA II is an effective evolution that uses the Pareto dominance approach to generate a set of Pareto optimal solutions [77, 96, 97].

Different operators are used to modify initial solutions during the iteration process. A similar algorithm set-up employed in chapter 3 is also used in this section for finding Pareto-optimal solutions. The algorithm steps to achieve the optimal coverage motion is summarized in the following subsections.

5.4.2.1 Working space discretization and encoding solutions

The working space consists of several options for the path and trajectory of the coverage motion. As a result, the optimal path and trajectory must be determined in the processing region simultaneously. The working space is discretized into several grid points to generate the desired geometric path. The grid points are stored using the x and y coordinates to represent the location points as path references during optimization process. Grid points provide displacement information along the linear segment. Each point on the grid is assigned an integer number to represent the geometry of the path in the optimization process using NSGA II. The integers generate different solutions representing several coverage paths. In NSGA II, each integer represents a gene with point information whereby all genes forming feasible geometric path combine to form chromosomes known as population.

5.4.2.2 Population initialization

The initial population is the set of chromosomes representing different potential solutions for the coverage motion. Two initialization methods are adopted in this chapter, random and the heuristic method. To ensure diversity and optimality in the solutions, in this chapter, 80% of the population is generated randomly and the remaining 20% is heuristically initialized.

5.4.2.3 Feasibility check

During optimization process, each population solution is checked so that segment motion time exists, and machine kinematic limits are satisfied. Constraints are checked for the time interval segment $0 \leq t_{\mathrm{h}}$, $0 \leq t_{\mathrm{cj}}$, $0 \leq t_{\mathrm{ca}}$, $0 \leq T_{\mathrm{v}}$, and all machine kinematic limits (5.9). If any constraints are not satisfied, the fitness value of the solution is set to zero. In addition, the

Table 5.1: Crossover operation.

Chromosome	Genes
parent (1)	$1 \rightarrow 2 \rightarrow \underbrace{3 \rightarrow 4 \rightarrow 5} \rightarrow 6 \rightarrow 7$
parent (2)	$1 \rightarrow 5 \rightarrow \underbrace{6 \rightarrow 2 \rightarrow 7} \rightarrow 4 \rightarrow 3$
offspring (1)	$1 \rightarrow 3 \rightarrow \underbrace{6 \rightarrow 2 \rightarrow 7} \rightarrow 4 \rightarrow 5$
offspring (2)	$1 \rightarrow 6 \rightarrow \underbrace{3 \rightarrow 4 \rightarrow 5} \rightarrow 2 \rightarrow 7$

scale parameter β is included in the optimization process to achieve the optimal path, set between 0 and 0.5.

5.4.2.4 Fitness evaluation

Each population is evaluated using the fitness functions from (5.8) as

$$T = \sum_{i=1}^{n} \left(T_{\mathrm{v},i} + 2t_{\mathrm{ca},i} + 4t_{\mathrm{cj},i} + 8t_{\mathrm{h},i} \right), \tag{5.12}$$

and Equation (5.10),

where T is the total motion time.

5.4.2.5 Non-dominated sorting and selection-I

In this process, different solutions are sorted based on the order of non-domination. Furthermore, the population solutions are assigned with the crowding distance parameter and rank [96]. Binary tournament selection is used to choose participants based on the crowding distance and the rank. The selected individuals are parents used to generate new offspring.

5.4.2.6 Creation of the offspring

The order crossover and inversion mutation are used in creating offspring from the parents. The crossover probability pc is set to the algorithm as the occurrence of a crossover during the algorithm runs. The crossover operator works with two parents to create two offspring and ensure no repetition of the genes (path locations) in a generated offspring [87]. The order crossover operation is depicted in Table 5.1. Based on genes order, the two random cuts are generated to divide each of the selected parents into three separate substrings. In order to create the first offspring, the substring between the two cuts for the second parent is copied to the first offspring while maintaining their position, and the remaining part of the offspring is filled by substrings of the first parent not occupied in the offspring. Likewise, the procedure is used to create the second offspring.

The inversion mutation is used to improve the newly formed offspring after the crossover operation [88]. The operator works on a single selected offspring by dividing it into three substrings using the generated random two cuts. The order of the substring genes between the cuts is inverted, forming new offspring, and the local search process finds the best mutated offspring relative to an initial individual; if the initial individual is superior to the mutated offspring, there is no improvement. During the local search operation, the created offspring solution values are evaluated using (5.10) and (5.12). The mutation process occurs with a certain mutation probability pm.

5.4.2.7 Recombination and selection-II

The generated offspring population is combined with the parent population to form the population size of $2N$. Non-dominating sorting is performed. Using elitism strategy [96], the sorted population size N is selected as the new population for the next generation or the final Pareto solutions.

5.4.2.8 Termination condition

In this chapter, the maximum number of iterations is predefined. The number is selected by analyzing the algorithm output from the set of parameter inputs by running the algorithm

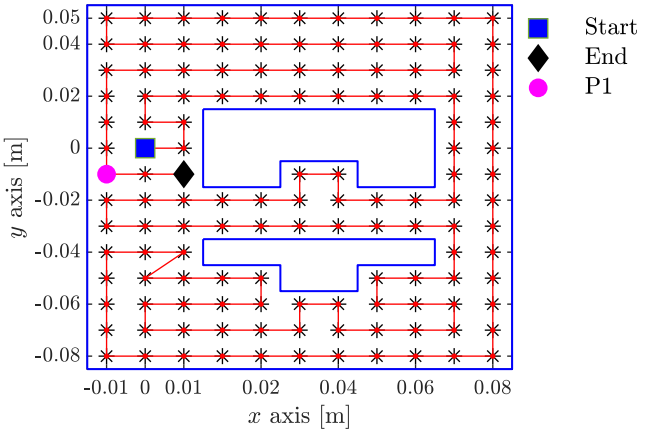

Fig. 5.1: Optimal path motion on rectangle working space moving from one point to another.

several times while observing output solutions. When there is no further improvement to the objective function values, the number is selected. In this chapter, the maximum number of iterations selected is 150.

5.5 Simulation

5.5.1 Simulation condition

The 2D rectangle geometry part in Fig. 5.1 is used for path and trajectory optimization. The working space area is 110 mm x 140 mm in size, with two islands inside. The point locations are generated on the working space with a distance of 10 mm from one point equal to another. The point locations are grids for the path references during path optimization.

The optimization problems of (5.10) and (5.12) are used as fitness functions in NSGA II to determine optimal coverage motion time and energy consumption along the paths. The settings for the NSGA II are as follows: population size is 200, crossover probability $pc = 0.8$, mutation probability $pm = 0.2$, and the maximum number of iterations is 150. The algorithm parameters are chosen based on test runs with various parameter sets, including pc, pm, population size, and a maximum number of iterations, by determining whether the solutions do not further increase the fitness values. The machine kinematic limits velocity, acceleration, and jerk are

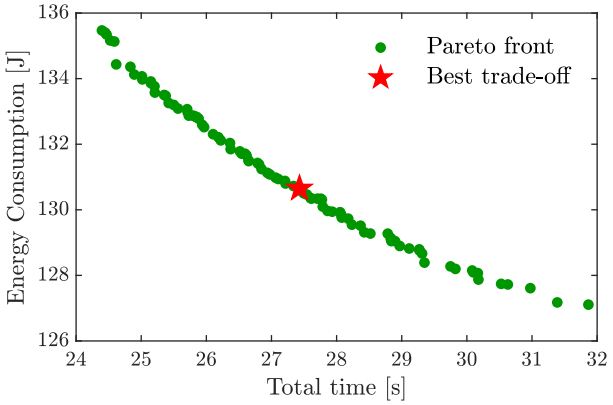

Fig. 5.2: Pareto front representing optimization results.

0.08 m/s, 1 m/s^2, and 20 m/s^3, respectively. The machine kinematic limits and parameters used in optimization are selected based on machine limits and working conditions. To generate optimal solutions, optimization is carried out in a MATLAB® 2021a environment using a laptop with a core i7-1165G7 processor running at 2.80 GHz, 16 GB of RAM, and Windows 10 as the operating system.

5.5.2 Simulation results

Fig. 5.2 shows simulation results of the Pareto front between the two objectives for the coverage motions. The results demonstrate the effectiveness of the proposed approach to obtain the trade-off between time and energy consumption. The best trade-off solution is selected from the normalized objective function space nearest to the origin. The selected best trade-off solution uses the total time 27.43 s and 130.67 J energy, the time-optimal path total time is 24.40 s and 135.47 J energy consumption, and the energy-optimal path motion, the total time is 31.86 s with energy consumption 127.11 J. Therefore, using overall extreme points, the best trade-off solution achieves time reduction and energy saving of 13.90% and 3.54%, respectively.

The optimized results for the trajectories jerk, acceleration, and velocity of the best trade-off optimal case for the x axis are shown in Fig. 5.3 which corresponds to a linear segment motion from $P1$ to the endpoint in Fig. 5.1. Additionally, as shown in detail of Fig. 5.3, the jerk profile has smooth continuity, unlike the jerk-limited acceleration profile. All the machine kinematic

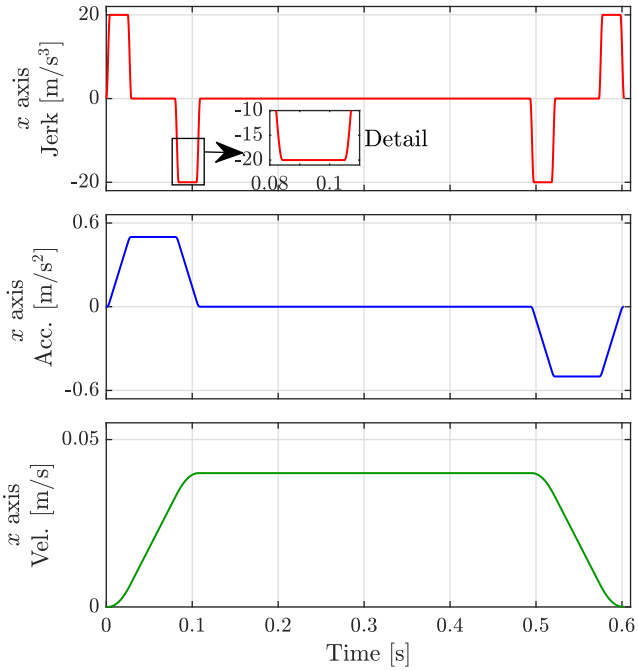

Fig. 5.3: Illustration of the jerk, acceleration, and velocity profiles of the linear segment for the best trade-off optimal path.

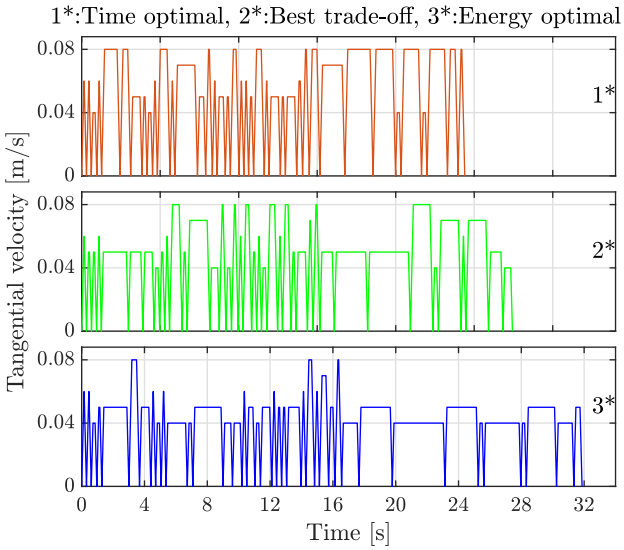

Fig. 5.4: Tangential velocities generated for time, best trade-off, and energy optimality cases.

limits are satisfied. Fig. 5.4 depicts tangential velocities for the time, best trade-off, and energy-optimal paths. Each linear segment generates velocity trajectories consisting of acceleration, constant velocity, and deceleration phases.

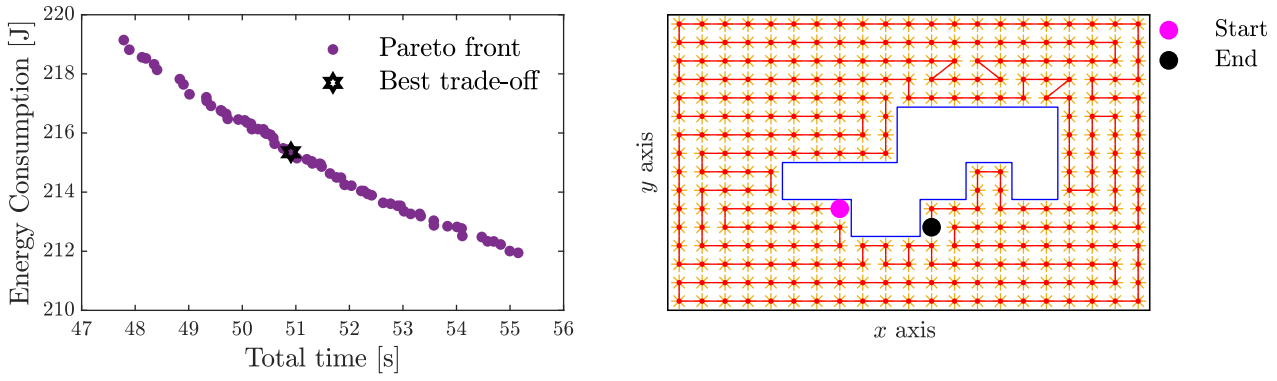

(a) Pareto front (b) Best trade-off path

Fig. 5.5: Pareto-optimal results and geometric path at the best trade-off for working surface two.

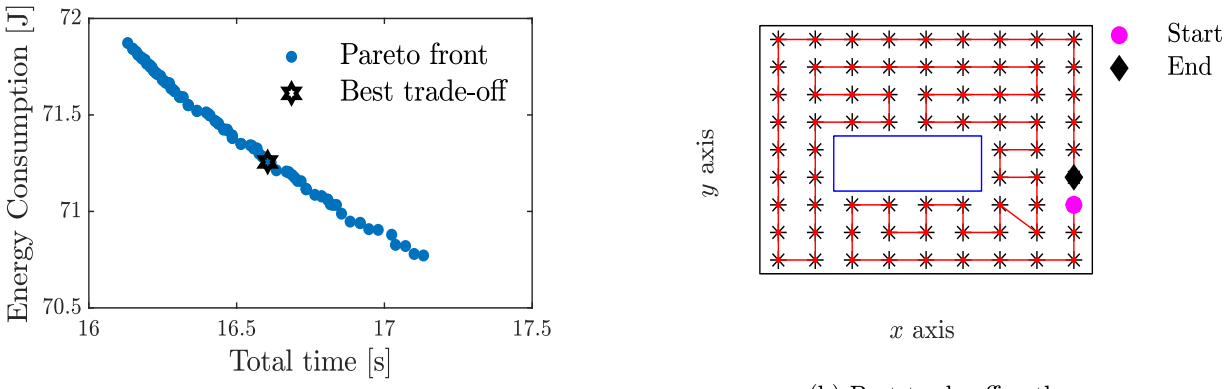

(a) Pareto front (b) Best trade-off path

Fig. 5.6: Pareto-optimal results and geometric path at the best trade-off for working surface three.

5.5.3 Motion optimization of the other two working surfaces

Two other working surfaces are optimized using similar strategies presented in section 5.4. The working surface of 2D pocket geometry with an island inside Fig. 5.5 (b) is used for simultaneous path and trajectory optimization. The size of the working surface is 158.5 mm x 120 mm with point locations of equal distance 7.5 mm from one point to another. Starting with population initialization and executing an optimization to the maximum number of iterations (150), the optimal coverage motion results are determined. Fig. 5.5 (a) shows the Pareto front for the trade-off between time and energy consumption, and Fig. 5.5 (b) presents the geometric path

for the best trade-off solution. The best trade-off solution values for time and energy are 50.91s and 215.35J. The time-optimal path total time is 47.78 s and 218.92 J energy consumption, and the energy-optimal path motion, the total time is 55.15 s with energy consumption 211.73 J. Using three optimal cases from Pareto-optimal solutions, the best trade-off solution achieves time reduction and energy saving of 7.69% and 1.63%, respectively.

In addition, motion optimization on the working surface Fig. 5.6 (b) is considered. The size of working surface area is 100 mm x 100 mm, the point locations are generated on it with equal distance of 10 mm from one point to another. The Pareto front for the trade-off time and energy consumption is determined as shown in Fig. 5.6 (a). The best trade-off solution achieves time and energy values of 16.61 s and 71.26 J, respectively, and Fig. 5.6 (b) shows the best trade-off geometric path. The best trade-off solution provides time reduction and energy saving of about 3.06% and 1.4%, respectively, compared to three optimal cases of Pareto-optimal solutions.

5.6 Experiment

5.6.1 Experimental procedure

An industrial two-axis machine shown in Fig. 5.7 is also used in this chapter for the experiment to validate the optimized results. The machine comprises of two AC servomotors, where the linear motion is acquired via ball-screw drive systems connected to each axis. The axial position of each axis of the table is measured using rotary encoders with a resolution of 76.29 nm and 0.2 ms sampling time. Experiments are carried out on the optimized paths from the Pareto front. Reference trajectory motion of selected points along the Pareto front are used for experimental verification. Five points are selected for experimental verification; the selected solutions are the best trade-off, energy-optimal, time-optimal, and two other optimal solutions. Reference trajectories for the paths are prepared to move the machine. Each experiment is performed seven times to avoid inaccuracies in the energy measures. The consumed energy is measured using a power analyzer (HIOKI3390) installed between a motor driver and a motor, directly measuring the energy consumption at a 50 ms data update interval.

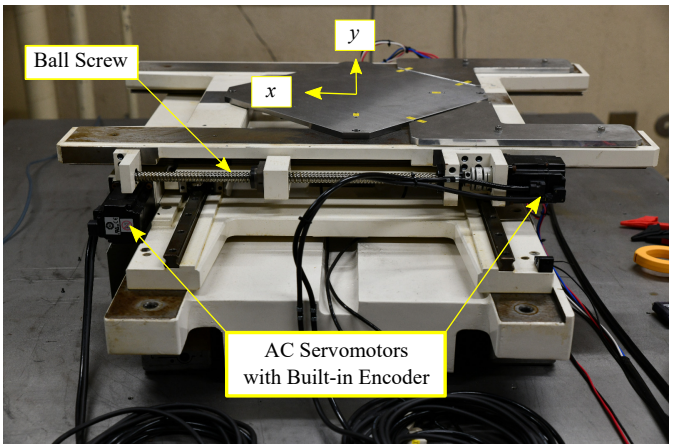

Fig. 5.7: Industrial two-axis feed drive system.

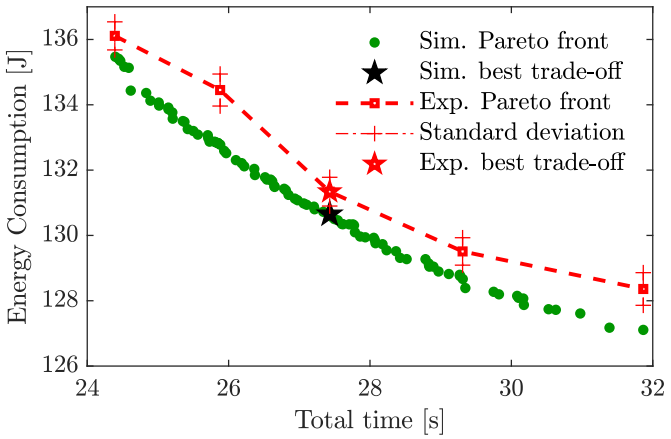

Fig. 5.8: Simulation and experimental energy consumption for the selected solutions.

5.6.2 Experimental results

The average experimental results of energy consumption for five solutions and simulation results are shown in Fig. 5.8. The experimental results are similar to that of simulation. The experimental results for time and energy consumption for the best trade-off solution are 27.43 s and 131.35 J, respectively, the time-optimal path total time is 24.40 s and 136.11 J energy consumption, and the energy-optimal path motion, the total time is 31.86 s with energy consumption 128.78 J. Therefore, using three optimal cases from the experiment, the best trade-off solution achieves time reduction and energy saving of 13.9% and 3.5%, respectively. The experimental velocity profiles for the x and y axes for all three optimal cases are shown in Fig. 5.9. All the limitations are satisfied.

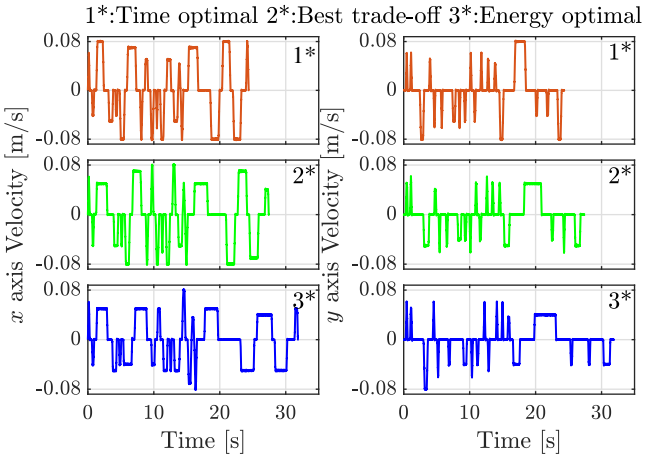

Fig. 5.9: Experimental velocity profiles for the time, best trade-off, and energy optimal paths in x and y axes.

5.6.3 Comparative study with the Jerk-limited acceleration profile (JLAP)

The motion performance accuracy of the proposed approach is compared with the JLAP method commonly used in trajectory generation. The JLAP profile is generated based on the approach proposed in [20, 49]. Similar optimization strategies and the same limits are used in the optimization process. The algorithm presented in section 5.4.2 and case study Fig. 5.1 is used to achieve the optimal path. Similar steps are used except for fitness functions described as from (4.4) given as

$$T = \sum_{i=1}^{n} \left(T_{\mathrm{c},i} + 2t_{\mathrm{c},i} + 4t_{\mathrm{a},i} \right), \tag{5.13}$$

and Equation (5.10),

Comparative experimental results

In this section, the experimental test of the geometric path is performed. The optimal path described by JLAP is prepared to move the machine. The experimental test is done for the

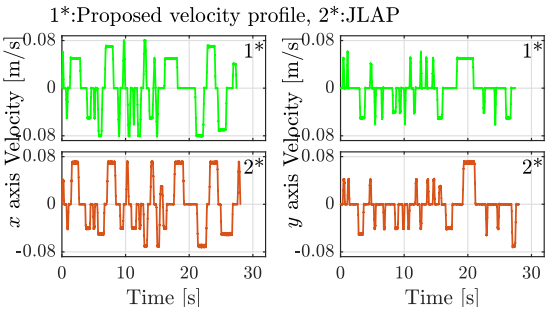

Fig. 5.10: Experimental velocity profiles for the proposed and JLAP in x and y axes.

JLAP path and the best trade-off path of the proposed approach, and similar machine working conditions and limits are used for the experimental test.

Fig. 5.10 shows experimental velocity profile for the best trade-off paths of the proposed approach and JLAP method. The motion profiles for the two approaches satisfy the machine velocity limits. During the experiment, the tracking performance for the path motions is measured by a rotary encoder. Fig. 5.11 shows the absolute mean tracking error for the x and y axes of each motor. The proposed approach improves the accuracy by about 16.2% and 14.9% for the x and y axes, respectively, compared to the JLAP approach. In addition, Fig. 5.12 depicts the single-sided amplitude spectrums of the tracking error for the proposed and JLAP optimal paths. The tracking error for the proposed is damped with a reduction in their amplitudes. The above results show that path optimization with the proposed approach achieves high tracking accuracy than the JLAP. In addition, the energy consumption for the JLAP path is 132.46 J, which is 1.3% higher than the best trade-off path of the proposed one.

5.7 Discussion

Fig. 5.8 shows the average experimental energy consumption Pareto-optimal solutions for the proposed approach, which is similar to the results of simulation in Fig. 5.2. The proposed approach achieves the trade-off between time and energy consumption. This contributes to research gap, whereby most trajectory generation aims to achieve a single objective time-optimal path [69, 105, 109, 113, 118–122]. In addition, as shown in Figs. 5.1, 5.3, and 5.9, the proposed approach attain the simultaneous path and trajectory generation while observing the machine limits.

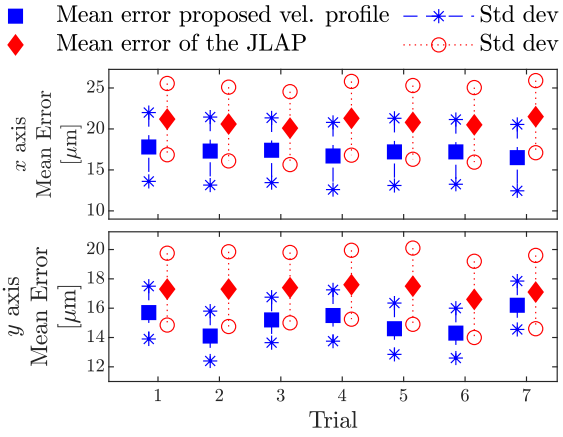

Fig. 5.11: Absolute mean tracking error for the proposed velocity profile and JLAP paths in x and y axes.

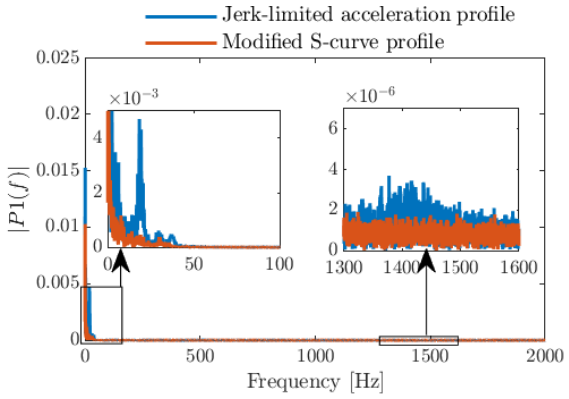

Fig. 5.12: Single-sided amplitude spectrums of tracking errors.

From the experimental comparison results Figs. 5.11 and 5.12, it shows that the proposed method outperforms the JLAP by achieving smooth motion and increase the accuracy by about 16.2% and 14.9% for the x and y axes, respectively. The achievement of the smoothness is contributed by scale parameter β and harmonic motion which are introduced to ensure the smooth jerk continuity. Therefore, it is reasonable to conclude that the proposed method improves the motion performance while achieving the trade-off between the two objectives.

A feed drive system is considered for optimal trajectory generation and experimental verification, which is widely used in the manufacturing sector with the operations such as pocket milling, inspection, polishing, gluing, and additive manufacturing. Therefore, the proposed approach can be widely applied in various industrial machines.

5.8 Conclusion

This chapter illustrates motion profiles with smooth jerk continuity for time and energy optimal coverage motion. The modified S-curve trajectory is generated to describe the motion by introducing the harmonic motion into the JLAP and achieve smooth jerk continuity. Simulation and experiments are carried out to demonstrate the effectiveness of the proposed method in terms of energy consumption and tracking performance enhancement in industrial two-axis feed drive system. Pareto front is generated by the NSGA II, where the solution nearest to the origin point in the normalized objective space is selected as the best trade-off solution. Experimental results show that the best trade-off solution achieves time reduction and energy saving by 13.9% and 3.5%, respectively, compared to single objective optimal solutions. Compared to the JLAP, the best trade-off optimal path reduces the mean error by 16.2% and 14.9% for the x and y axes, respectively.

Chapter 6

Conclusions and Future Works

6.1 Conclusions

Industrial machines are crucial in the manufacturing sector and are widely used. Industrial machine operations are currently driven by the need for accurate motion, shorter operating times, and energy efficiency. This can be achieved by ensuring that the machines operate at high efficiency. In the literature, several studies are presented to improve the efficiency of industrial machines in terms of time and energy consumption. However, the multi-objective problem of simultaneous trajectory generation and path optimization in industrial machines for time and energy optimal coverage motions has not been explored much. Thus, this thesis presents multi-objective problem-solving for time and energy optimal trajectory generation with simultaneous geometric path optimization. Furthermore, a single-objective optimization problem is presented for simultaneous trajectory generation and geometric path optimization for energy consumption when a single best solution is required. A typical industrial two-axis feed drive system is used in simulations and experiments to verify the effectiveness of the proposed methods for coverage motion. The proposed solutions can be used for industrial machine operations such as milling, laser cutting, inspection, gluing, and polishing.

In chapter 3, Pareto-optimal solutions are generated of simultaneous trajectory generation and geometric path optimization for time and energy optimal coverage motion. To generate the trajectory along the path, Jerk-limited acceleration profile (JLAP) is used to describe the

trajectory in which velocity profiles are generated for each linear segment to achieve the desired velocities. To solve the optimization problem, an energy model of the industrial two-axis feed drive system is used and Non-dominated Sorting Genetic Algorithm II (NSGA II) generates Pareto-optimal solutions that trade-off between time and energy. Experimental results show the effectiveness of the proposed approach, where the best trade-off solution achieves time and energy savings of about 10.05% and 2.1%, respectively. The best trade-off is that solution nearest to the origin of the normalized function space. In addition, the proposed method is compared with an approach in which the trajectory of each segment along a path is described by a constant velocity. The proposed method with variable velocities for each segment reduces the maximum error by about 76.6% compared to the optimized coverage motion using the constant commanded velocity approach.

Moreover, an energy optimal solution is achieved for a single-objective optimization problem in chapter 4. Energy optimization approach for the coverage motion of industrial machines which simultaneously integrates trajectory generation and geometric path optimization is proposed. In this chapter, a modified S-curve is used to describe the trajectory of each linear segment. The modified S-curve is generated by introducing the harmonic motion into the JLAP and achieving smooth jerk continuity. To achieve energy optimality, Genetic Algorithm (GA) is applied to optimize an energy consumption model of the feed drive system. Experimental results show that the energy optimal of the feed drive system is achieved under machine kinematic limits, ensuring smooth motion. Compared to the initial/unoptimized solutions, the final optimized solution achieves about 14.6% energy reduction. Moreover, the proposed approach is compared to fourth-order motion profile. Experimental results show that the proposed method outperforms the fourth-order motion profile in achieving higher motion accuracy and energy saving.

Using the Pareto optimization method, chapter 5 proposes a method for time and energy optimal trajectory generation with a simultaneous path optimization using the modified S-curve. The modified S-curve is used to describe the trajectory for each linear segment along the path to solve the multi-objective time and energy problem. The energy model of an industrial two-axis feed drive system is used in finding solutions to the optimization problem. NSGA II is used to generate a Pareto-optimal solutions for trade-off between time and energy consumption. The best trade-off solution is chosen as the optimal solution nearest to the origin of the normalized objective function space. The multi-objective optimization is solved, and the best trade-off solution is obtained, which achieves a time reduction and energy saving of about 13.9% and

3.5%, respectively. Furthermore, the proposed approach is compared to the approach in which JLAP is used to describe the trajectory of each linear segment along the path. Experimental results reveal that the optimal path of the proposed approach reduces the mean error by 16.2% and 14.9% for the x and y axes, respectively.

6.2 Future works

In this thesis, the proposed methods are limited to only considering the 2D working surface; for this reason, cannot be applied to industrial machines with more than three axes. In future works, the extension on freeform working surfaces that can be executed using three- and five-axis machines can be further explored.

Furthermore, for the machining operations, a cutting force model and other constraints of machining parameters, such as spindle speed, maximum cutting force, axial and radial depth of cut, and workpiece surface roughness, should be incorporated into the energy model and problem formulation to enhance the machining performance. This can be embodied in formulating the multi-objective problem as an extension to the proposed methods.

The JLAP and modified S-curve are used to describe the trajectory for linear segments along the paths. These profiles are symmetrical, which achieves equal acceleration and deceleration magnitudes; with the acceleration and deceleration phases taking the same motion time. Consideration of the asymmetrical S-curve profile to describe the trajectory for each linear segment provides more variables during the optimization of the problem; thus, using an asymmetrical profile to describe the trajectory can possibly provide better solutions.

In addition, the proposed method is based on PTP motions. By incorporating continuous corner smoothing into this proposed method with PTP motions, smooth transitions can be achieved in linear interpolation along the path from one segment to another.

The proposed methods considered solving single- and two-objective optimization problems. Since machine efficiency improvement has several measures, multiple objectives can be added to find the Pareto-optimal solutions.

Bibliography

[1] J. Zhao, L. Li, Y. Wang, and J. W. Sutherland, "Impact of surface machining complexity on energy consumption and efficiency in cnc milling," *The International Journal of Advanced Manufacturing Technology*, vol. 102, no. 9, pp. 2891–2905, 2019.

[2] W. Cai, F. Liu, X. Zhou, and J. Xie, "Fine energy consumption allowance of workpieces in the mechanical manufacturing industry," *Energy*, vol. 114, pp. 623–633, 2016.

[3] V. C. Panagiotopoulou, P. Stavropoulos, and G. Chryssolouris, "A critical review on the environmental impact of manufacturing: a holistic perspective," *The International Journal of Advanced Manufacturing Technology*, pp. 1–23, 2021.

[4] J. C. Lopes, G. A. de Carvalho, G. B. Moretti, B. N. Ávila, M. de Souza Rodrigues, M. V. Garcia, F. S. F. Ribeiro, A. R. Rodrigues, L. E. de Angelo Sanchez, and E. C. Bianchi, "Sustainable thinking toward to industry's future combined with new knowledge on greenhouse effect mitigation generated by the grinding process," *Journal of Cleaner Production*, vol. 386, p. 135810, 2023.

[5] Y. Xiao, Z. Jiang, Q. Gu, W. Yan, and R. Wang, "A novel approach to cnc machining center processing parameters optimization considering energy-saving and low-cost," *Journal of Manufacturing Systems*, vol. 59, pp. 535–548, 2021.

[6] X. Chen, C. Li, Y. Tang, L. Li, Y. Du, and L. Li, "Integrated optimization of cutting tool and cutting parameters in face milling for minimizing energy footprint and production time," *Energy*, vol. 175, pp. 1021–1037, 2019.

[7] C. Li, L. Li, Y. Tang, Y. Zhu, and L. Li, "A comprehensive approach to parameters optimization of energy-aware cnc milling," *Journal of Intelligent Manufacturing*, vol. 30, pp. 123–138, 2019.

[8] M. Moradi, M. K. Moghadam, M. Shamsborhan, Z. M. Beiranvand, A. Rasouli, M. Vahdati, A. Bakhtiari, and M. Bodaghi, "Simulation, statistical modeling, and optimization of co2 laser cutting process of polycarbonate sheets," *Optik*, vol. 225, p. 164932, 2021.

[9] M. R. Msukwa, E. W. Nshama, and N. Uchiyama, "Adaptive sliding mode control with feedforward compensator for energy-efficient and high-speed precision motion of feed drive systems," *IEEE Access*, vol. 8, pp. 43 571–43 581, 2020.

[10] A. Farrage and N. Uchiyama, "Improvement of motion accuracy and energy consumption for industrial feed drive systems using adaptive sliding mode control," *ISA transactions*, vol. 106, pp. 382–391, 2020.

[11] Q. Ji, C. Li, D. Zhu, Y. Jin, Y. Lv, and J. He, "Structural design optimization of moving component in cnc machine tool for energy saving," *Journal of Cleaner Production*, vol. 246, p. 118976, 2020.

[12] P. Albertelli, "Energy saving opportunities in direct drive machine tool spindles," *Journal of cleaner production*, vol. 165, pp. 855–873, 2017.

[13] M. Endo and B. Sencer, "Accurate prediction of machining cycle times by data-driven modelling of nc system's interpolation dynamics," *CIRP Annals*, vol. 71, no. 1, pp. 405–408, 2022.

[14] K. Erkorkmaz, S. E. Layegh, I. Lazoglu, and H. Erdim, "Feedrate optimization for freeform milling considering constraints from the feed drive system and process mechanics," *CIRP Annals*, vol. 62, no. 1, pp. 395–398, 2013.

[15] Y. Sun, M. Chen, J. Jia, Y.-S. Lee, and D. Guo, "Jerk-limited feedrate scheduling and optimization for five-axis machining using new piecewise linear programming approach," *Science china technological sciences*, vol. 62, no. 7, pp. 1067–1081, 2019.

[16] R. Ward, B. Sencer, B. Jones, and E. Ozturk, "Accurate prediction of machining feedrate and cycle times considering interpolator dynamics," *The International Journal of Advanced Manufacturing Technology*, vol. 116, no. 1, pp. 417–438, 2021.

[17] E. Barnett and C. Gosselin, "A bisection algorithm for time-optimal trajectory planning along fully specified paths," *IEEE Transactions on Robotics*, vol. 37, no. 1, pp. 131–145, 2020.

[18] P. Bosetti and E. Bertolazzi, "Feed-rate and trajectory optimization for cnc machine tools," *Robotics and Computer-Integrated Manufacturing*, vol. 30, no. 6, pp. 667–677, 2014.

[19] P. Shen, X. Zhang, Y. Fang, and M. Yuan, "Real-time acceleration-continuous path-constrained trajectory planning with built-in tradeoff between cruise and time-optimal motions," *IEEE Transactions on Automation Science and Engineering*, vol. 17, no. 4, pp. 1911–1924, 2020.

[20] N. Uchiyama, K. Goto, and S. Sano, "Analysis of energy consumption in fundamental motion of industrial machines and experimental verification," *2015 American Control Conference (ACC)*, pp. 2179–2184, 2015.

[21] E. W. Nshama and N. Uchiyama, "Pareto optimization of cycle time and motion accuracy in trajectory planning for industrial feed drive systems," *IEEE Access*, vol. 9, pp. 114 104–114 119, 2021.

[22] G. Carabin and L. Scalera, "On the trajectory planning for energy efficiency in industrial robotic systems," *Robotics*, vol. 9, no. 4, p. 89, 2020.

[23] J. Zhou, H. Cao, P. Jiang, C. Li, H. Yi, and M. Liu, "Energy-saving trajectory planning for robotic high-speed milling of sculptured surfaces," *IEEE Transactions on Automation Science and Engineering*, vol. 19, no. 3, pp. 2278–2294, 2021.

[24] L. Li, X. Deng, J. Zhao, F. Zhao, and J. W. Sutherland, "Multi-objective optimization of tool path considering efficiency, energy-saving and carbon-emission for free-form surface milling," *Journal of Cleaner Production*, vol. 172, pp. 3311–3322, 2018.

[25] G. Zhou, C. Zhang, F. Lu, and J. Zhang, "Integrated optimization of cutting parameters and tool path for cavity milling considering carbon emissions," *Journal of Cleaner Production*, vol. 250, p. 119454, 2020.

[26] K. Xu, Y. Li, and B. Xiang, "Image processing-based contour parallel tool path optimization for arbitrary pocket shape," *The International Journal of Advanced Manufacturing Technology*, vol. 102, no. 5, pp. 1091–1105, 2019.

[27] N. Hatem, Y. Yusof, A. Z. A. Kadir, K. Latif, and M. Mohammed, "A novel integrating between tool path optimization using an aco algorithm and interpreter for open architecture cnc system," *Expert Systems with Applications*, vol. 178, p. 114988, 2021.

[28] M. Kumar and P. Khatak, "Development of a discretization methodology for 2.5 d milling toolpath optimization using genetic algorithm," *Advances in Computing and Intelligent Systems*, pp. 93–104, 2020.

[29] B. R. C. Karuppanan and M. Saravanan, "Optimized sequencing of cnc milling toolpath segments using metaheuristic algorithms," *Journal of Mechanical Science and Technology*, vol. 33, no. 2, pp. 791–800, 2019.

[30] T. Moriwaki, "Multi-functional machine tool," *CIRP annals*, vol. 57, no. 2, pp. 736–749, 2008.

[31] S. Ma, Y. Zhang, Y. Liu, H. Yang, J. Lv, and S. Ren, "Data-driven sustainable intelligent manufacturing based on demand response for energy-intensive industries," *Journal of Cleaner Production*, vol. 274, p. 123155, 2020.

[32] S. T. Hassan, B. Batool, M. Sadiq, and B. Zhu, "How do green energy investment, economic policy uncertainty, and natural resources affect greenhouse gas emissions? a markov-switching equilibrium approach," *Environmental Impact Assessment Review*, vol. 97, p. 106887, 2022.

[33] K. O. Yoro and M. O. Daramola, "Co2 emission sources, greenhouse gases, and the global warming effect," *Advances in carbon capture*, pp. 3–28, 2020.

[34] A. Aramcharoen and P. T. Mativenga, "Critical factors in energy demand modelling for cnc milling and impact of toolpath strategy," *Journal of Cleaner Production*, vol. 78, pp. 63–74, 2014.

[35] W. Cai, L. Wang, L. Li, J. Xie, S. Jia, X. Zhang, Z. Jiang, and K.-h. Lai, "A review on methods of energy performance improvement towards sustainable manufacturing from perspectives of energy monitoring, evaluation, optimization and benchmarking," *Renewable and Sustainable Energy Reviews*, vol. 159, p. 112227, 2022.

[36] W. Wang, G. Tian, M. Chen, F. Tao, C. Zhang, A.-A. Abdulraham, Z. Li, and Z. Jiang, "Dual-objective program and improved artificial bee colony for the optimization of energy-conscious milling parameters subject to multiple constraints," *Journal of cleaner production*, vol. 245, p. 118714, 2020.

[37] X. Chen, C. Li, Y. Tang, L. Li, and H. Li, "Energy efficient cutting parameter optimization," *Frontiers of Mechanical Engineering*, pp. 1–28, 2021.

[38] S. Jia, S. Wang, J. Lv, W. Cai, N. Zhang, Z. Zhang, and S. Bai, "Multi-objective optimization of cnc turning process parameters considering transient-steady state energy consumption," *Sustainability*, vol. 13, no. 24, p. 13803, 2021.

[39] F. Han, L. Li, W. Cai, C. Li, X. Deng, and J. W. Sutherland, "Parameters optimization considering the trade-off between cutting power and mrr based on linear decreasing particle swarm algorithm in milling," *Journal of Cleaner Production*, vol. 262, p. 121388, 2020.

[40] J. Lv, T. Peng, and R. Tang, "Energy modeling and a method for reducing energy loss due to cutting load during machining operations," *Proceedings of the Institution of Mechanical Engineers, Part B: Journal of Engineering Manufacture*, vol. 233, no. 3, pp. 699–710, 2019.

[41] Y. He, X. Tian, Y. Li, Y. Wang, Y. Wang, and S. Wang, "Modeling and analyses of energy consumption for machining features with flexible machining configurations," *Journal of Manufacturing Systems*, vol. 62, pp. 463–476, 2022.

[42] M. R. Msukwa and N. Uchiyama, "Design and experimental verification of adaptive sliding mode control for precision motion and energy saving in feed drive systems," *IEEE Access*, vol. 7, pp. 20 178–20 186, 2019.

[43] Y. Altintas, A. Verl, C. Brecher, L. Uriarte, and G. Pritschow, "Machine tool feed drives," *CIRP Annals*, vol. 60, no. 2, pp. 779–796, 2011.

[44] I. Edem and V. Balogun, "Energy efficiency analyses of toolpaths in a pocket milling process," *International Journal of Engineering*, vol. 31, no. 5, pp. 847–855, 2018.

[45] M. Rigacci, R. Sato, and K. Shirase, "Experimental evaluation of mechanical and electrical power consumption of feed drive systems driven by a ball-screw," *Precision Engineering*, vol. 64, pp. 280–287, 2020.

[46] A. HYASHI, Y. INOUE, R. SATO, and K. SHIRASE, "A028 motion path evaluation based on energy consumption of feed drive system in nc machine tool," *Proceedings of International Conference on Leading Edge Manufacturing in 21st century: LEM21 2013.7*, pp. 129–134, 2013.

[47] A. Rangarajan and D. Dornfeld, "Efficient tool paths and part orientation for face milling," *CIRP Annals*, vol. 53, no. 1, pp. 73–76, 2004.

[48] D. Prévost, S. Lavernhe, C. Lartigue, and D. Dumur, "Feed drive modelling for the simulation of tool path tracking in multi-axis high speed machining," *International Journal of Mechatronics and Manufacturing Systems*, vol. 4, no. 3-4, pp. 266–284, 2011.

[49] E. W. Nshama, M. R. Msukwa, and N. Uchiyama, "A trade-off between energy saving and cycle time reduction by pareto optimal corner smoothing in industrial feed drive systems," *IEEE Access*, vol. 9, pp. 23 579–23 594, 2021.

[50] N. Baskar, P. Asokan, R. Saravanan, and G. Prabhaharan, "Selection of optimal machining parameters for multi-tool milling operations using a memetic algorithm," *Journal of Materials processing technology*, vol. 174, no. 1-3, pp. 239–249, 2006.

[51] S. Shaji and V. Radhakrishnan, "Analysis of process parameters in surface grinding with graphite as lubricant based on the taguchi method," *Journal of Materials Processing Technology*, vol. 141, no. 1, pp. 51–59, 2003.

[52] M. V. Andulkar, S. S. Chiddarwar, and A. S. Marathe, "Novel integrated offline trajectory generation approach for robot assisted spray painting operation," *Journal of Manufacturing Systems*, vol. 37, pp. 201–216, 2015.

[53] Y. Han, L. Zhang, M. Guo, C. Fan, and F. Liang, "Tool paths generation strategy for polishing of freeform surface with physically uniform coverage," *The International Journal of Advanced Manufacturing Technology*, vol. 95, pp. 2125–2144, 2018.

[54] M. H. Gadallah and H. M. Abdu, "Modeling and optimization of laser cutting operations," *Manufacturing Review*, vol. 2, p. 20, 2015.

[55] A. A. Petunin and C. Stylios, "Optimization models of tool path problem for cnc sheet metal cutting machines," *IFAC-PapersOnLine*, vol. 49, no. 12, pp. 23–28, 2016.

[56] F. Zhao, X. Xu, and S. Q. Xie, "Computer-aided inspection planning—the state of the art," *Computers in industry*, vol. 60, no. 7, pp. 453–466, 2009.

[57] H. Rico-Garcia, J.-L. Sanchez-Romero, H. M. Gomis, and R. V. Rao, "Parallel implementation of metaheuristics for optimizing tool path computation on cnc machining," *Computers in Industry*, vol. 123, p. 103322, 2020.

[58] C. Feng, X. Chen, J. Zhang, Y. Huang, and Z. Qu, "Minimizing the energy consumption of hole machining integrating the optimization of tool path and cutting parameters on cnc machines," *The International Journal of Advanced Manufacturing Technology*, pp. 1–14, 2022.

[59] X. Qu, Q. Liu, H. Wang, H. Liu, J. Liu, and H. Sun, "Optimization of polishing path and material removal for uniform material removal in optical surface polishing," *The International Journal of Advanced Manufacturing Technology*, vol. 124, no. 5-6, pp. 1699–1722, 2023.

[60] M. Hajad, V. Tangwarodomnukun, C. Jaturanonda, and C. Dumkum, "Laser cutting path optimization using simulated annealing with an adaptive large neighborhood search," *The International Journal of Advanced Manufacturing Technology*, vol. 103, pp. 781–792, 2019.

[61] Y. Altintas, A. Verl, C. Brecher, L. Uriarte, and G. Pritschow, "Machine tool feed drives," *CIRP annals*, vol. 60, no. 2, pp. 779–796, 2011.

[62] Y.-L. Kuo, C.-C. Lin, and Z.-T. Lin, "Dual-optimization trajectory planning based on parametric curves for a robot manipulator," *International Journal of Advanced Robotic Systems*, vol. 17, no. 3, p. 1729881420920046, 2020.

[63] N. Uchiyama, Y. Honda, and S. Sano, "Residual vibration suppression and energy saving in industrial machines using a trapezoidal velocity profile," *2014 American Control Conference*, pp. 323–328, 2014.

[64] G. Carabin, R. Vidoni, and E. Wehrle, "Energy saving in mechatronic systems through optimal point-to-point trajectory generation via standard primitives," *The International Conference of IFToMM Italy*, pp. 20–28, 2018.

[65] Z. Yu, C. Han, and M. Haihua, "A novel approach of tuning trapezoidal velocity profile for energy saving in servomotor systems," *2015 34th Chinese Control Conference (CCC)*, pp. 4412–4417, 2015.

[66] H.-J. Heo, Y. Son, and J.-M. Kim, "A trapezoidal velocity profile generator for position control using a feedback strategy," *Energies*, vol. 12, no. 7, p. 1222, 2019.

[67] T.-C. Lu, S.-L. Chen, and E. C.-Y. Yang, "Near time-optimal s-curve velocity planning for multiple line segments under axis constraints," *IEEE Transactions on Industrial Electronics*, vol. 65, no. 12, pp. 9582–9592, 2018.

[68] K.-H. Rew, C.-W. Ha, and K.-S. Kim, "A practically efficient method for motion control based on asymmetric velocity profile," *International Journal of Machine Tools and Manufacture*, vol. 49, no. 7, pp. 678–682, 2009.

[69] Y. Fang, J. Hu, W. Liu, Q. Shao, J. Qi, and Y. Peng, "Smooth and time-optimal s-curve trajectory planning for automated robots and machines," *Mechanism and Machine Theory*, vol. 137, pp. 127–153, 2019.

[70] P. M. Ho, N. Uchiyama, S. Sano, Y. Honda, A. Kato, and T. Yonezawa, "Simple motion trajectory generation for energy saving of industrial machines," *SICE Journal of Control, Measurement, and System Integration*, vol. 7, no. 1, pp. 29–34, 2014.

[71] D. Fouskakis and D. Draper, "Stochastic optimization: a review," *International Statistical Review*, vol. 70, no. 3, pp. 315–349, 2002.

[72] K. Deb, *Multi-objective optimisation using evolutionary algorithms: an introduction*. Springer, 2011.

[73] A. T. Abbas, M. F. Aly, and K. Hamza, "Optimum drilling path planning for a rectangular matrix of holes using ant colony optimisation," *International Journal of Production Research*, vol. 49, no. 19, pp. 5877–5891, 2011.

[74] M. Brand, M. Masuda, N. Wehner, and X.-H. Yu, "Ant colony optimization algorithm for robot path planning," *2010 international conference on computer design and applications*, vol. 3, pp. V3–436, 2010.

[75] J. Balic and M. Korosec, "Intelligent tool path generation for milling of free surfaces using neural networks," *International Journal of Machine Tools and Manufacture*, vol. 42, no. 10, pp. 1171–1179, 2002.

[76] Y. Yang, H.-z. Xu, S.-h. Li, L.-l. Zhang, and X.-m. Yao, "Time-optimal trajectory optimization of serial robotic manipulator with kinematic and dynamic limits based on improved particle swarm optimization," *The International Journal of Advanced Manufacturing Technology*, vol. 120, no. 1-2, pp. 1253–1264, 2022.

[77] Y. Xue, "Mobile robot path planning with a non-dominated sorting genetic algorithm," *Applied Sciences*, vol. 8, no. 11, p. 2253, 2018.

[78] B. A. Beirigo and A. G. dos Santos, "Application of nsga-ii framework to the travel planning problem using real-world travel data," *2016 IEEE Congress on Evolutionary Computation (CEC)*, pp. 746–753, 2016.

[79] H. R. Maier, S. Razavi, Z. Kapelan, L. S. Matott, J. Kasprzyk, and B. A. Tolson, "Introductory overview: Optimization using evolutionary algorithms and other metaheuristics," *Environmental modelling & software*, vol. 114, pp. 195–213, 2019.

[80] K. Kamandanipour, M. M. Nasiri, D. Konur, and S. H. Yakhchali, "Stochastic data-driven optimization for multi-class dynamic pricing and capacity allocation in the passenger railroad transportation," *Expert Systems with Applications*, vol. 158, p. 113568, 2020.

[81] L. A. Bewoor, V. C. Prakash, and S. U. Sapkal, "Production scheduling optimization in foundry using hybrid particle swarm optimization algorithm," *Procedia Manufacturing*, vol. 22, pp. 57–64, 2018.

[82] S. Katoch, S. S. Chauhan, and V. Kumar, "A review on genetic algorithm: past, present, and future," *Multimedia Tools and Applications*, vol. 80, pp. 8091–8126, 2021.

[83] T. Zhou, Y. Zhou, and K. Sundmacher, "A hybrid stochastic–deterministic optimization approach for integrated solvent and process design," *Chemical Engineering Science*, vol. 159, pp. 207–216, 2017.

[84] A. Bajaj and O. P. Sangwan, "A systematic literature review of test case prioritization using genetic algorithms," *IEEE Access*, vol. 7, pp. 126 355–126 375, 2019.

[85] A. Kumar, "Encoding schemes in genetic algorithm," *International Journal of Advanced Research in IT and Engineering*, vol. 2, no. 3, pp. 1–7, 2013.

[86] A. B. Hassanat, V. Prasath, M. A. Abbadi, S. A. Abu-Qdari, and H. Faris, "An improved genetic algorithm with a new initialization mechanism based on regression techniques," *Information*, vol. 9, no. 7, p. 167, 2018.

[87] A. Arram and M. Ayob, "A novel multi-parent order crossover in genetic algorithm for combinatorial optimization problems," *Computers & Industrial Engineering*, vol. 133, pp. 267–274, 2019.

[88] J. Xin, J. Zhong, F. Yang, Y. Cui, and J. Sheng, "An improved genetic algorithm for path-planning of unmanned surface vehicle," *Sensors*, vol. 19, no. 11, p. 2640, 2019.

[89] N. Gunantara, "A review of multi-objective optimization: Methods and its applications," *Cogent Engineering*, vol. 5, no. 1, p. 1502242, 2018.

[90] R. Kasimbeyli, Z. K. Ozturk, N. Kasimbeyli, G. D. Yalcin, and B. I. Erdem, "Comparison of some scalarization methods in multiobjective optimization: comparison of scalarization methods," *Bulletin of the Malaysian Mathematical Sciences Society*, vol. 42, pp. 1875–1905, 2019.

[91] T. Chen and M. Li, "The weights can be harmful: Pareto search versus weighted search in multi-objective search-based software engineering," *ACM Transactions on Software Engineering and Methodology*, vol. 32, no. 1, pp. 1–40, 2023.

[92] H. Ishibuchi, K. Doi, and Y. Nojima, "On the effect of normalization in moea/d for multi-objective and many-objective optimization," *Complex & Intelligent Systems*, vol. 3, no. 4, pp. 279–294, 2017.

[93] K. Deb, A. Pratap, S. Agarwal, and T. Meyarivan, "A fast and elitist multiobjective genetic algorithm: Nsga-ii," *IEEE transactions on evolutionary computation*, vol. 6, no. 2, pp. 182–197, 2002.

[94] J. E. Alvarez-Benitez, R. M. Everson, and J. E. Fieldsend, "A mopso algorithm based exclusively on pareto dominance concepts," *Evolutionary Multi-Criterion Optimization: Third International Conference, EMO 2005, Proceedings 3*, pp. 459–473, 2005.

[95] A. Konak, D. W. Coit, and A. E. Smith, "Multi-objective optimization using genetic algorithms: A tutorial," *Reliability Engineering & System Safety*, vol. 91, no. 9, pp. 992–1007, 2006.

[96] S. Verma, M. Pant, and V. Snasel, "A comprehensive review on nsga-ii for multi-objective combinatorial optimization problems," *IEEE Access*, vol. 9, pp. 57 757–57 791, 2021.

[97] Z. Che, T.-A. Chiang, and T.-T. Lin, "A multi-objective genetic algorithm for assembly planning and supplier selection with capacity constraints," *Applied Soft Computing*, vol. 101, p. 107030, 2021.

[98] I. F. Edem and P. T. Mativenga, "Modelling of energy demand from computer numerical control (cnc) toolpaths," *Journal of cleaner production*, vol. 157, pp. 310–321, 2017.

[99] B. Alpers, "On fast jerk–, acceleration–and velocity–restricted motion functions for online trajectory generation," *Robotics*, vol. 10, no. 1, p. 25, 2021.

[100] S. Tajima and B. Sencer, "Global tool-path smoothing for cnc machine tools with uninterrupted acceleration," *International Journal of Machine Tools and Manufacture*, vol. 121, pp. 81–95, 2017.

[101] C. Li, Z. Zhu, H. Yang, and R. Li, "An innovative hybrid system for wind speed forecasting based on fuzzy preprocessing scheme and multi-objective optimization," *Energy*, vol. 174, pp. 1219–1237, 2019.

[102] Y. Tian, H. Wang, X. Zhang, and Y. Jin, "Effectiveness and efficiency of non-dominated sorting for evolutionary multi-and many-objective optimization," *Complex & Intelligent Systems*, vol. 3, no. 4, pp. 247–263, 2017.

[103] W. Cai, L. Wang, L. Li, J. Xie, S. Jia, X. Zhang, Z. Jiang, and K. hung Lai, "A review on methods of energy performance improvement towards sustainable manufacturing from perspectives of energy monitoring, evaluation, optimization and benchmarking," *Renewable and Sustainable Energy Reviews*, vol. 159, p. 112227, 2022.

[104] J. R. G. Martínez, J. R. Reséndiz, M. Á. M. Prado, and E. E. C. Miguel, "Assessment of jerk performance s-curve and trapezoidal velocity profiles," *2017 XIII International Engineering Congress (CONIIN)*, pp. 1–7, 2017.

[105] Y. Fang, J. Qi, J. Hu, W. Wang, and Y. Peng, "An approach for jerk-continuous trajectory generation of robotic manipulators with kinematical constraints," *Mechanism and Machine Theory*, vol. 153, p. 103957, 2020.

[106] C.-C. Liu, M.-S. Tsai, M.-Q. Hong, and P.-Y. Tang, "Development of a novel tuning approach of the notch filter of the servo feed drive system," *Journal of Manufacturing and Materials Processing*, vol. 4, no. 1, p. 21, 2020.

[107] A. Dumanli and B. Sencer, "Data-driven iterative trajectory shaping for precision control of flexible feed drives," *IEEE/ASME Transactions on Mechatronics*, vol. 26, no. 5, pp. 2735–2746, 2020.

[108] S. Tajima, B. Sencer, and E. Shamoto, "Accurate interpolation of machining tool-paths based on fir filtering," *Precision Engineering*, vol. 52, pp. 332–344, 2018.

[109] Z. Wu, J. Chen, T. Bao, J. Wang, L. Zhang, and F. Xu, "A novel point-to-point trajectory planning algorithm for industrial robots based on a locally asymmetrical jerk motion profile," *Processes*, vol. 10, no. 4, p. 728, 2022.

[110] I. F. Edem, V. A. Balogun, B. D. Nkanang, and P. T. Mativenga, "Software analyses of optimum toolpath strategies from computer numerical control (cnc) codes," *The International Journal of Advanced Manufacturing Technology*, vol. 103, no. 1, pp. 997–1007, 2019.

[111] P. Lambrechts, M. Boerlage, and M. Steinbuch, "Trajectory planning and feedforward design for high performance motion systems," *Proceedings of the 2004 American control conference*, vol. 5, pp. 4637–4642, 2004.

[112] B. Alpers, "On fast jerk-continuous motion functions with higher-order kinematic restrictions for online trajectory generation," *Robotics*, vol. 11, no. 4, p. 73, 2022.

[113] K. D. Nguyen, T.-C. Ng, and I.-M. Chen, "On algorithms for planning s-curve motion profiles," *International Journal of Advanced Robotic Systems*, vol. 5, no. 1, p. 11, 2008.

[114] P. Lambrechts, M. Boerlage, and M. Steinbuch, "Trajectory planning and feedforward design for electromechanical motion systems," *Control Engineering Practice*, vol. 13, no. 2, pp. 145–157, 2005.

[115] Y. Li and F. Liang, "Ga-based time-optimal feedrate scheduling on nurbs tool path with geometric and drive constraints," *The International Journal of Advanced Manufacturing Technology*, pp. 1–23, 2022.

[116] X. Lü, Y. Wu, J. Lian, Y. Zhang, C. Chen, P. Wang, and L. Meng, "Energy management of hybrid electric vehicles: A review of energy optimization of fuel cell hybrid power system based on genetic algorithm," *Energy Conversion and Management*, vol. 205, p. 112474, 2020.

[117] G. Carabin and R. Vidoni, "Energy-saving optimization method for point-to-point trajectories planned via standard primitives in 1-dof mechatronic systems," *The International Journal of Advanced Manufacturing Technology*, vol. 116, no. 1, pp. 331–344, 2021.

[118] F. Song, S. Yu, T. Chen, and L.-N. Sun, "Research on cnc simulation system with instruction interpretations possessed of wireless communication," *The Journal of Supercomputing*, vol. 72, no. 7, pp. 2703–2719, 2016.

[119] W. Fan, X.-S. Gao, W. Yan, and C.-M. Yuan, "Interpolation of parametric cnc machining path under confined jounce," *The International Journal of Advanced Manufacturing Technology*, vol. 62, no. 5, pp. 719–739, 2012.

[120] A. Y. Lee and Y. Choi, "Smooth trajectory planning methods using physical limits," *Proceedings of the Institution of Mechanical Engineers, Part C: Journal of Mechanical Engineering Science*, vol. 229, no. 12, pp. 2127–2143, 2015.

[121] H. Li, Z. Gong, W. Lin, and T. Lippa, "Motion profile planning for reduced jerk and vibration residuals," *SIMTech technical reports*, vol. 8, no. 1, pp. 32–37, 2007.

[122] J. Huang and L.-M. Zhu, "Feedrate scheduling for interpolation of parametric tool path using the sine series representation of jerk profile," *Proceedings of the Institution of Mechanical Engineers, Part B: Journal of Engineering Manufacture*, vol. 231, no. 13, pp. 2359–2371, 2017.

Publication list

International journal papers

- H. J. Nyobuya, M. S. Halinga, and N. Uchiyama, "Simple Adaptive Control Approach to Motion Accuracy and Energy-Saving for Industrial Feed Drive System Using Jerk-Based Augmented Output Signal,". (Accepted), *The International Journal of Advanced Manufacturing Technology* . (Impact Factor 3.563)
- M. S. Halinga, E. W. Nshama, T. R. Schäfle and N. Uchiyama, "Time and Energy Optimal Trajectory Generation for Coverage Motion in Industrial Machines,". *ISA Transactions*, 138, pp. 735-745 (2023). (Impact Factor 5.911)
- M. S. Halinga, H. J. Nyobuya and N. Uchiyama, "Generation and Experimental Verification of Time and Energy Optimal Coverage Motion for Industrial Machines using a Modified S-curve Trajectory,". *The International Journal of Advanced Manufacturing Technology*, 125, pp. 3593-3605 (2023). (Impact Factor 3.563)

International conference papers

- M. S. Halinga, H. J. Nyobuya and N. Uchiyama, "Energy-Optimal Coverage Motion Trajectory Generation for Industrial Machines," in *The 22nd World Congress of the International Federation of Automatic Control (IFAC)*, Yokohama, Japan, pp. 9906-9911, 2023.
- H. J. Nyobuya, M. S. Halinga, and N. Uchiyama, "Enhanced Motion Accuracy in Industrial Feed Drive Systems using Simple Adaptive Control with a Jerk-Based Augmented Signal," in *The 22nd World Congress of the International Federation of Automatic Control (IFAC)*, Yokohama, Japan, pp. 9452-9457, 2023.

- M. S. Halinga, H. J. Nyobuya and N. Uchiyama, "Generation of Time and Energy Optimal Coverage Motion for Industrial Machines using a Modified S-curve Trajectory," *2023 IEEE/SICE International Symposium on System Integration*, Atlanta, USA, pp. 448-453, 2023.